Hybrid modelling of erythropoiesis and blood disorders

Polina Kurbatova

Numéro d'ordre : 258-2011 Année 2011

Université Claude Bernard - Lyon 1

Institut Camille Jordan - CNRS UMR 5208
École doctorale InfoMaths

Thèse de l'université de Lyon

pour obtenir le titre de

Docteur en Sciences
Mention : Mathématiques appliquées

présentée par

Polina Kurbatova

Modélisation hybride de l'érythropoïèse et des maladies sanguines

Thèse dirigée par Vitaly Volpert et Grigory Panasenko
soutenue publiquement le 24 novembre 2011

Jury :

Mark Chaplain	Professeur, Université de Dundee	Rapporteur
Ionel Sorin Ciuperca	Maître de Conférence, Université Lyon 1	Examinateur
Florence Hubert	Maître de Conférence, l'Université de Provence	Examinateur
Grigory Panasenko	Professeur, Université Jean Monnet de St. Etienne	Directeur
Luigi Preziosi	Professeur, Université Polytechnique de Turin	Rapporteur
Philippe Tracqui	DR au CNRS, Université Joseph Fourier	Examinateur
Vitaly Volpert	DR au CNRS, Université Lyon 1	Directeur

Remerciements

Tout d'abord je voudrais exprimer ma profonde gratitude envers mes deux directeurs de thèse, Grigory Panansenko et Vitaly Volpert. Je les remercie pour leur soutien aussi bien sur le plan scientifique que personnel, ainsi que le temps qu'ils ont consacré à moi et à mes questions pendant toute la durée de la thèse. J'ai eu beaucoup de chance d'avoir de tels directeurs. Merci beaucoup. Je voudrais exprimer ma reconnaissance à Nicolai Bessonov, c'était un grand plaisir pour moi de travailler et d'apprendre avec lui.

Je remercie Mark Chaplain et Luigi Preziosi d'avoir accepté d'être rapporteurs et d'avoir effectué une lecture aussi précise et intéressée de mon manuscrit.

Je remercie aussi Ionel Sorin Ciuperca, Florence Hubert et Philippe Tracqui de m'avoir fait l'honneur d'accepter de faire partie de mon jury.

Cette thèse a été effectuée à l'Institut Camille Jordan, au sein de l'équipe de modélisation mathématique en médecine et en biologie. Je tiens à remercier tous ses membres avec qui j'ai eu grand plaisir à travailler. En particulier, je tiens à remercier Samuel Bernard et Fabien Crauste pour leur collaboration et les réunions fructeuses mais aussi parce que grâce à eux je me suis sentie beaucoup plus à l'aise dès mon arrivée au laboratoire. Merci. Je voudrais aussi remercier Stephan Fischer et Nathalie Eymard pour leur collaboration pendant les différentes périodes de ma thèse.

Je voudrais remercier mes amis que j'ai eu la chance de rencontrer en France : Ivan, Gaelle, Nastia et Vladimir pour avoir pris une place importante dans ma vie. Je voudrais aussi remercier Fred, Laurent, Rémi et les autres thésards de l'ICJ pour les moments agréables passés ensemble. Je voudrais aussi, remercier Vika, Tania et Serega ; malgré la distance, j'ai toujours senti qu'ils étaient près de moi. Je tiens à remercier Paule, Lionel et Laura pour leur gentillesse et leur chaleur qui m'ont soutenue pendant tout ce temps.

Enfin, je voudrais remercier mes parents et grand-parents, mon frère et Larissa pour leur soutien et pour avoir toujours cru en moi. Je voudrais remercier, toi, mon chèri Nicolas, je n'y imagine même pas comment je pourrais d'être ici (et ailleurs aussi) sans toi.

Résumé

La thèse est consacrée au développement de nouvelles méthodes de modélisations mathématiques en biologie et en médecine, du type "off-lattice" modèles hybrides discret-continus, et de leurs applications à l'hématopoïèse et aux maladies sanguines telles la leucémie et l'anémie. Dans cette approche, les cellules biologiques sont considérées comme des objets discrets alors que les réseaux intracellulaire et extracellulaire sont décrits avec des modèles continus régis par des équations aux dérivées partielles et des équations différentielles ordinaires. Les cellules interagissent mécaniquement et biochimiquement entre elles et avec le milieu environnant. Elles peuvent se diviser, mourir par apoptose ou se différencier. Le comportement des cellules est déterminé par le réseau de régulation intracellulaire et influencé par le contrôle local des cellules voisines ou par la régulation globale d'autres organes.

Dans la première partie de la thèse, les modèles hybrides du type "off-lattice" dynamiques sont introduits. Des exemples de modèles, spécifiques aux processus biologiques, qui décrivent au sein de chaque cellule la concurrence entre la prolifération et l'apoptose, la prolifération et la différenciation et entre le cycle cellulaire et de l'état de repos sont étudiés. L'émergence des structures biologiques est étudiée avec les modèles hybrides. L'application à la modélisation des filamente de bactéries est illustrée.

Dans le chapitre suivant, les modèle hybrides sont appliqués afin de modéliser l'érythropoïèse ou production de globules rouges dans la moelle osseuse. Le modèle inclut des cellules sanguines immatures appelées progéniteurs érythroïdes, qui peuvent s'auto-renouveler, se différencier ou mourir par apoptose, des cellules plus matures appelées les réticulocytes, qui influent les progéniteurs érythroïdes par le facteur de croissance Fas-ligand, et des macrophages, qui sont présents dans les îlots érythroblastiques *in vivo*. Les régulations intracellulaire et extracellulaire par les protéines et les facteurs de croissance sont précisées et les rétrocontrôles par les hormones érythropoïétine et glucocorticoïdes sont pris en compte. Le rôle des macrophages pour stabiliser les îlots érythroblastiques est montré. La comparaison des résultats de modélisation avec les expériences sur l'anémie chez les souris est effectuée.

Le quatrième chapitre est consacré à la modélisation et au traitement de la leucémie. L'érythroleucémie, un sous-type de leucémie myéloblastique aigüe (LAM), se développe à cause de la différenciation insuffisante des progéniteurs érythroïdes et de leur auto-renouvellement excessif. Un modèle de type "Physiologically Based Pharmacokinetics-Pharmacodynamic" du traitement de la leucémie par AraC et un modèle de traitement chronothérapeutique de la leucémie sont examinés. La comparaison avec les données cliniques sur le nombre de blast dans le sang est effectuée.

Le dernier chapitre traite du passage d'un modèle hybride à un modèle continu dans le cas 1D. Un théorème de convergence est prouvé. Les simulations numériques confirment un bon accord entre ces deux approches.

Mots-clés : modèles hybrides discret-continus, "off-lattice" dynamiques des cellules, réseau de régulation intracellulaire et extracellulaire, équations aux dérivées partielles, équations différentielles ordinaires, érythropoïèse, modèle de type PBPKPD du treatement de leucémie.

Abstract

This dissertation is devoted to the development of new methods of mathematical modelling in biology and medicine, off-lattice discrete-continuous hybrid models, and their applications to modelling of hematopoiesis and blood disorders, such as leukemia and anemia. In this approach, biological cells are considered as discrete objects while intracellular and extracellular networks are described with continuous models, ordinary or partial differential equations. Cells interact mechanically and biochemically between each other and with the surrounding medium. They can divide, die by apoptosis or differentiate. Their fate is determined by intracellular regulation and influenced by local control from the surrounding cells or by global regulation from other organs.

In the first part of the thesis, hybrid models with off-lattice cell dynamics are introduced. Model examples specific for biological processes and describing competition between cell proliferation and apoptosis, proliferation and differentiation and between cell cycling and quiescent state are investigated. Biological pattern formation with hybrid models is discussed. Application to bacteria filament is illustrated.

In the next chapter, hybrid model are applied in order to model erythropoiesis, red blood cell production in the bone marrow. The model includes immature blood cells, erythroid progenitors, which can self-renew, differentiate or die by apoptosis, more mature cells, reticulocytes, which influence erythroid progenitors by means of growth factor Fas-ligand, and macrophages, which are present in erythroblastic islands *in vivo*. Intracellular and extracellular regulation by proteins and growth factors are specified and the feedback by the hormones erythropoietin and glucocorticoids is taken into account. The role of macrophages to stabilize erythroblastic islands is shown. Comparison of modelling with experiments on anemia in mice is carried out.

The following chapter is devoted to leukemia modelling and treatment. Erythroleukemia, a subtype of Acute Myeloblastic Leukemia (AML), develops due to insufficient differentiation of erythroid progenitors and their excessive slef-renewal. A Physiologically Based Pharmacokinetics-Pharmacodynamics (PBPKPD) model of leukemia treatment with AraC drug and chronotherapeutic treatments of leukemia are examined. Comparison with clinical data on blast count in blood is carried out.

The last chapter deals with the passage from a hybrid model to a continuous model in the 1D case. A convergence theorem is proved. Numerical simulations confirm a good agreement between these approaches.

Keywords : discrete-continuous hybrid models, off-lattice cell dynamics, intracellular and extracellular regulatory networks, ordinary and partial differential equations, erytropoiesis, PBPKPD modelling of leukemia treatment.

Publications

1. N. Bessonov, I. Demin , P. Kurbatova, L. Pujo-Menjouet, V. Volpert, Chapter *Multi-agent systems and blood cell formation.* in Book *Multi-Agent Systems - Modeling, Interactions, Simulations and Case Studies*. Intech, 2011.
2. S. Fischer, P. Kurbatova, N. Bessonov, O. Gandrillon, V. Volpert, F. Crauste, *Erythroblastic Islands : Using a Hybrid Model to Assess the Function of Central Macrophage.* Submitted in Journal of Theoretical Biology, 2011.
3. P. Kurbatova, S. Bernard, N. Bessonov, F. Crauste, I. Demin, C. Dumontet, S. Fischer, V. Volpert, *Hybrid Model of Erythropoiesis and Leukemia Treatment with Cytosine Arabinoside.* Submitted and accepted in SIAM J. Appl. Math., 2011.
4. P. Kurbatova, G. Panasenko, V. Volpert, *Asymptotic numerical analysis of the diffusion-discrete absorption equation*, Math. Meth. Appl. Sci., 2011.
5. N. Bessonov, P. Kurbatova, V. Volpert, *Pattern Formation in Hybrid Models of Cell Populations.* Proceedings of a conference Pattern Formation in Morphogenesis, Springer, in press, 2010.
6. N. Bessonov, F. Crauste, S. Fischer, P. Kurbatova, and V. Volpert, *Application of Hybrid Models to Blood Cell Production in the Bone Marrow.* In press Math. Model. Nat. Phenom.
7. N. Bessonov, P. Kurbatova, V. Volpert, *Dynamics of growing cell populations.* CRM, preprint num. 931 for Mathematical biology, University of Barcelona, February 2010.
8. N. Bessonov, P. Kurbatova, V. Volpert, *Particle dynamics modelling of cell populations.* Math. Model. Nat. Phenom., JANO9 – The 9th International Conference on Numerical Analysis and Optimization, Volume 5, Number 7, 2010, pp. 42 – 47.
9. N. Bessonov, P. Kurbatova, V. Volpert, *Dynamics of growing cell populations.* Special Issue "Actual problems of mathematical hydrodynamics", Izvestiya Vuzov, 2009.

Table des matières

1 Introduction **9**
1.1 Hybrid models in biology . . . 9
1.2 Mathematical modelling of hematopoiesis . . . 12
1.2.1 Biological background . . . 12
1.2.2 Continuous models . . . 13
1.2.3 Leukemia modeling and treatment . . . 14
1.3 Summary of the results . . . 18
1.3.1 Hybrid Method . . . 18
1.3.2 Erythropoiesis . . . 20
1.3.3 Leukemia . . . 22
1.3.4 From hybrid to continuous models . . . 24

2 Hybrid method and model examples **25**
2.1 Method description . . . 25
2.2 Particle dynamics and continuum mechanics . . . 28
2.2.1 From cells to particle dynamics . . . 29
2.2.2 Particles and discrete equations . . . 29
2.2.3 Continuous model . . . 30
2.2.4 Energy . . . 31
2.2.5 1D model of particle flow . . . 31
2.2.6 Model problem with a point source of particles . . . 32
2.2.6.1 1D case . . . 32
2.2.6.2 2D case . . . 37
2.2.7 Motion of dividing cells . . . 38
2.3 1D hybrid models . . . 38
2.3.1 Cell differentiation and apoptosis . . . 38
2.3.2 Cell division and differentiation . . . 42
2.3.3 Quiescent state of cells . . . 42
2.4 2D modelling. . . . 46
2.4.1 Cell differentiation and apoptosis. . . . 46
2.4.2 Modelling of tumor growth . . . 46
2.5 Modelling of Pattern Formation in Bacteria Filament . . . 51

3 Hybrid modeling of erythropoiesis **55**
3.1 Model . . . 56
3.1.1 Intracellular Scale : Mathematical Model . . . 56
3.1.1.1 ODE System . . . 56
3.1.1.2 Brief Analysis : Existence and Stability of Steady States . . . 57
3.1.1.3 Dynamics of the ODE System . . . 60
3.1.1.4 Feedback Control Role . . . 63
3.1.2 Extracellular Scale . . . 64
3.1.3 Coupling Both Scales . . . 67
3.2 Results : Stability of Erythroblastic Island and Function of Central Macrophage 68
3.2.1 Erythroblastic Island without Macrophage . . . 68
3.2.1.1 Stability Analysis . . . 69
3.2.1.2 Feedback Relevance and Relation to Stability . . . 70
3.2.2 Island with macrophage . . . 72
3.2.2.1 Stability Analysis . . . 73
3.2.2.2 Feedback Relevance and Relation to Stability . . . 74
3.3 Parameter Estimation . . . 75
3.4 Responsiveness of the system to stress situations . . . 78
3.5 Discussion . . . 81

4 Pharmacokinetics-Pharmacodynamics model of leukemia treatment **85**
4.1 Mathematical model . . . 85
4.1.1 Intracellular and extracellular regulation of normal erythropoiesis . . . 85
4.1.2 Ara-C kinetics . . . 88
4.1.3 Organization and duration of cell cycle . . . 89
4.1.4 Circadian rhythm in the cell cycle . . . 91
4.2 Results . . . 92
4.2.1 Treatment protocol depending on cell cycle duration . . . 93
4.2.2 Optimal administration of Ara-C related to circadian rhythm . . . 94
4.3 Comparison with clinical data of leukemia treatment . . . 97
4.4 Discussion . . . 100

5 From hybrid to continuous models **103**
5.1 Formulation of the problem. . . . 104
5.2 Comparison of the discrete and continuous models. . . . 105
5.3 Numerical experiments . . . 109

Conclusions and Perspectives **110**

A Addition to chapter 3 and 4 **115**
A.1 Computational algorithm . . . 115

Bibliographie **130**

Chapitre 1

Introduction

1.1 Hybrid models in biology

In recent years, mathematical models that exploit the advantages of both continuous and discrete models have emerged. Hybrid discrete-continuous models are widely used in investigation of the dynamics of cell populations in biological tissues and organisms that involve processes at different scales. This approach receives more and more attention in modelling cellular systems due to the availability of "individual cell data" such as metabolic, genetic and proteomic.

In hybrid methods cells are considered as discrete objects described either by cellular automata or by various lattice or off-lattice models while intracellular and extracellular concentrations are described with continuous models, ordinary or partial differential equations. Hybrid methods can be divided into three main groups : (i) cellular Potts models ([6, 105]) that can be thought of as a generalized cellular automaton (CA) models ([4, 5, 7, 8, 34, 40, 72, 113]), (ii) off-lattice cell models ([32, 33, 39, 53, 91, 116]) and (iii) viscoelastic cell models [38, 57, 94]. In off-lattice models cell shape can be explicitly modeled and cell interactions with neighbouring cells and surrounding medium can be investigated. The viscoelastic cell models are also lattice free, besides this approach takes into account cell elasticity. That allows cell deformation simultaneously preserving cell volume.

There are several types of cellular automaton model where each individual cell can be represented as a single site of lattice, as several connected lattice sites or the lattice site can be larger than an individual cell. In each particular CA model the state of rules determines the motion of cells. It can be influenced by the interaction of cells with the elements of their immediate surrounding and by processes that involve cellular response to external signals like chemotaxis. The numerous models with gradient fields of chemical concentrations that govern motility of cells have been suggested. Cellular automaton have been used extensively to model a wide range of problems. The numerous models analyse the different stages of tumor development from initial avascular phase to invasion and metastasis through angiogenesis.

Cellular automata are applied to model tumor invasion in [7, 8] where tumor is considered as a collection of many individual cancer cells that interact and modify the environment

through which they grow and migrate. The movement probability of each single cell is based on coefficients of a discretization system of partial differential equations that control the chemical extracellular matrix dynamics. By means of hybrid model it was shown that evolution of cell phenotypes/genotypes arises in tumors growing in different oxygen concentrations. Other cellular automaton modele, studied by Dormann and Deutsch [40], focuses on avascular tumor growth *in vitro* by means of multicellular spheroids. The model reproduces experimental results of growth saturation observed in multicellular spheroids due to the introduction into the model of not only movement of the cell population towards nutrients coming from outside the tumor but also of a chemotactic migration of tumor cells into the direction of the necrotic signal gradient that means towards the center. That explains why an initial exponential growth phase of spheroid is significantly slowed down with appearance of necrotic cells even if further nutrient is supplied. Diffusion of chemicals (nutrient and necrotic signal) is modeled with the continuous diffusion equations. Tumor-induced angiogenesis has been modeled using a cellular automaton approach in Anderson and Chaplain [5]. In this work the growth of the vascular network outside the solid tumor in response to tumor angiogenic factors (TAF) is described by both continuous and discrete mathematical models. In the continuum approach by means of a system of coupled nonlinear partial differential equations, chemotactic response of the endothelial cells is modeled. Using the resulting coefficients of discretized form with Euler finite difference approximation of these governing partial differential equations provides the migration of each individual cell. In the discrete approach the ability of cells to proliferate is incorporated. Based partially on the work of Anderson and Chaplain other mathematical models of angiogenic networks this time in connection with chemotherapeutic strategies were developed [72, 113]. In McDougall et al. [72] blood flow is incorporated by adapting computational techniques used in petroleum engineering industry to model flow through porous media. The blood is assumed to be a Newtonian fluid and no kinetics reactions are included in drug functions. The flow through vascular network with different architecture was examined and applied for the study of delivery of chemotherapeutic drugs to the tumor. Later this model was extended in Stéphanou et al. [113] to the 3D case. Other mathematical model of flow in capillary networks has been considered by Alarcon et al. [4] in order to investigate the influence of red blood cell heterogeneity on normal and cancerous cell growth.

A generalized cellular automaton approach is presented by the cellular Potts models (CPM). The CPM is a more sophisticated cellular automaton that describes individual cells as extended objects of variable shapes. This model suggests the consideration of differential surface energies between cells and their surrounding extracellular medium. The CPM effective energy can control cell behaviors including cell adhesion, signalling, volume and surface area or even chemotaxis, elongation and haptotaxis [6]. In [105] M. Scianna and co-workers applied the cellular Potts model to study the scattering process in colonies of two cell lines, thyroid carcinoma-derived cells (ARO) and mouse liver progenitor cells (MLP-29) induced by hepatocyte growth factor (HGF) which influences the cell-cell adhesion energy and the system motility. In the case of ARO cells the effective energy determines adhesion and target area deviation while for a culture of MLP-29 cells it was necessary to add a term related to

cell polarization and persistence in conjunction with a chemotactic response. In [47] CPM, combining with continuum methods, is used to reproduce transmesothelial migration assays of ovarian cancer cells, isolated or aggregated in multicellular spheroids. This process is regulated by the activity of matrix metalloproteinases (MMPs) and by the interaction of the cells with the extracellular matrix and with other cells. Effective energy is responsible for cell-cell adhesion, cell shape and the response of a cell to chemotactic and haptotactic gradients. Concentration of chemical substances, released by mesothelial cells and molecules of extracellular matrix, and MMPs, released from tumor cells, are described by partial differential equations. They determine cancer cell's motility. Results of simulations are in good agreement with experimental evidences.

Lattice-free models are important to those biological situations in which the shape of individual cells can influence the dynamics or geometry of the whole population of cells. In these models, shape of cells can be explicitly modeled and response to local mechanical forces, interaction with neighboring cells and environment can be investigated. Indeed, all models of this type have the freedom to move each cell in any direction and they can be distinguished into several main types : (i) spherical cell-centered models [32, 33, 53, 91], (ii) ellipsoidal cell-centered models [57], (iii) viscoelastic cell models [38, 57, 94] that allows to include elastic or viscoelastic properties of individual cells. To use this modeling approach special algorithms to handle efficiently cell-cell interaction should be designed. Some interpolation techniques need to be applied to couple the cellular off-lattice individuals with the chemical fields.

The method is ideal to understand macroscopic behaviour of discrete systems interacting with continuum systems. J. C. Dallon [32] models with such a method distyostelium discoideum where individual amoebae are treated as discrete entities. Each cell is thought of as a point mass. They move and communicate with each other through a extracellular diffusible chemical which is determined by a partial differential equation. Each individual cell modify the continuum variable which in turn modify the behavior of the cells. This communication is carried out by interpolation the information from the cell locations to the lattice of discretized domain of partial differential equation. Intracellular dynamics of various chemical complexes, one of them determines cell movement, is modeled with ordinary differential equations defined in the previous works of Tang&Othmer [116] and Dallon&Othmer [33]. The cells move in the direction of the gradient of the chemoattractant. The second model in [32] describes scar tissue formation with the same basic framework.

Hybrid lattice-off models, not limited in possible directions of cell motion, are widely applied to the modeling of tumor growth and invasion where cell migration is thought to be central. For example, in the recent work of J. Jeon and co-workers [53] an off-lattice hybrid discrete-continuum model of tumor growth and invasion is proposed. The cells are represented as the spherical discrete objects while the extracellular concentrations represent continuum part. All cells interact with each other and with extracellular matrix. Cell migration is described with the Langevin equation. In [91] multiscale modeling approach is used to determine regulation of cell adhesion by interactions between E-cadherin and β-catenin and its implications for cell migration and cancer invasion. Each cell in isolation has a spherical shape. The β-catenin kinetics is governed by a system of differential equations in each indivi-

dual cell. The concentration of β-catenin control the decision of a cell to migrate. In J. Kim et al. [57] the model of tumor spheroidal growth consists of both continuum and cell-level description. All cells are deformable and have ellipsoidal shape in the absence of external forces. Extracellular concentrations of oxygen and glucose are governed by reaction-diffusion equations. Cells which are at the periphery of the tumor proliferate.

Fluid-based elastic cell modeling is applied to early tumor development in an article of K. A. Rejniak [94]. The cell membranes and cell nuclei are treated as neutrally buoyant bodies which are moved by the fluid inside and outside the cell. The fluid inside the cells represents the cell cytoplasm and the fluid outside the cells represents the extracellular matrix. The motion of the fluid is described by the Navier-Stokes equations. The cell nuclei inside the cell is modeled as the source of fluid and cell bounders as the collection of springs that apply the force to the fluid. All cells have the ability to proliferate and to exchange mechanical and chemical signals with their immediate neighbors. The growth of early tumor under different conditions of its initiation and progression is presented. Other model with the fluid-elastic structure of the cells was considered in by R. Dillon et al. in [38]. Extracellular chemicals, required for cell growth, are described by a system of reaction-diffusion-advection equations. The model is applied to solid tumor growth and ductal carcinoma.

1.2 Mathematical modelling of hematopoiesis

1.2.1 Biological background

Haematopoiesis is the process by which immature cells proliferate and differentiate into mature blood cells. It starts with very few primitive haematopoietic stem cells and ends up with a huge number of mature erythrocytes (red blood cells), leukocytes (white blood cells) and platelets. We are concerned, in this work, with the red blood cell lineage, through the process of production and regulation of red blood cells, called erythropoiesis.

The whole process of erythropoiesis happens in the bone marrow where erythroid progenitors, immature blood cells with abilities to proliferate and differentiate, divide to produce erythroblasts (mature progenitors), then reticulocytes (precursor cells), which are almost differentiated red blood cells. Reticulocytes eject their nuclei, enter the bloodstream and finish their differentiation process to become erythrocytes (mature red blood cells). At every step of this differentiation process, erythroid cells can die by apoptosis (programmed cell death), and erythroid progenitors have been shown to be able to self-renew under stress conditions [14, 45, 46, 84]. Moreover, cell fate is partially controlled by external feedback controls. For instance, death by apoptosis has been proved to be mainly negatively regulated by erythropoietin (Epo), a growth factor released by the kidneys when the organism lacks red blood cells [60]. Self-renewal is induced by glucocorticoids [14, 45, 46, 84], but also by Epo [99, 112] and some intracellular autocrine loops [46, 104]. Global feedback control mediated by the population of mature red blood cells (through erythropoietin release) is supposed to influence erythroid progenitor proliferation [99, 112] and inhibit their death by apoptosis [60]. Local feedback control, mediated by reticulocytes and based upon Fas-ligand

activity, is supposed to induce both differentiation and death by apoptosis [79]. Global and local feedback controls modify the activity of intracellular proteins. A set of two proteins, previously considered by the authors [29], Erk and Fas, are thought to be determinant for the regulation of self-renewal, differentiation and apoptosis. It has been shown [99], that Erk and Fas are involved in an antagonist loop where Erk, from the MAPK family, inhibits Fas (a TNF family member) and self-activates, high levels of Erk inducing cell proliferation depending on Epo levels, whereas Fas inhibits Erk and induces apoptosis and differentiation. Competition between these two proteins sets a relevant frame to observe, within a single cell, all three possible cell fates depending on the level of each protein.

In addition to intracellular regulation of cell fate and feedback induced either by mature red blood cells or reticulocytes on erythroid progenitors, an important aspect of erythropoiesis lays in the structure of bone marrow. Erythroid progenitors are indeed produced in specific micro-environments, called niches [115], where erythroblastic islands develop. An erythroblastic island consists in a central macrophage surrounded by erythroid progenitors [27]. The macrophage appears to act on surrounding cells, by affecting their proliferation and differentiation programs. For years, however, erythropoiesis has been studied under the influence of erythropoietin, which may induce differentiation and proliferation in vitro without the presence of the macrophage. Hence, the roles of the macrophage and the erythroblastic island have been more or less neglected. Consequently, spatial aspects of erythropoiesis (and hematopoiesis, in general) have usually not been considered when modelling cell population evolution or hematological diseases appearance and treatment.

1.2.2 Continuous models

Hematopoiesis has been the topic of modelling works for decades. Dynamics of hematopoietic stem cells have been described by Mackey's early works [69, 70]. The author developed hypothesis that aplastic anaemia (lower counts of all three blood cell types) and periodic haematopoiesis in humans are probably due to irreversible cellular loss from the proliferating pluripotential stem cell population. A model for pluripotential stem cell population is described by delay equations. In the later developed model a population dynamics of cells capable of both proliferation and maturation was analysed [71]. This model is described by the first order differential equations. Further development of mathematical model devoted to periodic diseases of blood production was proposed to explain the origin of oscillations of circulating blood neutrophil number in Bernard et al. [15]. They demonstrated that an increase in the rate of stem cell apoptosis can lead to long period oscillations in the neutrophil count. By coupling the previous models in [26] Colijn and Mackey applied mathematical model, through systems of delay differential equations, to explain coupled oscillations of leukocytes, platelets and erythrocytes in cyclical neutropenia and determined necessary parameters to fit data during its treatment. Another work on haematopoiesis modeling was proposed by Roeder[96].

The platelet production process (thrombopoiesis) attracted less attention through years [41, 119]. Cyclical platelet disease was a subject of mathematical modeling in Santillan et al.

[103] and was enriched in Apostu et al. [11].

The red blood cell production process (erythropoiesis) has recently been the focus of modelling in hematopoiesis. Pioneering mathematical model which describes the regulation of erythropoiesis in mice and rats has been developed by Wichmann, Loeffler and co-workers [121]. In the following paper proposed model was validated by comparing with experimental data during stress erythropoiesis as hypoxia and different forms of induced anaemia [120]. Analysis of the regulating mechanisms in erythropoiesis was enriched in [125]. In 1995, Bélair et al. proposed age-structured model of erythropoiesis where erythropoietin (EPO) causes differentiation, without taking into account erythropoietin control of apoptosis found out in 1990 by Koury and Bondurant in [60]. In 1998 Mahaffy et al. [67] expanded this model by including the apoptosis possibility. Age-stuctured model is detailed in [1] with assumption that decay rate of erythropoietin depends on the number of precursor cells. In [28] Crauste et al. included in the model the influence of EPO upon progenitors apoptosis and showed the importance of erythroid progenitor self-renewing by confronting their model with experimental data on anaemia in mice. Multiscale approaches include both cell population kinetics [18, 19] or erythroid progenitor dynamics [28, 29] and intracellular regulatory networks dynamics in the models, in order to give insight in the mechanisms involved in erythropoiesis.

A model of all hematopoietic cell lineages has been proposed by Colijn and Mackey [25, 26], including dynamics of hematopoietic stem cells, white cell lineage, red blood cell lineage and platelet lineage.

All the previously mentioned approaches did not consider spatial aspects of hematopoiesis. Models describe cell population kinetics, either in the bone marrow or the spleen (where cell production and maturation occur) or in the bloodstream (where differentiated and mature cells ultimately end up). Consequently, cellular regulation by cell-cell interaction was neither considered in these models.

In this thesis we propose a new multiscale model for cell proliferation [18, 19], applied to erythropoiesis in the bone marrow, based on hybrid modelling. This approach, taking into account both interactions at the cell population level and regulation at the intracellular level, allows studying cell proliferation at different scales. Moreover, the "hybrid" modelling consists in considering a continuous model at the intracellular scale (that is, deterministic or stochastic differential equations), where protein competition occurs, and a discrete model to describe cell evolution (every cell is a single object evolving individually and interacting with surrounding cells and the medium).

1.2.3 Leukemia modeling and treatment

Leukemia. Leukaemia is a malignant disease characterized by abnormal proliferation of immature blood cells or haematopoietic stem cells within the bonne marrow. These cells finally enter and invade bloodstream. There are four types of leukemia : myelogenous and lymphocytic (according to the haematopoietic lineage involved in the disease), each of which being acute (rapid increase of immature blood cells) or chronic (excessive production of relatively mature blood cells). We focus our attention on the acute myeloid leukemia (AML).

According to the French-American-British (FAB) classification, AML has eight different subtypes. In this work we concentrate ourselves on erythroleukemia, designated by M6 in the FAB classification (see Figure 1.1). Erythroleukemia was first described by Di Guglielmo in the early twentieth century [68], it is characterized by a proliferation of erythroid and myeloid (white cells) progenitors, and sometimes a pure erythroid proliferation is observed [59]. The origin of erythroleukemia lies in a destabilization of erythropoiesis at the immature level, that is at the erythroid progenitor level. A dysfunction of the Epo-mediated apoptosis regulation has been stressed to be a causative agent of erythroleukemia. Evidences for self-activation of Epo-receptors at the surface of erythroid progenitors [36] could explain the sudden proliferation of immature erythroid cells. Yet, experiments conducted by Madan et al. [66] indicated that autocrine stimulation by erythropoietin in mice could result in intense proliferation of erythroid progenitors but never triggered erythroleukemia. Self-activation of Epo-receptors could not then explain appearance of erythroleukemia without considering other signaling pathways (for instance, including Erk or Fas) destabilization.

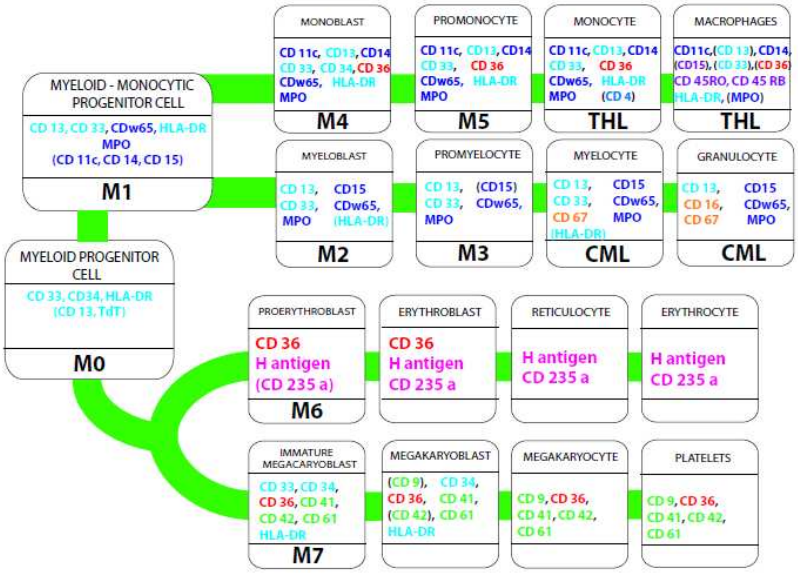

Fig. 1.1 – Myeloid cell differentiation - Schematic figure of myeloid differentiation including the corresponding leukaemia and non-Hodgkin lymphomas as well as cell markers involved in each stage, adapted from [89].

Leukemia treatment. During past decade the first line therapy for AML patients was daunorubicin or idarubicin in combination with cytosine arabinoside (Ara-C), yet nowadays new investigational options exist [42]. In the thesis we consider the chemotherapeutic treatment based on Ara-C. This drug is characterized by a short half-life and targets cells during DNA synthesis (S-phase of the cell cycle). After intravenous administration, the drug is rapidly metabolized, by deamination in the liver and kidney, to its inactive form uracil

arabinoside (Ara-U). When in the bone marrow, it penetrates proliferating cells membrane and it can be transformed into its active form arabinoside triphosphate (Ara-CTP), which participates in the DNA duplication, replacing natural nucleotides. When the proportion of Ara-CTP in the DNA becomes sufficiently high, the cell dies by apoptosis.

It is not always clear what dose of Ara-C should be administrated to each concrete patient to achieve the best efficacy. However, some standard protocol is usually applied. The desired therapeutic effect is to bring the disease into remission that means reappearance of normal haemapoiesis with less than 5% blast cells in bone marrow. From 1980th the pharmacokinetics of high-dose Ara-C was studied [108]. Further clinical studies was needed to determine the correct balance between efficacy an toxicity. Some trials were recently carried out where authors showed [56] that the high-dose of Ara-C improve long-term disease control, but no differences between high-dose and standard-dose were found with regard to complete remission rates.

Ara-C acts on all proliferating cells whether they are leukemic or normal. Therefore, the aim in optimizing drug administration schedule is to increase cytotoxicity for leukemic cells and tolerance for normal cells. One possible approaches to this problem is based on chronotherapy, which takes into account the small differences in the temporal organisation of the cell cycle between normal and leukemic cells.

Chronotherapy. Chronotherapy signifies drug delivery synchronized with biological rhythms in order to optimize the therapeutic outcomes. Cell physiology is regulated along the 24-h time [93]. The suprachiasmatic nucleus, a hypothalamic pacemaker clock and at least 12 circadian genes act to generate and coordinate biological rhythms. The aim of anti-cancer chronomodulated treatment is to decrease toxicity and improve efficacy of the treatment. The same temporal pattern of phase-specific drug administration should have minimum cytotoxicity toward population of normal cells and at the same time should show high cytotoxicity toward cancer cells. It was shown that the survival rate of children with acute lymphoblastic leukemia (ALL) is greater for the evening schedule than for the morning one [92]. The clinical relevance of the chronotherapy principle was tested in large population of patient with metastatic colorectal cancer [63, 64, 77]. Significant improvements in tolerability and anticancer efficacy were demonstrated in men, since women still displayed significantly toxicities. It means that the response of patients to chronotherapy can be heterogeneous and protocol should be personalized to each patient or to subgroups of patients. Mathematical modeling is a good additional utility for that kind of research [9, 10].

Leukemia modeling. Mathematical modelling of leukemia has attracted much attention since the beginning of the 1970's. In 1976, Rubinow and al. [97] proposed mathematical model of acute myeloid leukemia where population of normal neutrophilic cells and leukemic myeloblasts was considered as distinct but interacting populations. Dynamics of the number of cells in each population was described by ordinary differential-difference equations taking into account the age or maturity of cells. Cells of both population can be in the phase G_0. Including the phase G_0 was important to control the proliferation rate which depended on

total number of cells. In the presence of leukemic cells, normal cells were destabilized and production of normal cells began to turn off. As a result, total population entirely consisted of leukemic cells and there were no normal cells. Mathematical models of chronic myeloid leukemia and cancer stem cells was proposed by F. Michor in [73, 74, 75]. Basing on [97] model Rubinow et al. [98] proposed a mathematical model of chemotherapeutic treatment of acute myeloid leukemia. In order to model drug-treatment regime all cells, whether normal or leukemic, which are not in the resting phase G_0, were subdivided into three compartments G_1, S, $G_2{+}M$ according to their phase. It was assumed that 90 % of all cells in the phase S in the moment of drug administration were killed. It was shown that even small changes in protocol can have significant effects on the results of treatment. An optimal protocol of drug administration was proposed. Another mathematical model of acute myeloid leukemia was suggested in [3]. Populations of normal and leukemic cells were considered in the model. Two cell population dynamics followed a process of Gompertzian growth. Leukemic cells exhibited inhibiting effect on the growth of the normal cells. The kinetic equations and steady-state properties of the model were described. A treatment model was proposed and numerically simulated. It was shown that aggressive treatment of the disease with heavy doses of drugs is plausible. Very detailed description of PK/PD model of AML treatment with AraC was proposed by P. F. Morrison and collaborators in [65, 78]. They introduced the model of drug distribution and metabolism of AraC in the different parts of the organism and estimated the pharmacokinetic parameters for L1210 cell line (lymphocytic leukemia cells derived from mice). In the [65] authors carried out computer simulations of the treatment. A PK/PD model presented in this thesis is based on these works.

PK/PD modeling. With the development of mathematical modeling of cancer, pharmacokinetic-pharmacodynamic (PK/PD) models have received wide application. Pharmacodynamics is often summarized as the study of what a drug does to the diseased organs and whole body, whereas pharmacokinetics is the study of what the body does to a drug and provides a metabolism scheme of drug transformation of its active form. PK/PD approach answers such important questions as (i) if the right drug has been selected and (ii) if the optimal dosage regimen has been established.

PK/PD modeling approach developed by Veng-Pedersen and co-workers [30, 117] deals with stress erythropoiesis. Such approaches are usually centered on parameter estimation and model fitting to data (statistical approaches). S. Chapel et al. investigated the reticulocyte response resulting from phlebotomy-induced erythropoietin (EPO) in adult sheep by means of PK/PD modeling [30]. This study was extended in the subsequent article [117] by considering the hemoglobin data to identify the relevant parameters of the cellular kinetics of erythropoiesis in acute anemia and showed a good agreement with the observed data. PK/PD model of the erythropoietic responses to single i.v. and s.c. (subcutaneous) administration of recombinant human erythropoietin (rHuEPO) in rats was studied in [123]. A two-compartment pharmacokinetic model of rHuEPO involving linear first-order elimination and Michaelis-Menten saturable kinetics after i.v. administration was used. In order to describe s.c. administration the absorbtion kinetics is assumed. Proposed pharmacodynamic

model was based on combination of cell production and loss model and of indirect response model. Several types of cells were considered among them earliest progenitor cells, which, in turn, converted to erythroblasts, reticulocytes and red blood cells. Indirect response model was considered trough stimulation of responses by rHuEPO. In another article of S. Woo [124], a physiology-based PD model was developed in order to describe progression of anemia caused by carboplatin in rats. A three-compartment PK model with plasma concentration and amounts of carboplatin in peripheral tissue was presented. The PD model for carboplatin-induced anemia that include erythroid progenitors, erythroblasts, reticulocytes and mature red blood cells with taking into account stimulation through EPO concentration was considered. Such models could give an assess to optimization of erythropoietic treatment of anemia.

1.3 Summary of the results

This dissertation is devoted to the development of hybrid models of cell population dynamics. It is applied to study hematopoiesis and blood disorders, such as anemia and leukemia.

The thesis contains four chapters. In the first chapter we present the description of the method developed in this work and model examples of particle dynamics. In the second chapter, a hybrid model of erythropoiesis is suggested and studied. The third chapter is devoted to PK/PD modeling of leukemia treatment with AraC. In the last chapter the passage from a hybrid model to a continuous model in the 1D case is investigated.

1.3.1 Hybrid Method

Cell populations represent complex multi-level systems where different levels (intracellular, cellular, tissue, organism) interact with each other providing normal functioning of the whole system. We introduce and study a hybrid model with off-lattice cell dynamics which describe biological processes different levels.

Cells are considered as discrete objects. They can interact with each other and with the surrounding medium mechanically and biochemically, they can divide, differentiate and die due to apoptosis. Cell behavior is determined by intracellular regulatory networks described by ordinary differential equations and by extracellular bio-chemical substances described by partial differential equations. Each cell has ability of growing, moving, dividing and exchanging biochemical substances with surrounding medium. We describe motion of each cell by the displacement of its center by Newton's second law.

For each particular application intracellular and extracellular regulation should be specified for each cell type as well as how cell fate (proliferation, differentiation and apoptosis) depends on regulatory networks. In this thesis the approach discussed above is applied to multi-scale modelling of normal and leukaemic erythropoiesis.

1D hybrid models. We consider a hybrid model for multi-scale modelling of cells population. We start with the 1D case and study three model problems. In the first one, each cell

can self-renew or die by apoptosis. In the second model, the case where cells self-renew or differentiate into another type of cells is studied. In the last model, we investigate the case where cells can divide or be in a quiescent state. Finally, we illustrate application of these models to bacteria filament.

The fate of each cell in considered models is determined by intracellular and extracellular regulation. In the first (second) model we suppose that cell division and death (differentiation) are determined by some bio-chemical substances produced by the cells themselves. We consider the case where there are two such substances, u and v, which influence cell division and death. We come to the following system of equations :

$$\begin{cases} \frac{du}{dt} = d_1 \frac{\partial^2 u}{\partial x^2} + b_1 c - q_1 u, \\ \\ \frac{dv}{dt} = d_2 \frac{\partial^2 v}{\partial x^2} + b_2 c - q_2 v. \end{cases} \tag{1.1}$$

These equations describe the evolution of the extracellular concentrations u and v with their diffusion, production terms proportional to the concentration of cells c and with the degradation term. We consider the no-flux boundary conditions.

Intracellular concentrations u_i and v_i in the i-th cell are described by the equations :

$$\begin{cases} \frac{du_i}{dt} = k_1^{(1)} u(x,t) - k_2^{(1)} u_i(t) + H_1, \\ \\ \frac{dv_i}{dt} = k_1^{(2)} v(x,t) - k_2^{(2)} v_i(t) + H_2. \end{cases} \tag{1.2}$$

The first term in the right-hand side of the first equation shows that the intracellular concentration u_i grows proportionally to the value of the extracellular concentration $u(x,t)$ at the space point x_i where the cell is located. In the first and second studied models the intracellular concentration of u_i controls cell division while the concentration of v_i controls cell death (first model) and differentiation (second model).

In the third model we suppose that cells can be either in quiescent state or in cell cycle. When a cell enters cell cycle, it grows and then divides into two identical to itself cells. Extracellular regulation is described by system of partial differential equations. Intracellular regulatory networks is described by system of ordinary differential equations.

For each model pattern formation due to different values of parameters is studied and discussed. Extension of the first model where cells can either divide or die to 2D case was carried out.

Bacteria filament growth. The filamentous cyanobacterium *Anabaena* sp. PCC 7120 represents a chain of cells connected to each other and is a good model to study cell differentiation and pattern formation. Due to nitrogen starvation 5-10% of cells differentiate into heterocytes, cells that fix nitrogen. This process is regulated by different internal and external signals. The intracellular regulation which determines cell differentiation is shown in Figure 1.2, [101]. Cell division is initiated by protein FtsZ, cell differentiation starts with

accumulation of 2-oxoglutorate. DNA-binding protein, HetR, and a diffusible inhibitor produce by differentiated cells, PatS, play a central role in the decision of cell to differentiate. We describe this regulation by system of ordinary differential equations :

$$\begin{cases} \frac{du_i}{dt} = H_u \\ \frac{dG_i}{dt} = H_g \\ \frac{dh_i}{dt} = k_1^{(h)} G_i(t) + k_2^{(h)} h_i^2(t) - k_3^{(h)} p_i(t) h_i(t) \\ \frac{dp_i}{dt} = d(p_{i-1} - p_i) + d(p_{i+1} - p_i) + k_1^{(p)} h_i(t) - k_2^{(p)} p_i(t) \end{cases} \tag{1.3}$$

where u_i denotes the intracellular concentration of the cell division protein, FtsZ, in the i-th cell, G_i is the concentration of 2-oxoglutarate, h_i is the self-enhancing differentiation regulatory protein HetR, p_i is the inhibitor encoded by the gene PatS, which is dependent on HetR for production. PatS is synthesized in the developing heterocyst and diffuses to the neighboring vegetative cells. We carry out computer simulation to test the model. Obtained results qualitatively represent heterocyst development observed *in vitro*.

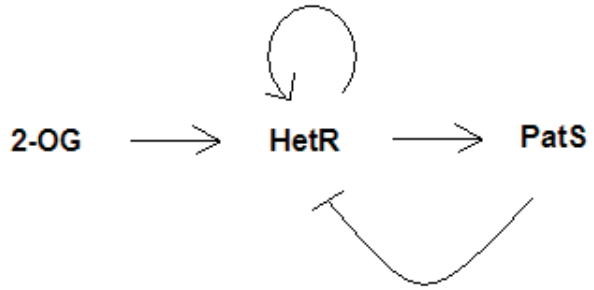

FIG. 1.2 – Intracellular regulation of heterocyst differentiation in anabaena.

1.3.2 Erythropoiesis

Erythropoiesis is the process of production and regulation of red blood cells, which occurs in the bone marrow. Different cell populations involved in their production (from the very immature ones to differentiated ones) are usually kept in a steady state through various and complex negative feedback controls. Inside the bone marrow, immature red blood cells proliferate and differentiate within particular structures, called erythroblastic islands. Erythroblastic island consists of macrophage (white cell) in the center of island, surrounded by erythroid cells of different maturation stage with more mature cells on the periphery of

the island, ready to leave the bone marrow and enter the bloodstream. The role of the macrophage as well as the different feedback mechanisms involved in red blood cell production (erythropoiesis) are not completely understood. Our results bring new information on the role of the macrophage and the erythroblastic island in the production and regulation of red blood cells, the macrophage being shown to play a key role in the stability and robustness of the production process, and will improve our understanding of in vivo erythropoiesis.

A hybrid model of red blood cell production, proposed in this work, considers both mechanisms at the intracellular scale (protein regulation, cell fate decision) and at the cell population scale (cell-cell interactions, influence of feedback controls), and allows to investigate the role of the central macrophage in normal erythropoiesis. There are number of intracellular proteins and growth factors that lead the erythroid cell to either proliferation, differentiation, or death by apoptosis. The regulation scheme can be found in Figure 1.4. Two intracellular two proteins, Erk and Fas, are supposed to be determinant in this regulation. Erk favors self-renewal, while Fas control differentiation and apoptosis. Competition between these proteins, considered as the main regulatory network for erythroid progenitor fate is then described by the following system,

$$\frac{dE}{dt} = (\alpha(Epo, GF) + \beta E^k)(1 - E) - aE - bEF, \tag{1.4}$$

$$\frac{dF}{dt} = \gamma(F_L)(1 - F) - cEF - dF, \tag{1.5}$$

where E and F are Erk and Fas concentrations, functions $\alpha(Epo, GF)$ and $\gamma(F_L)$ describe feedback controls trough considering of extracellular scale [29]. Reticulocytes express Fas-ligand (F_L) on their surfaces, Fas-ligand does not diffuse (at least in the bone marrow). Yet the expression of Fas-ligand is modeled by short-diffusion and described with the following reaction-diffusion equations :

$$\frac{\partial F_L}{\partial t} = D_{F_L}\Delta F_L + W_{F_L} - \sigma_{F_L}F_L, \tag{1.6}$$

$$\tag{1.7}$$

with a source term depending on the number of reticulocytes W_{F_L}.

The spatial aspects of erythropoiesis are taken into account. To analyze the role of macrophage, two models with different structure of erythroblastic island with and without macrophage were investigated (Figure 1.3). In the second model macrophage releases pro-survival cytokine which diffuse into extracellular matrix,

$$\frac{\partial GF}{\partial t} = D_{GF}\Delta GF + W_{GF} - \sigma_{GF}GF, \tag{1.8}$$

with a constant source term W_{GF} for growth factor concentration. A strong effect of the central macrophage on the stability of an erythroblastic island is shown while in the absence of macrophages, erythroblastic islands lose their stability. Investigation of the stress

erythropoiesis model concludes that stability does not decrease responsiveness of the model. Comparison of modelling with experiments on anemia in mice is carried out.

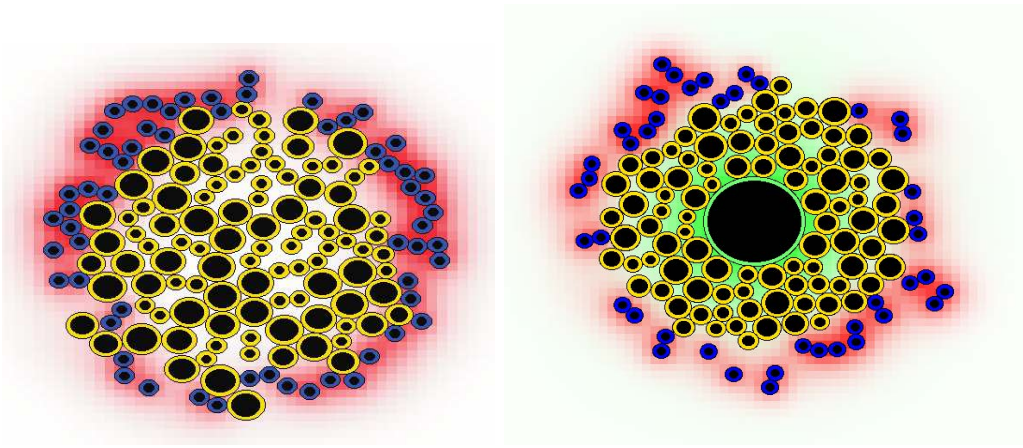

FIG. 1.3 – Erythroblastic island with and without macrophage. The green cell is a macrophage, yellow cells are immature cells (erythroblasts) and blue cells are differentiated cells (reticulocytes). The green substance is secreted by the macrophage (growth factors) and the red substance by reticulocytes (Fas-ligand). In each cell, the black area represents the incompressible part of the cell.

1.3.3 Leukemia

In the fourth chapter we apply developed method to the modeling of Acute Myeloid Leukemia (AML) and its treatment with Ara-C. A pharmacodynamic/pharmacokinetic model of Ara-C is proposed and used to simulate the treatment. We describe metabolism of Ara-C after its intravenous introduction in the organism. Inside cells, part of Ara-C is phosphorylated into its active form, Ara-CTP, which arrests DNA synthesis and induces cell apoptosis. Ara-C is deaminated into its inactive form Ara-U. Ara-CTP, in turn, can be dephosphorylated back to Ara-C. We take into account these three reactions in order to model the intracellular kinetics of Ara-C and Ara-CTP (see Figure 1.5). We describe them by Michaelis-Menten mechanisms. The phosphorylation rate of Ara-C is described with following equation,

$$r_p = \frac{V_k}{1 + \frac{K_m K_a}{w_i}},$$

Ara-CTP dephosphorylation rate is given by

$$r_{dp} = \frac{V_{dp}}{1 + \frac{\alpha^1 K_{dp}}{w_i^a}},$$

Finally, deamination of Ara-C follows similar kinetics,

$$r_{da} = \frac{V_{da}}{1 + \frac{K_{da}}{w_i}},$$

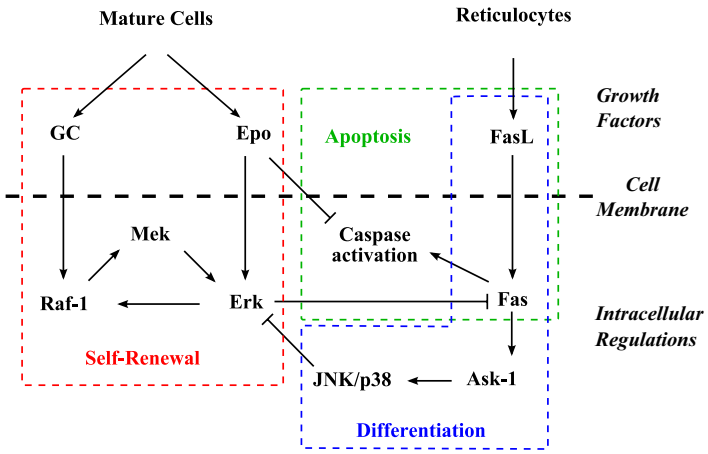

FIG. 1.4 – Summary of intracellular protein interactions that determine erythroid progenitor fate, partially adapted from Rubiolo et al. [99].

The kinetics of intracellular Ara-C concentration in the i-th cell is then described by the following equation,

$$\frac{dw_i}{dt} = k_1(w - w_i(t)) - k_2 w_i(t) - (r_p - r_{dp} + r_{da}), \tag{1.9}$$

where w is the extracellular concentration of Ara-C in the bone marrow, supposed to be uniformly distributed in the bone marrow.

The balance equation for the intracellular concentration of Ara-CTP is

$$\frac{dw_i^a}{dt} = k_\alpha(r_p - r_{dp}). \tag{1.10}$$

Ara-CTP exerts a cytotoxic effect on all dividing cells, arresting DNA synthesis and inducing apoptosis. Evolution of the quantity of Ara-CTP in DNA is described with the following equation,

$$\frac{dp_i}{dt} = k_\beta w_i^a, \tag{1.11}$$

Above equations and parameters for Ara-C metabolism are derived from Morrison et al. [78].

In order to study pharmacodynamics two populations of cells were considered, normal cells and leukemic cells. Normal cells are supposed to have a circadian rhythm, that influences their cell cycle durations, whereas leukemic cells, appart from being characterized by excessive proliferation and insufficient differentiation and apoptosis, are supposed to escape circadian rhythms. We consider a treatment based on periodic administration of Ara-C, an anti-cancer agent targeting cells in DNA synthesis. The influence of the period of treatment and of the delivery time on the outcome of the treatment are investigated and stress the relevance of considering chronotherapeutic treatments to cure leukemia.

Next, we consider a simplified model, which consists of cell dynamics and pharmacokinetics, to reproduce with numerical simulations the number of blasts in blood due to chemotherapy of acute leukemia.

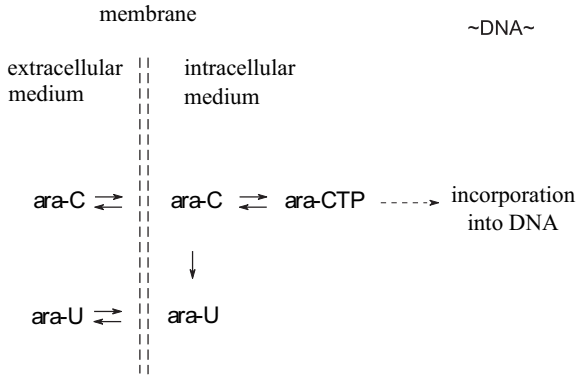

FIG. 1.5 – Metabolism of Ara-C, adapted from [78].

1.3.4 From hybrid to continuous models

Hybrid models are well adapted for numerical simulations of variable biological problems. However, it is difficult or even impossible to study them analytically. This is why it may be useful to investigate a possible transition from hybrid models to continuum models.

In the second and fifth chapter we carry out detailed comparison between particle dynamics and the corresponding equations of continuum mechanics. In the second chapter we consider particle flow in 1D case where particles are represented as discrete objects. Their motion is described by the equation

$$m\ddot{x}_i + \mu m\dot{x}_i - \sum_{j\neq i} f(h_{ij}) = 0, \tag{1.12}$$

where x_i is the coordinate of the i-th particle. Introducing particle velocity $v_i = \dot{x}_i$ we obtain

$$m\frac{dv_i}{dt} + \mu m v_i + \nabla p = 0. \tag{1.13}$$

Here p is the pressure determined by the force f_{ij} acting between the particles. From this equation it is clear that particle motion is related to Darcy's law of fluid motion in porous medium. We confront particle dynamics model with continuous approach for two different models : particle flow model and a problem with a point source of particles.

The fifth chapter presents asymptotic analysis of the diffusion-discrete absorption (DDA) equation. This differential-difference equation describes the steady state diffusion with the pointwise absorption. Such a model corresponds to a chain of cells (points) absorbing some substance, between the cells a steady diffusion process takes place. Equation (1.12) with $\mu = 0$ describes displacement of particles and can be considered as a discrete elasticity equation. We continualise DDA equation where the small parameter is the distance h between two neighboring cells (in the equilibrium state). The comparison of the exact solution of the DDA equation and the solution of the homogenized differential equation shows a good accuracy of the asymptotic approximation.

Chapitre 2

Hybrid method and model examples

2.1 Method description

In this thesis we introduce and study a hybrid model with off-lattice cell dynamics. Cells can interact with each other and with the surrounding medium mechanically and biochemically, they can divide, differentiate and die due to apoptosis. Cell behavior is determined by intracellular regulatory networks described by ordinary differential equations and by extracellular bio-chemical substances described by partial differential equations. Each cell has ability of growing, moving, dividing and exchanging biochemical substances with surrounding medium.

In order to describe mechanical interaction between cells, we restrict ourselves here to the simplest model where cells are represented as elastic balls. Consider two elastic balls with the centers at the points x_1 and x_2 and with the radii, respectively, r_1 and r_2. If the distance h_{12} between the centers is less then the sum of the radii, $r_1 + r_2$, then there is a repulsive force between them f_{12} which depends on the distance h_{12} (Figure 2.2 (left)). If a particle with the center at x_i is surrounded by several other particles with the centers at the points x_j, $j = 1, ..., k$, then we consider the pairwise forces f_{ij} assuming that they are independent of each other. This assumption corresponds to small deformation of the particles. Hence, we find the total force F_i acting on the i-th particle from all other particles, $F_i = \sum_{j \neq i} f_{ij}$. The motion of the particles can now be described as the motion of their centers by Newton's second law

$$m\ddot{x}_i + \mu m\dot{x} - \sum_{j \neq i} f(h_{ij}) = 0, \tag{2.1}$$

where m is the mass of the particle, the second term in the left-hand side describes the friction by the surrounding medium, the third term is the potential force between cells. We consider the force between particles in the following form

$$f_{ij} = \begin{cases} K\frac{h_0 - h_{ij}}{h_{ij} - (h_0 - h_1)}, h_0 - h_1 < h_{ij} < h_0 \\ 0, h_{ij} \geq h_0 \end{cases} \tag{2.2}$$

where h_{ij} is the distance between the particles i and j, h_0 is the sum of cell radii, K is a positive parameter, and h_1 accounts for the compressible part of each cell. This means that the internal part of the cell is incompressible. It allows us to control compressibility of the medium. The force between the particles tends to infinity when h_{ij} decreases to $h_0 - 2h_1$ (Figure 2.1). The force presented by equation (2.2) is considered in this form in the all applications of the thesis, except for Section 2.2.5 where cells do not have incompressible part.

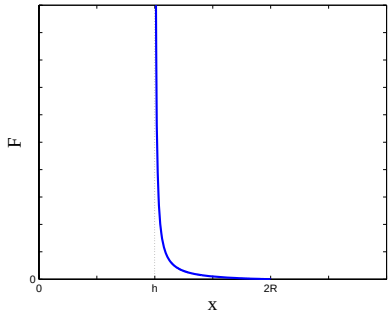

FIG. 2.1 – Force between the cells.

Intracellular regulatory networks for the i-th cell are described by a system of ordinary differential equations

$$\frac{du_i(t)}{dt} = F(u_i(t), u(x_i, t)), \tag{2.3}$$

where u_i is a vector of intracellular concentrations of cell i, u is a vector of extracellular concentrations, F is the vector of reaction rates which should be specified for each particular application. Intracellular concentrations u_i are supposed to be uniformly distributed inside the i-th cell. Therefore these functions depend on time t and they are independent of the space variable x. Values of intracellular concentrations can be different in different cells. At the same time, they can be influenced by extracellular concentrations $u(x;t)$ taken at $x = x_i$. As we saw above cell motion is reduced to motion of cell centers. The value of the extracellular concentration in the right-hand side of equation (2.3) is taken at the center x_i of the i-th cell (see also Figure 2.2). We solve the system of equations (2.3) with finite difference explicit method or mixed explicit-implicit method. The concentrations of the species in the extracellular matrix are described by reaction-diffusion equations

$$\frac{\partial u}{\partial t} = D\ \Delta u + G(u, c), \tag{2.4}$$

where c is the local cell density, G is the rate of consumption or production of different species by cells, which will be specified for each particular application, D is the extracellular diffusion rate. Numerical resolution of this equation is based on conventional implicit finite-difference methods. In 1D case we solve equation (2.4) with Thomas method and in 2D case with alternative direction method.

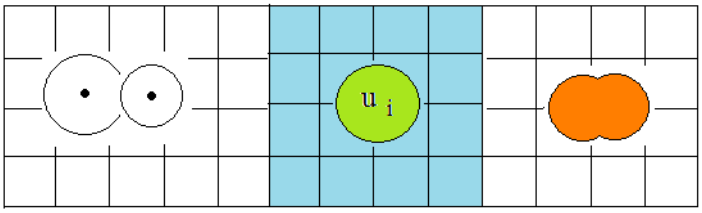

Fig. 2.2 – Schematic representation of the hybrid model. The square grid shows the numerical mesh to solve reaction-diffusion equations (2.4). Cell centers move according to equations (2.1). The force $f(h_{ij})$ between two cells depends on the distance between their centers (left). Intracellular concentrations $u_i(t)$ inside the i-th cell are described by equations (2.3). They can be influenced by the extracellular concentrations $u(x,t)$ shown schematically as a blue field (center). If a cell dies by apoptosis, it is removed from the computational domain. If it divides, it increases its area. It can remain a circle with a greater (time dependent) radius or change its shape preserving area after division (right).

We calculate cell concentration $c = h_0/h_{ij}$ in one dimensional case as the number of cells in the interval of the length h_0. In the 2D case, a local cell concentration c is computed as total cell area inside each square of the grid. For simplicity of calculation of cell concentration we make an assumption that cell is square (see Figure 2.4). If one square grid of numerical scheme is completely inside of the cell, then concentration is equal

$$c_1 = \frac{\frac{dxdy}{4R^2}}{dxdy} = \frac{1}{4R^2}$$

Otherwise, cell concentration is

$$c_2 = \frac{\frac{x_m y_m}{4R^2}}{dxdy}$$

Next, we distribute the concentration between the nodes dividing c_1 and c_2 by 4. Then we compute the values of the concentration at the nodes of the numerical grid corresponding to equation (2.4). The value of the concentration at the cell center $x = x_i$ is found as a result of linear interpolation with respect to the surrounding grid nodes (Figure 2.4).

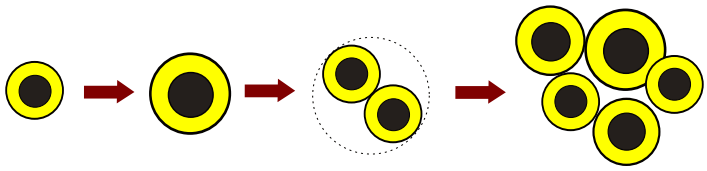

Fig. 2.3 – Cell division. In each cell, the black area represents the incompressible part of the cell.

Cells can divide, die by apoptosis or differentiate. Their fate is determined by intracellular concentrations. In particular, if a concentration of an intracellular protein exceeds some

critical value, the cell divides, if a concentration of another protein reaches its critical value, the cell differentiates. These assumptions are simplified but still realistic from the biological point of view. In the numerical model, if a cell dies by apoptosis, it is removed from the computational domain. Before a cell divides, it increases its area. It can preserve a circular shape during its growth or, if we need to compute more precisely the forces acting between the cells, it can take an ∞-shape (Figure 2.2 (right)) specific for cells in the process of division. In this model we prescribe that cells preserve a circular shape during growth. Mother cell increases twice the radii before its division and gives birth to two cells side by side with initial radius. The direction of division could be chosen in different ways depending on the application of the hybrid model. In this thesis we choose the direction of division randomly (Figure 2.3), except 1D case.

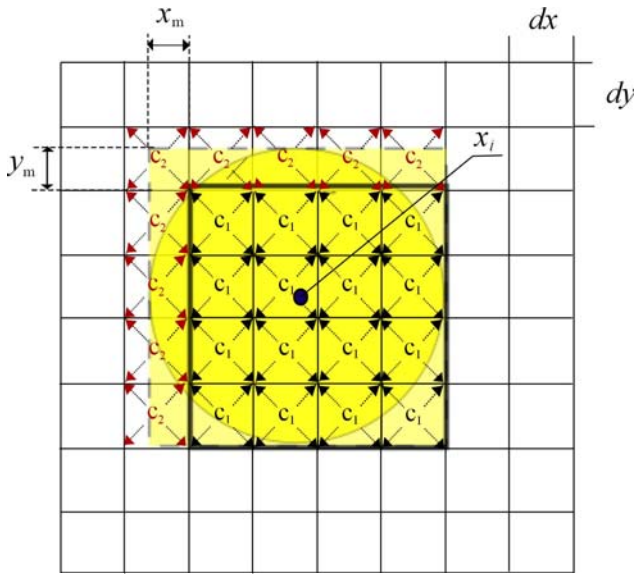

FIG. 2.4 – The square grid shows the numerical mesh used to solve reaction-diffusion equations. Concentration at all grid nodes is computed and then the values at the nodes are interpolated to the cell center $x = x_i$ of equation (2.3).

The approach described here represents general framework. For each particular application intracellular and extracellular regulation should be specified for each cell type as well as how cell fate (proliferation, differentiation and apoptosis) depends on regulatory networks.

2.2 Particle dynamics and continuum mechanics

Dissipative particles dynamics is developed as a method of simulation of complex media [54]. We apply it in order to study biological cell populations taking into account possible cell division, differentiation and death [20].

2.2.1 From cells to particle dynamics

Consider two elastic balls with the centers at the points x_1 and x_2 and with the radii, respectively, r_1 and r_2. If the distance h_{12} between the centers is less than the sum of the radii, $r_1 + r_2$, then there is a repulsive force between them f_{12} which depends on the distance h_{12}.

If a particle with the center at x_i is surrounded by several other particles with the centers at the points x_j, $j = 1, ..., k$, then we consider the pairwise forces f_{ij} assuming that they are independent of each other. This assumption corresponds to small deformation of the particles. Hence, we find the total force F_i acting on the i-th particle from all other particles,

$$F_i = \sum_{j \neq i} f_{ij}.$$

The motion of the particles can now be described as the motion of their centers.

2.2.2 Particles and discrete equations

Consider a system of N particles in the plane. Denote their coordinates by $x_1, ..., x_n$. Here x_i is a two-component vector. Suppose that all particles have the same mass m and consider the equation of motion of the i-th particles in the form

$$\ddot{x}_i + \mu m \dot{x}_i + \sum_{j \neq i} f_{ij} = 0. \tag{2.5}$$

The dot denotes the derivative with respect to time, $\ddot{x}_i$ is the particle acceleration, $\dot{x}_i$ is its speed. The second term in the left-hand side of this equation describes dissipation due to friction, the last term is the sum of forces acting on this particle from all other particles.

The force f_{ij} acting between the particles i and j can be expressed through the potential : $f_{ij} = -m\nabla\phi(|x - x_j|)_{x=x_i}$. Then

$$\ddot{x}_i + \mu \dot{x}_i + \nabla \left(\sum_{j \neq i} \phi(|x - x_j|) \right)_{x=x_i} = 0, \quad 1, ..., N. \tag{2.6}$$

Consider a square grid with the mesh points $\bar{x}_i$ and the step δx. Denote by s_i the square with the side 2 δx and the center at the point $\bar{x}_i$. Let $x_{i1}, ..., x_{ik} \in s_i$. Let us introduce velocity and density at the grid points :

$$v_i = \frac{1}{k} \sum_{j=1}^{k} \dot{x}_{ij}, \quad \rho_i = \frac{k}{|s_i|},$$

where $|s_i| = 4(\delta x)^2$ is the area of s_i. Then

$$\sum_j \phi(|x - x_j|) \approx \sum_m \phi(|x - \bar{x}_m|)\rho_m |s_m| \approx U(x),$$

where

$$U(x) = \int \phi(|x - x'|)\rho(x')dx'.$$

Taking a sum of equations (2.6) with respect to the points inside s_i, we obtain the discrete equation

$$\rho_i \frac{dv_i}{dt} + \mu\rho_i v_i + \rho_i(\nabla U)_i = 0, \tag{2.7}$$

where we use the approximation $\frac{1}{k}\sum_{j=1}^{k}\phi(|x_j - \bar{x}_m|) \approx \phi(|\bar{x}_i - \bar{x}_m|)$. Averaged equation (2.7) may not be equivalent to (2.6). Two particles $x_j, x_k \in s_i$ with opposite velocities cancel in (2.7) but not in (2.6). They result in the momentum transfer and can be taken into account in (2.7) by additional dissipative terms. In numerical simulations, the equivalence of these equations can be provided if we take an average velocity with respect to some ensembles of particles.

2.2.3 Continuous model

Consider the continuous analogue of discrete equation (2.7)

$$\rho\frac{dv}{dt} + \mu\rho v + \rho(\nabla U) = 0. \tag{2.8}$$

This equation of motion should be completed by the equation of mass conservation :

$$\frac{\partial\rho}{\partial t} + \nabla.(\rho v) = 0. \tag{2.9}$$

We can write equation (2.8) in the form

$$\rho(\frac{\partial v}{\partial t} + v.\nabla v) + \mu\rho v + \nabla p - U\nabla\rho = 0, \tag{2.10}$$

where p is the pressure, $p = \rho U$. This equation is nonlocal because the potential U contain the integral. Using the Taylor expansion of the density $\rho(x')$ around the point x and keeping the terms up to the second order, we obtain

$$\rho(\frac{\partial v}{\partial t} + v.\nabla v) + \mu\rho v + \nabla p - K\Delta\rho\nabla\rho = 0. \tag{2.11}$$

The pressure in this equation is different in comparison with the previous one but we keep for it the same notation. This equation does not contain the potential anymore. Therefore, we cannot express the pressure through it, and we need to complete system (2.9), (2.11) by an equation of state, $p = p(\rho)$. In the case $\mu = 0$ and $K = 0$, (2.11) is the Euleur equation and system (2.9), (2.11) becomes the classical model of gas dynamics.

2.2.4 Energy

Denote the left hand-side of equation (2.8) by $J(x,t)$. We take a scalar product of this vector with v and integrate over $\mathbb{R}^2$:

$$\int Jvdx = \frac{1}{2}\int \rho\frac{\partial|v|^2}{\partial t}dx + \frac{1}{2}\int(\rho v, \nabla|v|^2)dx + \mu\int \rho|v|^2dx + \int(\rho v, \nabla U)dx =$$

$$\frac{1}{2}\,\frac{d}{dt}\int(\rho|v|^2 + \rho U)dx + \mu\int \rho|v|^2dx.$$

We use here formal integration by parts, equation (2.9) and the equality

$$\int \frac{\partial\rho}{\partial t}\,Udx = \frac{1}{2}\,\frac{d}{dt}\int\int \phi(|x-x'|)\rho(x,t)\rho(x',t)dxdx' = \frac{1}{2}\,\frac{d}{dt}\int \rho Udx.$$

From (2.8) we obtain

$$\frac{dE}{dt} = -\mu\int \rho|v|^2dx, \tag{2.12}$$

where E is the sum of the kinetic and potential energy of the system :

$$E = \frac{1}{2}\int \rho|v|^2dx + \frac{1}{2}\int \rho Udx.$$

It follows from (2.12) that the total energy of the system decreases, its kinetic energy tends to zero while the potential energy to some constant. Total energy can also be introduced for the system of particles. Similar to the continuous case, it decreases with time.

2.2.5 1D model of particle flow

In the 1D case, the last term in the left-hand side of the equation (2.11) has the form $K\rho'\rho''$ and can be included in the pressure. In the stationary case, neglecting the inertial terms, we obtain from (2.9), (2.11) :

$$\mu\rho v + p' = 0, \quad \rho v = q, \tag{2.13}$$

where q is some constant. The force between two spherical particles is considered in the form

$$f(h) = \begin{cases} k\frac{h_0/h-1}{2-h_0/h} & , \quad h_0/2 < h < h_0, \\ 0 & , \qquad h > h_0 \end{cases}, \tag{2.14}$$

where h is the distance between their centers, k and h_0 are positive parameters. The force between the particles tends to infinity when h decreases to $h_0/2$. On the other hand, this force equals zero if $h \geq h_0$. Hence, every given particles interacts with at most one other particle from the left of it and another one from the right.

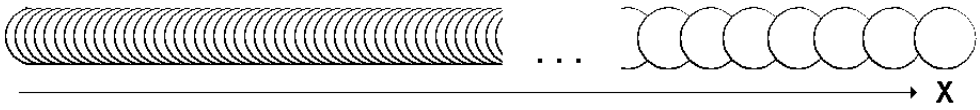

FIG. 2.5 – Particle flow in 1D model problem.

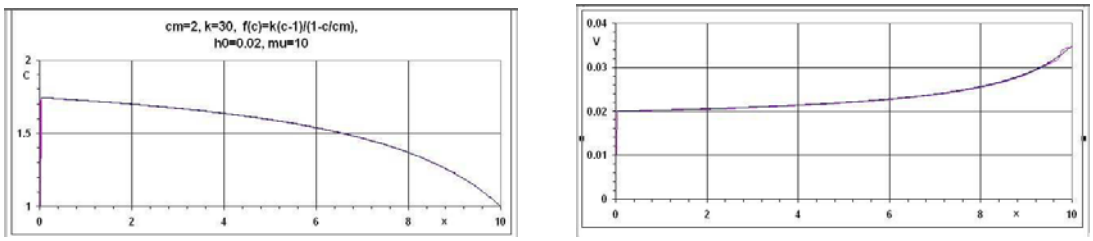

FIG. 2.6 – Particle dynamics (red) and analytical solution (black) for 1D particle flow, concentration (left) and velocity (right) of particles.

If $c = h_0/h$ is the number of particles in the interval of the length h_0, $c = h_0\rho$, then we obtain from the previous formula the equation of state, $p(c) = k(c-1)/(2-c)$. Together with (2.13) it allows us to find the function $c(x)$. Figure 2.5 shows an example of particle dynamics simulations, and Figure 2.6 the comparison of numerical simulations of particle dynamics with the analytical solution. The numerical and analytical curves exactly coincide.

2.2.6 Model problem with a point source of particles

2.2.6.1 1D case

We will study in this section the test case where a 1D interval is filled by cells of two types, A and B. Cells of the type A divide and after each division produce one cell A and one cell B. The cells of the type B do not divide. If initially there is a unique cell of the type A, then it will remain unique and the interval will be filled by cells of the type B. In the continuous analogue of this model, the cell A is a point source. We will compare the numerical solution of the cell problem with an analytical solution of the continuous problem.

In the 1D case, the last term in the left-hand side of the equation (2.11) has the form $K\rho'\rho''$ and can be included in the pressure. Consider the equation

$$\rho\frac{dv}{dt} + \mu\rho v + p' = 0. \tag{2.15}$$

This equation of motion should be completed by the equation of mass conservation :

$$\frac{d\rho}{dt} + \frac{\partial(\rho v)}{\partial x} = J, \tag{2.16}$$

where J the source of new particles (dividing cell). Let us consider the stationary case. Then we obtain

$$\mu(\rho v)' + p'' = 0, \tag{2.17}$$

$$p'' = -\mu J. \tag{2.18}$$

Cell division results in the mechanical interactions and the consequence their motion. This motion changes the position of the dividing cells. Thus, we come to the problem about the motion of point sources. Consider a 1D example where an analytical solution can be easily found :

$$p'' = -a\delta(x - \xi(t)), 0 < x < L, p(0) = p(L) = 0 \tag{2.19}$$

where $\xi(t)$ is a position of the point source. Let us introduce the function

$$p_0(x) = \begin{cases} \frac{a}{2}(x - \xi) + 1, x < \xi \\ \frac{a}{2}(\xi - x) + 1, x > \xi \end{cases} \tag{2.20}$$

and put $p = p_0 + p_1$. Then $p_1'' = 0$ and

$$\begin{cases} p_1(0) = -p_0(0) = -1 + \frac{a\xi}{2}, \\ p_1(L) = -p_0(L) = -1 + \frac{a}{2}(L - \xi). \end{cases}$$

We find

$$p_1(x) = \frac{\frac{a}{2}(L - \xi) - \frac{a\xi}{2}}{L}x + (\frac{a\xi}{2} - 1).$$

From (2.15) we obtain,

$$\xi'(t) = -\frac{p'(\xi(t))}{\mu\rho}.$$

Consider when $\rho = 1$. The analytical solution of this equation is

$$\xi(t) = (\xi(t_0) - \frac{L}{2})e^{\frac{a}{\mu L}(t - t_0)} + \frac{L}{2}.$$

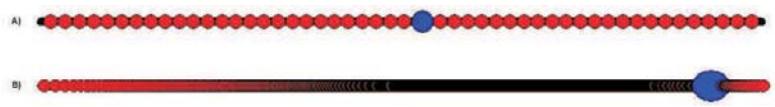

Fig. 2.7 – Example of particle dynamics simulation. Dividing cell (type A) is blue (big), not dividing cells (type B) are red (small).

We carry out the 1D simulation where cells can move along the interval of a fixed length L. We note that only two nearest particles can interact. We consider the equation of motion (2.5). The force between two particles is considered in the form

$$f_{ij} = \begin{cases} K\frac{h_0 - h_{ij}}{h_{ij} - (h_0 - h_1)}, h_0 - h_1 < h_{ij} < h_0, j = i \pm 1 \\ 0, h_{ij} \geq h_0 \end{cases} \tag{2.21}$$

Here h_{ij} is the distance between the particles i and j, h_0 is a diameter, $h_0 - 2h_1$ is incompressible part of each particle. This means that the distance between the centers of the particles can not be less than $h_0 - 2h_1$.

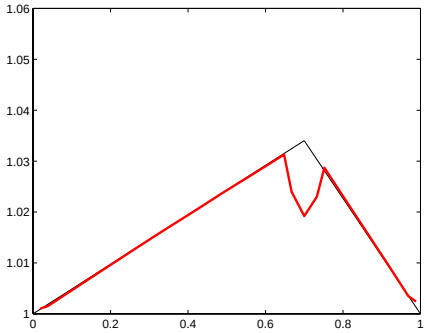

(a) K= 300, a=0.162

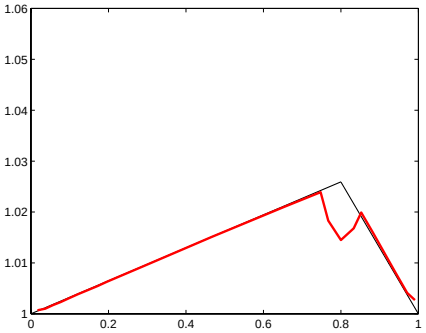

(b) K= 300, a=0.162

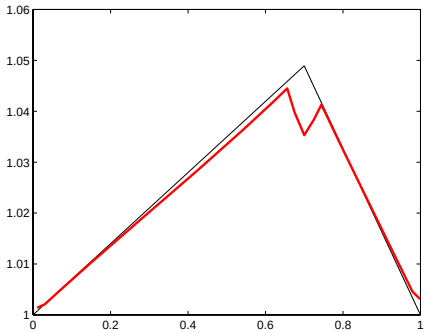

(c) K= 200, a=0.233

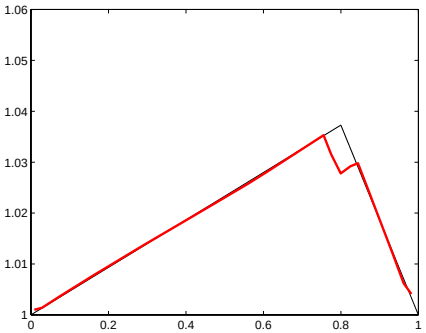

(d) K= 200, a=0.233

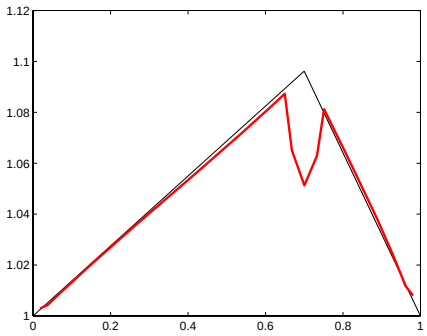

(e) K= 100, a=0.458

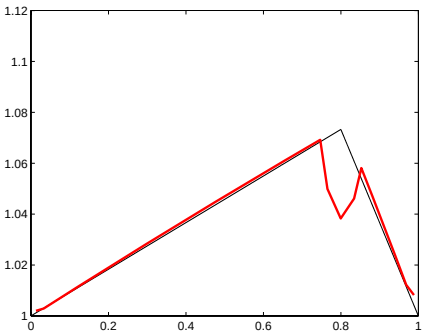

(f) K= 100, a=0.458

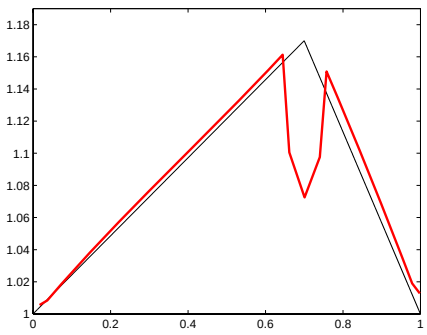

(g) K= 50, a=0.809

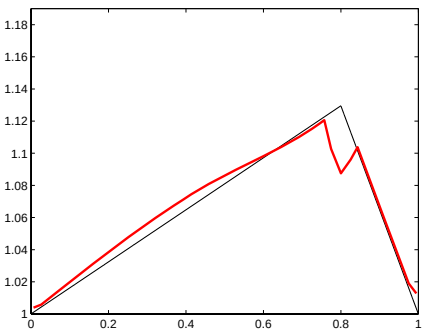

(h) K= 50, a=0.809

FIG. 2.8 – Pressure distribution at two consecutive moments of time found analytically (black thin line) and numerically (red thick line) ; μ= 10 000, h_0=0.01, h_1= 0.005.

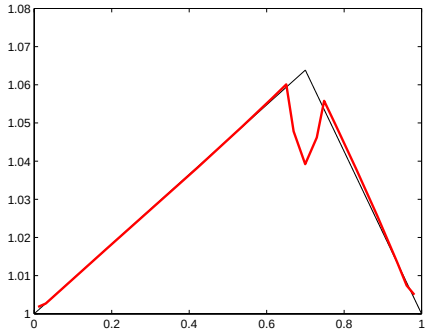

(a) K= 300, a=0.304

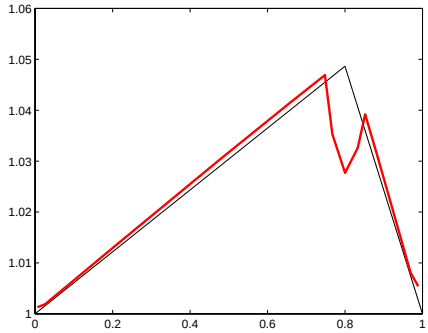

(b) K= 300, a=0.304

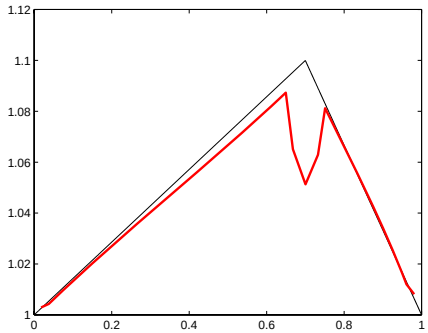

(c) K= 200, a=0.476

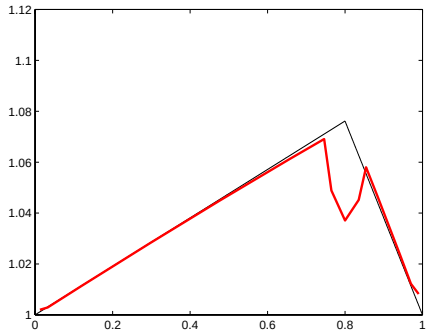

(d) K= 200, a=0.476

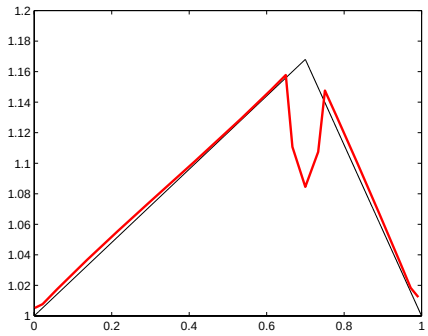

(e) K= 100, a=0.8

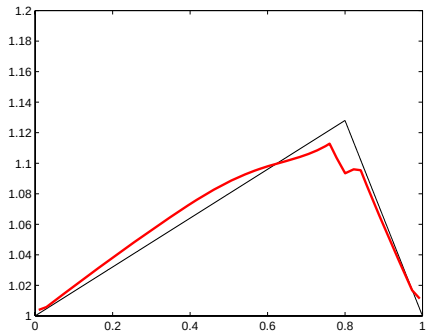

(f) K= 100, a=0.8

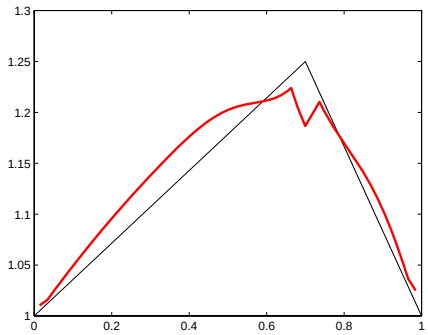

(g) K= 50, a=1.19

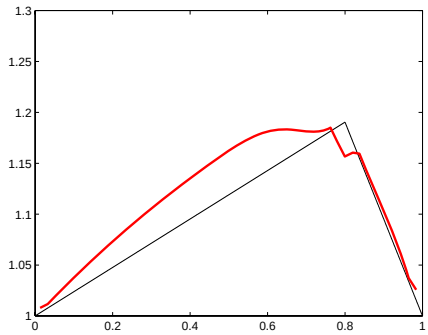

(h) K= 50, a=1.19

Fig. 2.9 – Pressure distribution at two consecutive moments of time found analytically (black thin line) and numerically (red thick line); μ= 20 000, h_0=0.01, h_1= 0.005.

We put the dividing particle in the middle of the interval (Figure 2.7A). In the beginning we keep it fixed. It divides and fills the whole interval by the particles of the type B which do not divide. Then we detach the dividing particle. It starts moving to the boundary due to the pressure gradient (Figure 2.7B). Figure 2.8 shows the pressure distribution found numerically in particle dynamics and analytically. When the value of coefficient K is sufficient large (Figure 2.8,a,b), that is the medium is weakly compressible, then the numerical and analytical results are in a good agreement. If the value of coefficient K is smaller then the difference between numerical and analytical results is more more essential (Figure 2.8,g,h). With increasing the coefficient of friction μ the medium becomes highly compressible and results of comparison numerical and analytical solution are not in a good agreement (Figure 2.9).

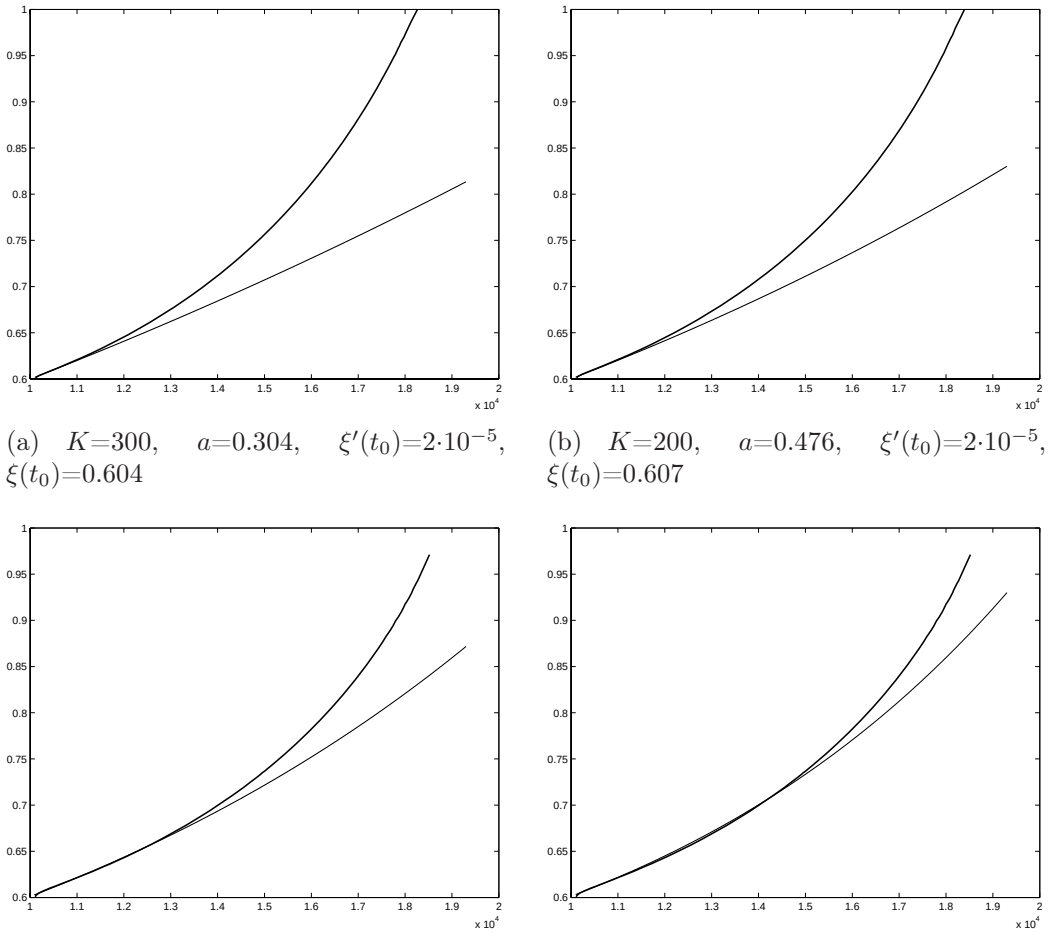

(a) K=300, a=0.304, $\xi'(t_0)$=2·10^{-5}, $\xi(t_0)$=0.604

(b) K=200, a=0.476, $\xi'(t_0)$=2·10^{-5}, $\xi(t_0)$=0.607

(c) K=100, a=0.8, $\xi'(t_0)$=2·10^{-5}, $\xi(t_0)$=0.606

(d) K=50, a=1.19, $\xi'(t_0)$=2·10^{-5}, $\xi(t_0)$=0.607

FIG. 2.10 – Coordinate of the growing particle as a function of time ; numerical simulations (upper curve), the analytical solution (lower curve), μ= 20 000, h_0=0.01, h_1= 0.005.

In spite of the good agreement for the pressure distribution, there is a big difference in the speed of the dividing cell found analytically and numerically (Figure 2.22). A possible explanation can be related to the fact that the analytical solution is found under the quasi-stationary approximation. It may not be well applicable for particle dynamics because of the periodic oscillations caused by cell division.

2.2.6.2 2D case

In the 2D model example we consider a square domain with a fixed dividing particle in its center. This particle produces other spherical particles with a given frequency. The direction of division, that is the angle of newly born particles with respect to the original particle is random. Thus we have a point source of particles from the center of the domain. The corresponding continuous model in the stationary case can be derived from equations (2.8), (2.9) :

$$\Delta p = J(x),\ x \in \Omega, \quad p = 0,\ x \in \partial\Omega. \tag{2.22}$$

Here $J(x)$ is a Dirac δ-function, in the case of a point source, or its approximation.

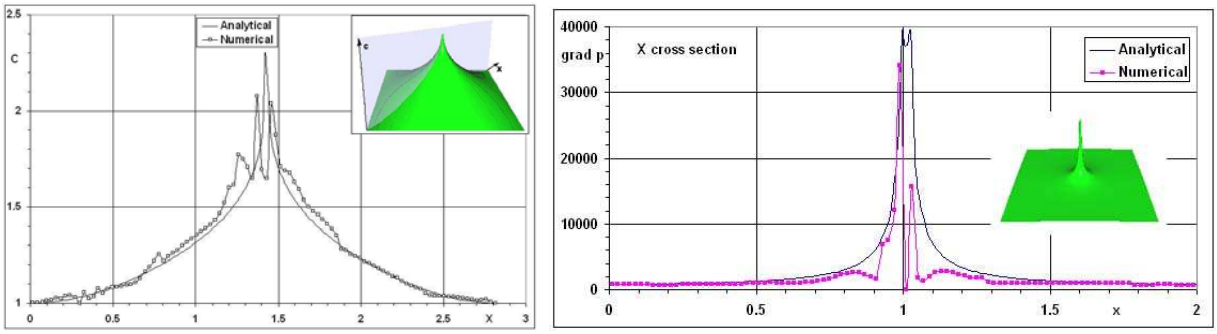

Fig. 2.11 – Left : concentration distribution for the discrete (dotted line) and continuous (smooth line) models along the diagonal of the square computational domain (upper right corner). Right : the modulus of ∇p along the x-direction.

This problem allows us to determine the pressure distribution. We need an equation of state to find the concentration. If the particles are locally uniformly distributed and form a square grid, then $c = (h_0/h)^2$. Simple computations allow us to find the expression for the pressure from the expression for the force between two neighboring particles (2.14) :

$$p(c) = k\sqrt{c}\,\frac{\sqrt{c}-1}{2-\sqrt{c}}\,.$$

A similar formula, though quantitatively different, holds if the packing of particles is different. In particular, it can be hexagonal.

Thus, we can determine the concentration distribution from particle dynamics and from the equations of continuum mechanics. Their comparison is shown in Figure 2.11.

2.2.7 Motion of dividing cells

Biological cells can divide and create a cell population around them. Appearance of new cells creates cell pressure and, as a consequence, their motion. This motion changes the position of the dividing cells. Thus, we come to the problem about the motion of dividing cells. From the biological point of view this is related to the distribution of stem cells, which possess the capacity to self-renew. Figure 2.12 shows the motion of a single dividing cell in a square filled by non-dividing cells. The dividing cell feels the shortest way to the wall and moves in this direction.

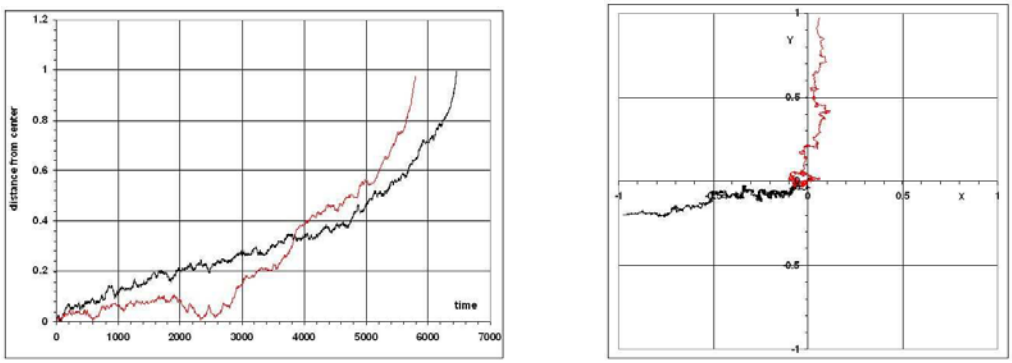

FIG. 2.12 – Motion of a dividing particle, distance from the center of the domain (left) and its trajectory (right). Two curves correspond to two different simulations.

The corresponding continuous problem writes

$$\Delta p = \delta(x - \xi(t)),\ x \in \Omega, \quad p = 0,\ x \in \partial\Omega, \quad \xi'(t) = \oint p\, ds\ ,$$

where $\xi(t)$ is a position of the point source. It is a 2D vector. The integral is taken over a contour around the point ξ. Solution of this problem can be sought as $p(x,t) = p_0(x,t) + a\ln(b/|x - \xi(t)|)$, where p_0 is a regular harmonic function with non-homogeneous boundary conditions. Then $\xi'(t) = \nabla p_0(\xi(t), t)$. Numerical solution of this problem shows the same qualitative behavior as for particle dynamics. The point source moves to the boundary by the shortest way. Its speed increases when it approaches the wall.

2.3 1D hybrid models

2.3.1 Cell differentiation and apoptosis

In this section we consider the complete model (2.1)-(2.4). We begin with the 1D model example where cells can move along the real line. Each cell can divide and die by apoptosis. After division cell gives two cells identical to itself. We suppose that cell division and death are determined by some bio-chemical substances produced by the cells themselves. We consider

the case where there are two such substances, u and v, which influence cell division and death. We come to the following system of equations :

$$\begin{cases} \frac{du}{dt} = d_1 \frac{\partial^2 u}{\partial x^2} + b_1 c - q_1 u, \\ \\ \frac{dv}{dt} = d_2 \frac{\partial^2 v}{\partial x^2} + b_2 c - q_2 v. \end{cases} \tag{2.23}$$

These equations describe the evolution of the extracellular concentrations u and v with their diffusion, production terms proportional to the concentration of cells c and with the degradation term. The equations above are completed by the no-flux boundary conditions.

Intracellular concentrations u_i and v_i in the i-th cell are described by the equations :

$$\begin{cases} \frac{du_i}{dt} = k_1^{(1)} u(x,t) - k_2^{(1)} u_i(t) + H_1, \\ \\ \frac{dv_i}{dt} = k_1^{(2)} v(x,t) - k_2^{(2)} v_i(t) + H_2. \end{cases} \tag{2.24}$$

The first term in the right-hand side of the first equation shows that the intracellular concentration u_i grows proportionally to the value of the extracellular concentration $u(x,t)$ at the space point x_i where the cell is located. These equations contain the degradation terms and constant production terms, H_1 and H_2. When a new cell appears, we put the concentrations u_i and v_i equal zero.

If the concentration u_i attains some critical value u_c, then the cell divides. If v_i becomes equal v_c, the cell dies. Consider first the case where $k_1^{(1)} = k_1^{(2)} = k_2^{(1)} = k_2^{(1)} = 0$. Then u_i and v_i are linear functions of time which reach their critical values at some moments of times $t = \tau_u$ and $t = \tau_v$, respectively. If $\tau_u < \tau_v$, then all cells will divide with a given frequency, if the inequality is opposite, then all cells will die. We notice that if $k_1^{(2)}$ equals zero, then the extracellular concentration v does not influence the evolution of v_i.

Next, consider the case where $k_1^{(1)}$ is different from zero. If it is positive, then cells stimulate proliferation of the surrounding cells, if it is negative, they suppress it. Both cases can be observed experimentally. We restrict ourselves here by the example of negative $k_1^{(1)}$. All other coefficients remain zero. Therefore, cells have a fixed life time. If they do not divide during this time, they die.

We carry out the 1D simulation where cells can move along the real line. Initially, there are two cells in the middle of the interval. Figure 2.13 shows the evolution of this population in time. Each blue dot shows one cell. For each moment of time (vertical axis) we observe the distribution of cell population in space (horizontal axis).

The distribution of u in the extracellular matrix is shown in Figure 2.14. It corresponds to the simulation shown in Figure 2.13 (e). This cell population spreads in space. The evolution of u in time corresponds to this propagation.

Dynamics of the cell population in Figure 2.13 (a) can be characterized by two main properties. First of all, it expands to the left and to the right with approximately constant speed. Second, the total population consists of relatively small sub-populations. Each of them starts from a small number of cells. Usually, these are two most right and left cells from the

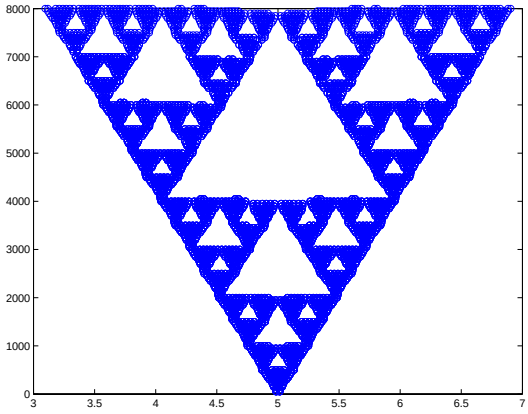

(a) $v_c = 2$, $k_1^{(1)} = -5 \cdot 10^{-3}$, $d_1 = 0.0001$, $b_1 = 0.2$

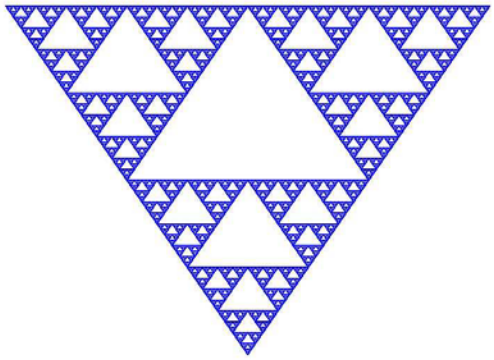

(b) Serpinsky carpet - fractal set

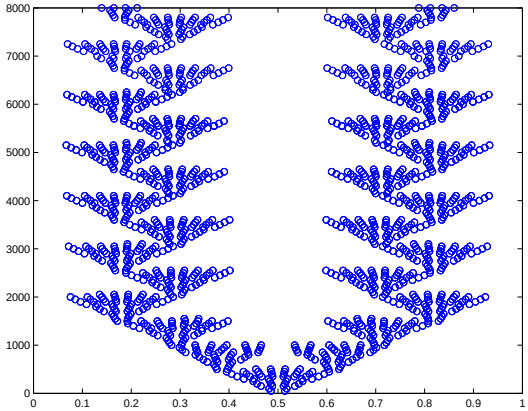

(c) $v_c = 2$, $k_1^{(1)} = -5.5 \cdot 10^{-3}$, $d_1 = 0.0001$, $b_1 = 0.2$

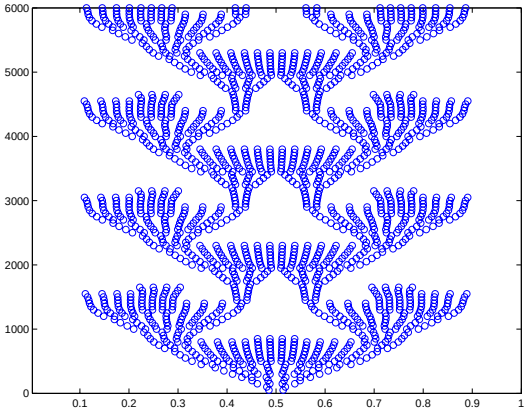

(d) $v_c = 4$, $k_1^{(1)} = -5 \cdot 10^{-3}$, $d_1 = 10^{-3}$,$b_1 = 3.1$

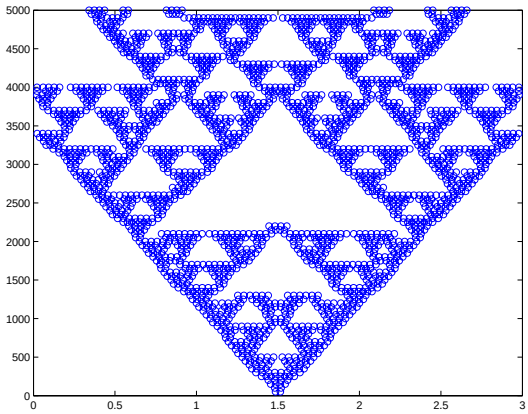

(e) $v_c = 1.01$, $k_1^{(1)} = 10^{-4}$, $d_1 = 0.0001$, $b_1 = 0.2$

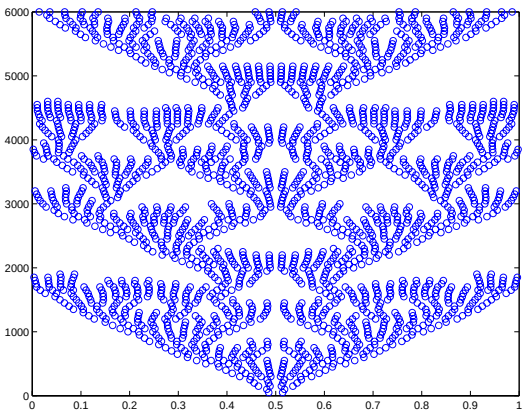

(f) $v_c = 3$, $k_1^{(1)} = -5 \cdot 10^{-3}$, $d_1 = 0.0001$, $b_1 = 0.2$

FIG. 2.13 – Evolution of cell population where $d_2 = 1$, $b_2 = 0.1$, $q_1 = 0.02$, $q_2 = 0.0001$, $k_2^{(1)} = k_1^{(2)} = k_2^{(2)} = 0$, $H_1 = 0.1$, $H_2 = 0.01$.

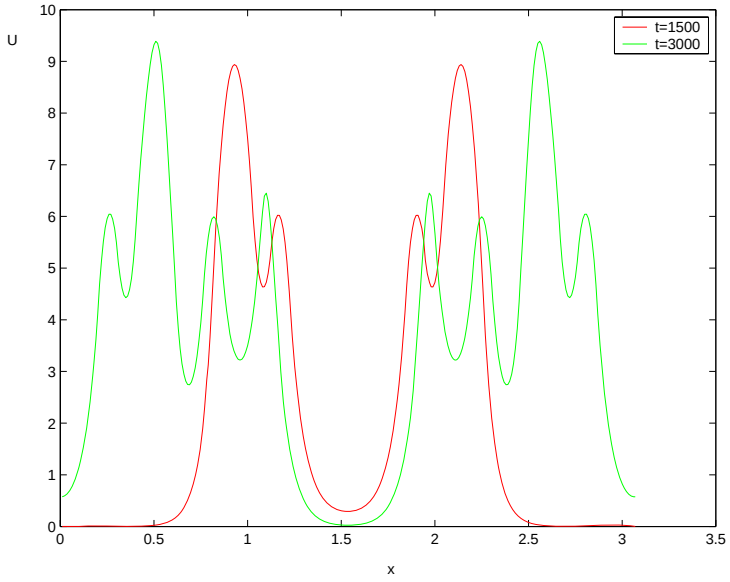

FIG. 2.14 – Distribution of u at different moments of time for the values of parameters $v_c = 1.01$, $d_1 = 0.0001$, $d_2 = 1$, $b_1 = 0.2$, $b_2 = 0.1$, $q_1 = 0.02$, $q_2 = 0.0001$, $k_2^{(1)} = k_1^{(2)} = k_2^{(2)} = 0$, $k_1^{(1)} = 10^{-4}$, $H_1 = 0.1$, $H_2 = 0.01$.

previous sub-population. During some time, the sub-population grows, reaches certain size and disappears giving birth to new sub-populations.

This behavior can be explained as follows. The characteristic time of cell division is less than of cell death. When the cell sub-population is small, the quantity of u is also small, and its influence on cell division is not significant. When the sub-population becomes larger, it slows down cell division because of growth of u. As a result the sub-population disappears. The outer cells can survive because the level of u there is less.

The geometrical pattern of cell distribution for these values of parameters reminds Serpinsky carpet (Figure 2.13, b), an example of fractal sets. It is obtained from an equilateral triangle by consecutive removing some of its parts. At the first step, the central triangle is removed. At the second step, the central part of each remaining triangle is removed and so on. In the case of cellular pattern, the minimal triangle is determined by the cell size. Since this patterns grows with time, we can scale it to a triangle of a constant size. In this case, we obtain a decreasing sequence of removed (white) triangles, as it is the case for Serpinsky carpet.

The pattern of cell distribution depends on the parameters. Other examples are shown in Figure 2.13. The cell population in Figure 2.13 (c,d) remains bounded, and the pattern is time periodic. In the simulation shown in Figure 2.13 (a,e,f) the cell population grows with approximately constant speed.

2.3.2 Cell division and differentiation

In this model we describe extracellular and intracellular concentrations by equations (2.23) and (2.24). When v_i becomes equal to v_c, cells differentiate into another type of cells. The new type of cells do not have the ability to grow and divide. Figure 2.15 presents the evolution of the cell population depending on the critical value of v_c. We begin the simulation with two cells in the middle of the interval. The cell population starts growing. When it is small, the quantity of u produced by cells is also small, and its influence on cell division is not significant. When the population becomes larger, there is more u in the extracellular matrix. It slows down cell division. As a result, the concentration v_i attains the critical value v_c faster than u_i reaches u_c. Then the cells start to differentiate. When the critical value v_c is small (Figure 2.15, a) all cells finally differentiate into another cell type. If we increase the critical value v_c (Figure 2.15, b), then there is a stationary group of differentiated cells in the middle of interval. Other differentiated cells periodically appear from the right and from the left, they move towards the borders of the interval and leave it. In Figure 2.15 (c), the population of differentiated cells in the middle of the interval becomes larger than before. There are also other differentiated cells which move to the borders of interval. This regime is not periodic anymore. Finally, for v_c sufficiently large differentiated cells appear only in the middle of interval. The number of both types of cells is shown in Figure 2.16.

2.3.3 Quiescent state of cells

In this model we suppose that cells can be either in quiescent state (type Q) or in cell cycle (type A). When a cell enters cell cycle, it grows and then divides into two identical to itself cells. We specify the model (2.1)-(2.4) in the following way. The equations which describe the evolution of the concentrations u and v in the extracellular matrix take the form :

$$\begin{cases} \frac{du}{dt} = d_1 \frac{\partial^2 u}{\partial x^2} + b_1^1 c_1 + b_1^2 c_2 - q_1 u, \\ \\ \frac{dv}{dt} = d_2 \frac{\partial^2 v}{\partial x^2} + b_2^1 c_1 + b_2^2 c_2 - q_2 v. \end{cases} \tag{2.25}$$

Here c_1 is the concentration of cells in cell cycle. We suppose that cells in quiescent state do not produce u and v. Therefore, $b_1^2 = b_2^2 = 0$. As before, we consider the no-flux boundary conditions.

Intracellular regulatory networks for the i-th cell in a cell cycle are described by system (2.26) of ordinary differential equations

$$\begin{cases} \frac{du_i}{dt} = k_1^{(u)} u(x,t) - k_2^{(u)} u_i(t) + H_u, \\ \\ \frac{dv_i}{dt} = k_1^{(v)} v(x,t) - k_2^{(v)} v_i(t) + H_v. \end{cases} \tag{2.26}$$

When the value of v_i overcomes v_c, the cell leaves cell cycle and becomes quiescent. It changes its type from A to Q. The intracellular concentrations for the i-th cell in a quiescent

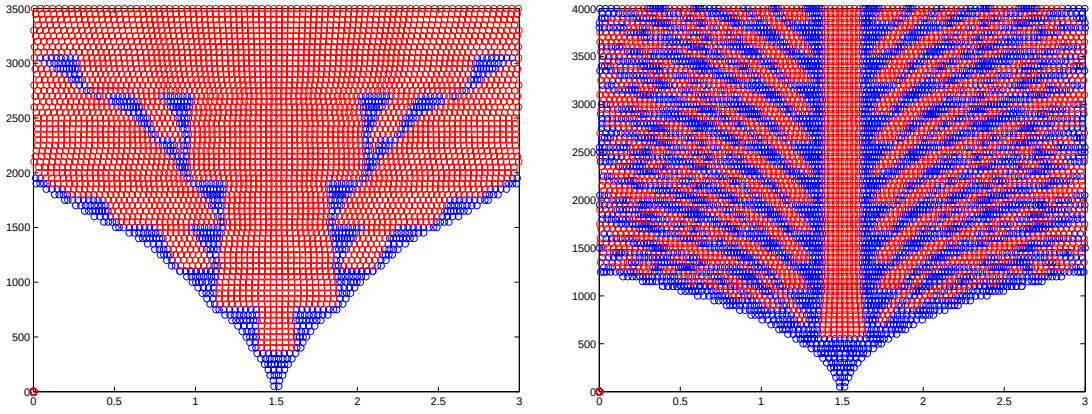

(a) $v_c = 1.4$ (b) $v_c = 1.8$

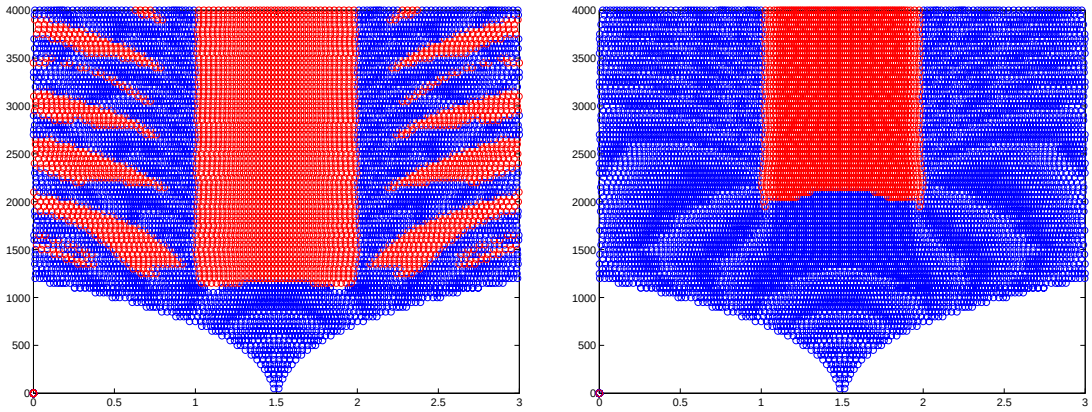

(c) $v_c = 3$ (d) $v_c = 8.2$

FIG. 2.15 – Evolution of cell population in the case of self-renewal and differentiation. Differentiated cells are shown in red; $d_1 = 0.0001$, $d_2 = 1$, $b_1 = 0.2$, $b_2 = 0.1$, $q_1 = 0.02$, $q_2 = 0.0001$, $k_1^{(1)} = -3 \cdot 10^{-3}$, $k_2^{(1)} = k_1^{(2)} = k_2^{(2)} = 0$, $H_1 = 0.1$, $H_2 = 0.01$.

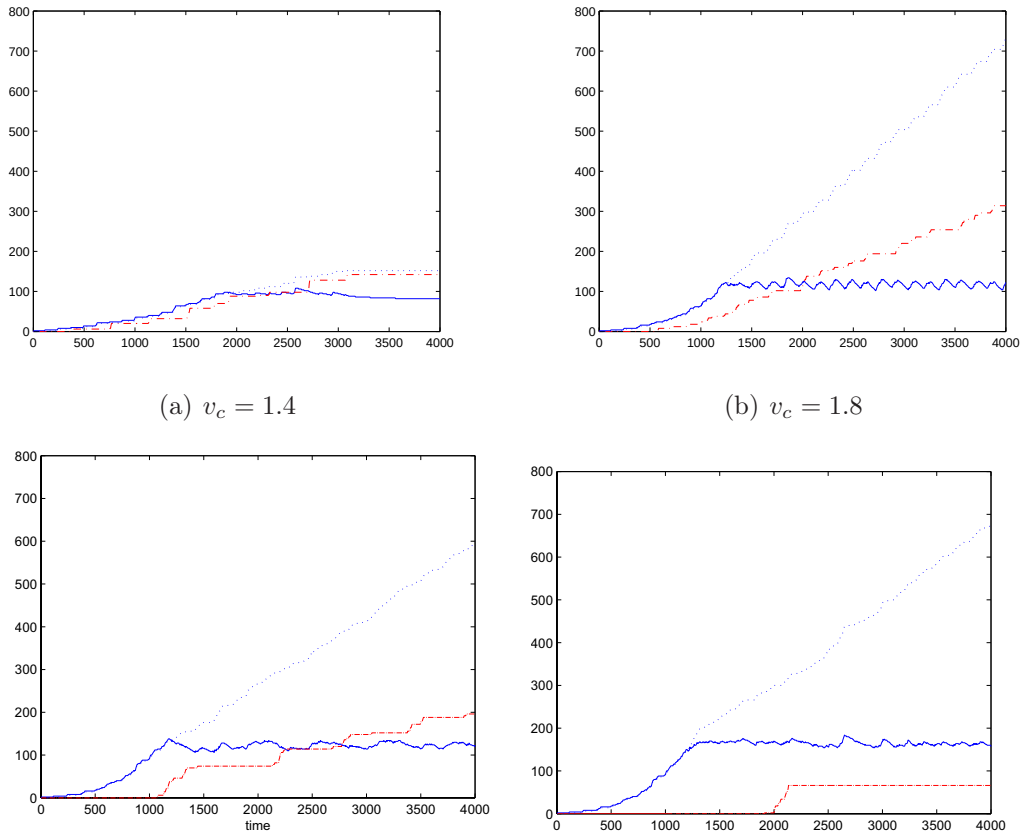

(a) $v_c = 1.4$ (b) $v_c = 1.8$

(c) $v_c = 3$ (d) $v_c = 8.2$

FIG. 2.16 – Number of cells. Summarized number of differentiated cells and cells in division are shown in red (dash-dot curve) and blue (dash curve), respectively. Blue solid curve represents the total number of cells; $d_1 = 0.0001$, $d_2 = 1$, $b_1 = 0.2$, $b_2 = 0.1$, $q_1 = 0.02$, $q_2 = 0.0001$, $k_1^{(1)} = -3 \cdot 10^{-3}$, $k_2^{(1)} = k_1^{(2)} = k_2^{(2)} = 0$, $H_1 = 0.1$, $H_2 = 0.01$.

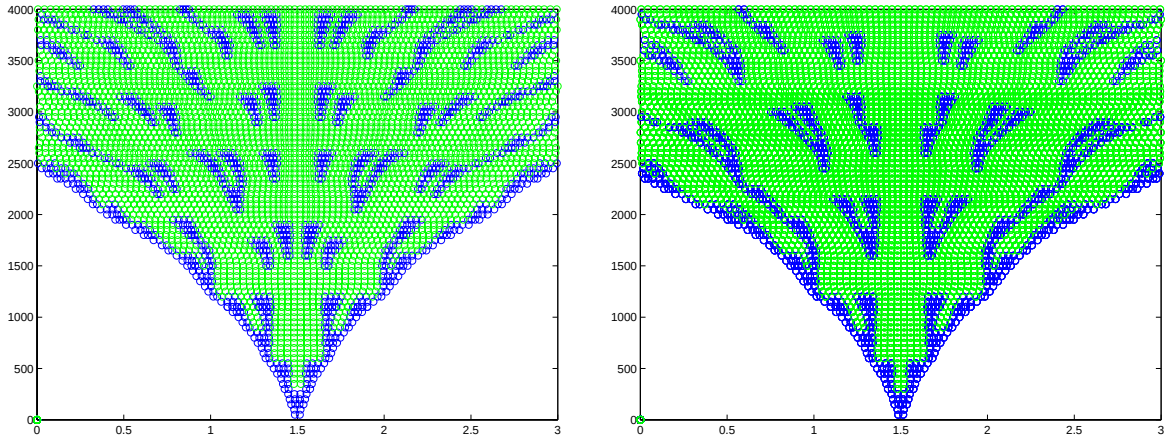

(a) $k_1^{(p)} = -5 \cdot 10^{-3}$ (b) $k_1^{(p)} = -7 \cdot 10^{-3}$

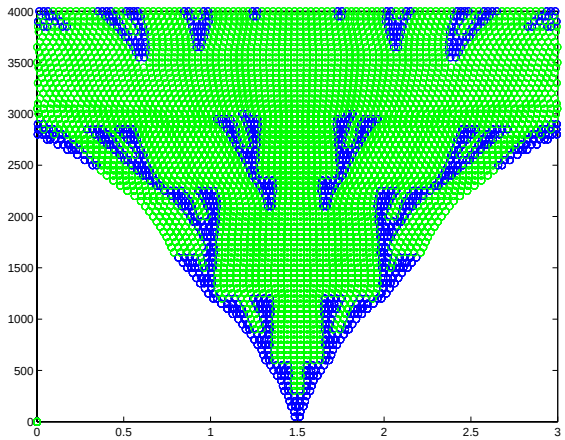

(c) $k_1^{(p)} = -1.8 \cdot 10^{-2}$

FIG. 2.17 – Evolution of cell population in the case where cells can self-renew (blue) or remain quiescent (green) ; $d_1 = 0.0001$, $d_2 = 1$, $b_1^1 = 0.2$, $b_2^1 = 0.1$, $q_1 = 0.02$, $q_2 = 0.0001$, $k_2^{(u)} = k_1^{(v)} = k_2^{(v)} = 0$, $k_1^{(u)} = -5 \cdot 10^{-3}$, $H_u = 0.1$, $H_v = 0.003$, $k_2^{(p)} = 0$, $H_p = 0.01$, $v_c = 0.5$, $p_c = 10$.

state is described by the equation :

$$\frac{dp_i}{dt} = k_1^{(p)} u(x,t) - k_2^{(p)} p_i(t) + H_p. \tag{2.27}$$

When p_i reaches the critical value p_c, the cell enters again cell cycle. Figure 2.17 presents three examples of this simulation. We observe that cells periodically enter and leave cell cycle. With decreasing the value of $k_1^{(p)}$ there are less cells in quiescent state.

2.4 2D modelling.

2.4.1 Cell differentiation and apoptosis.

We illustrate 2D simulation with one of the models considered in the previous section where cells can either self-renew or die. Evolution of extracellular and intracellular concentrations is described by systems (2.23)-(2.24) where 1D diffusion is replaced by the 2D Laplace operator.

We start simulation with a single cell at the center of a square domain. Cells grow, divide and die resulting in the emergence of various patterns which can be radially symmetric, asymmetric or even chaotic depending on the value of parameters. Four examples are shown in Figure 2.18.

2.4.2 Modelling of tumor growth

In this section we consider the complete model (2.1)-(2.4) assuming that u is a scalar variable. It describes the concentration of nutrients which diffuse from the boundary of the domain and which are consumed by cells inside the domain. We consider the equation

$$\frac{\partial u}{\partial t} = D\ \Delta u - kcu, \tag{2.28}$$

where c is cell concentration and k is a positive parameter. The rate of nutrient consumption is proportional to the product of the concentrations. The form of the domain and of the boundary conditions will be specified below.

Next, we consider the scalar intracellular variable u_i where the subscript i corresponds to the cell number. It is described by the equation

$$\frac{du_i}{dt} = k_1 u(x_i,t) - k_2 u_i. \tag{2.29}$$

The first term in the right-hand side of this equation shows that the intracellular concentration u_i grows proportionally to the value of the extracellular concentration $u(x,t)$ at the space point x_i where the cell is located. The second term describes consumption or destruction of u_i inside the cell. We suppose that the cell radius r_i grows proportionally to the increase of u_i :

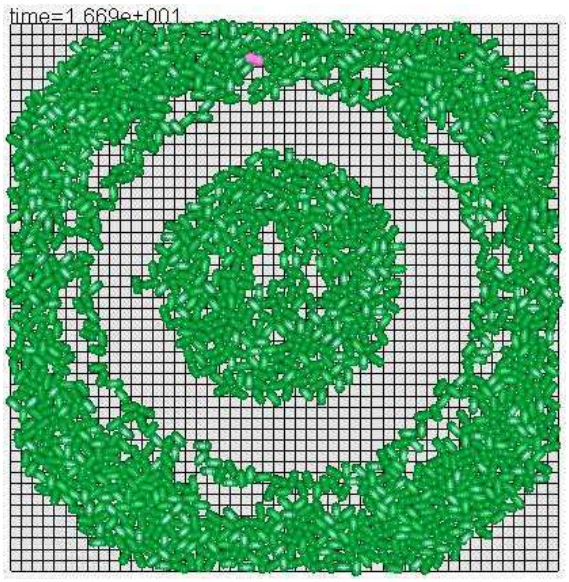

(a) $q_1 = 0.02$, $q_2 = 0.5$, $k_1^{(1)} = 0$, $k_1^{(2)} = 5$, $d_2 = 0.0001$, $V_{cr} = 1$

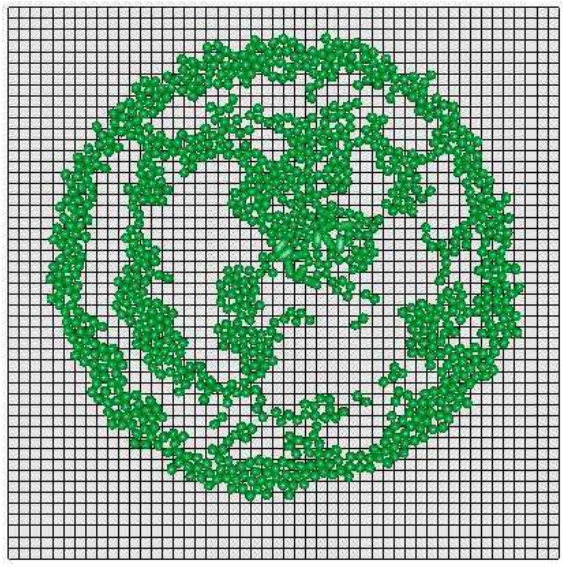

(b) $q_1 = -1$, $q_2 = -0.0001$, $k_1^{(1)} = -0.01$, $k_1^{(2)} = 0$, $d_2 = 1$, $V_{cr} = 1$

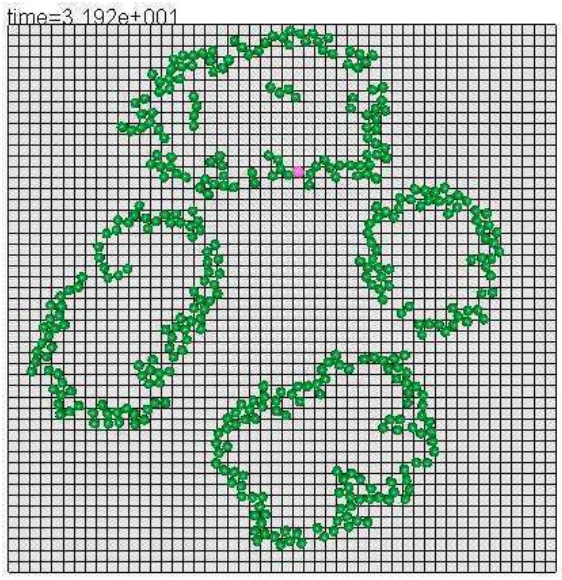

(c) $q_1 = -0.05$, $q_2 = -0.0001$, $k_1^{(1)} = -0.01$, $k_1^{(2)} = 0$, $d_2 = 1$, $V_{cr} = 16$

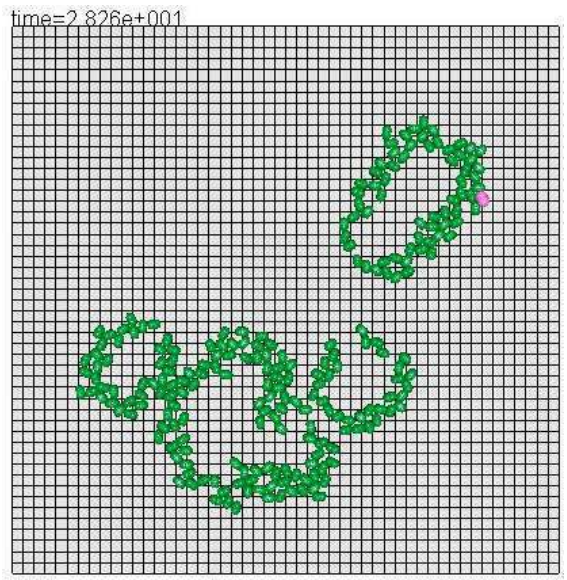

(d) $q_1 = -0.05$, $q_2 = -0.0001$, $k_1^{(1)} = -0.01$, $k_1^{(2)} = 0$, $d_2 = 1$, $V_{cr} = 20$

FIG. 2.18 – 2D simulations in the case of cell self-renewal and apoptosis ; snapshots of cell populations. $H_1 = 0.1$, $H_2 = 0.01$, $b_1 = 0.2$, $b_2 = 0.1$, $k_2^{(2)} = k_2^{(1)} = 0$, $d_1 = 0.0001$.

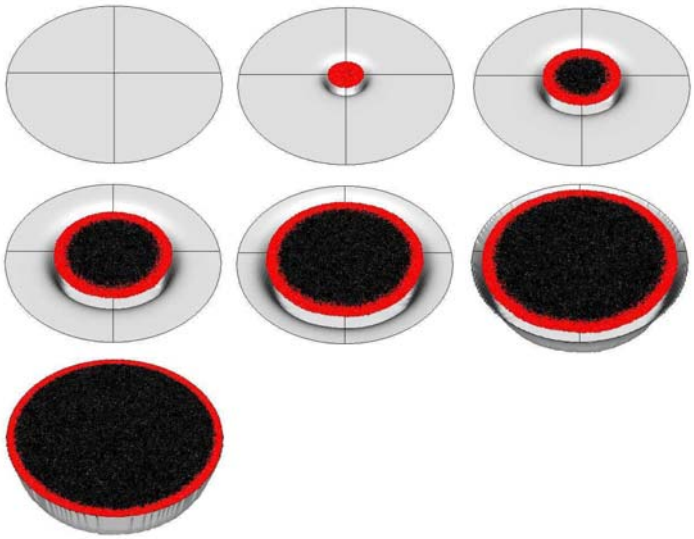

FIG. 2.19 – Consecutive moments of tumor growth. It starts with a single cell at the center of the circle. Living cells are shown in red, dead cells in black. 2D grey surface shows the level of nutrients.

$$\frac{dr_i}{dt} = \max\left(\frac{du_i}{dt}, 0\right). \tag{2.30}$$

The initial value of the radius for each new cell is r_0, the maximal radius r_m. When it is reached, the cell divides. If the cell does not divide before its maximal age, then it dies. The maximal cell age is a parameter of the problem.

Consider a circular domain Ω and complete equation (2.28) by the boundary condition $u = 1$ at the boundary $\partial\Omega$. We put a single cell in the center of the domain and begin numerical solution of system (2.28)-(2.30). The results of the simulations are shown in Figure 2.19 for several consecutive moments of time. The grey 2D surface shows the spatial distribution of the concentration $u(x,t)$. In the beginning it equals 1 everywhere in the domain. The constants k_1 and k_2, $k_1 > k_2$ are chosen in such a way that the intracellular concentration u_i growth. Consequently, the radius of the cell also grows and after some time the cell divides. The new cells also consume nutrients, grow and divide. The part of the domain filled by cells forms a disk while the concentration $u(x,t)$ decreases in the center of the domain (second figure in the upper row). Hence, the right-hand side of equation (2.30) also decreases, the intracellular concentration stops growing or even decreases, and cells cannot divide before their maximal age τ. As a result, they die and form the black region in the center. Living cells shown in red form a narrow external layer. The region filled by cells grows in time and finally approaches to the boundary of the domain.

Dynamics of the cell population can be more complex if we decrease the maximal life time τ. Cells now have less time to accumulate enough nutrients for division. In this case, even a small decrease in nutrient concentration can become crucial from the point of view

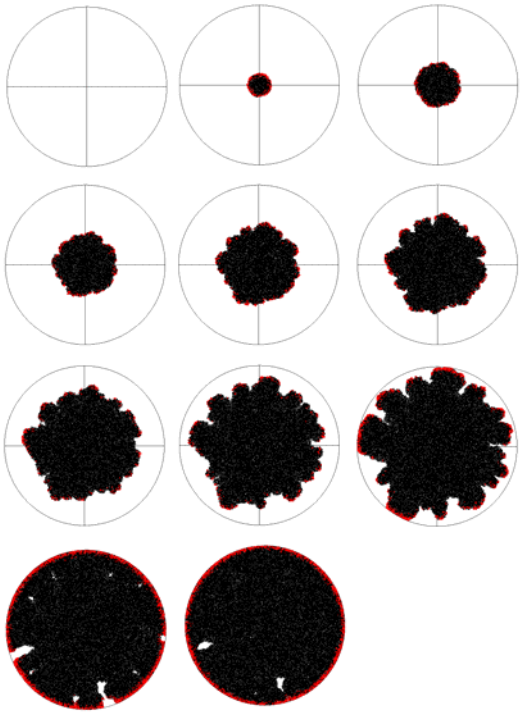

FIG. 2.20 – Consecutive moments of tumor growth. If the life time of cells is short, they become more sensitive to the lack of nutrient. The region filled by cells loses its radial symmetry.

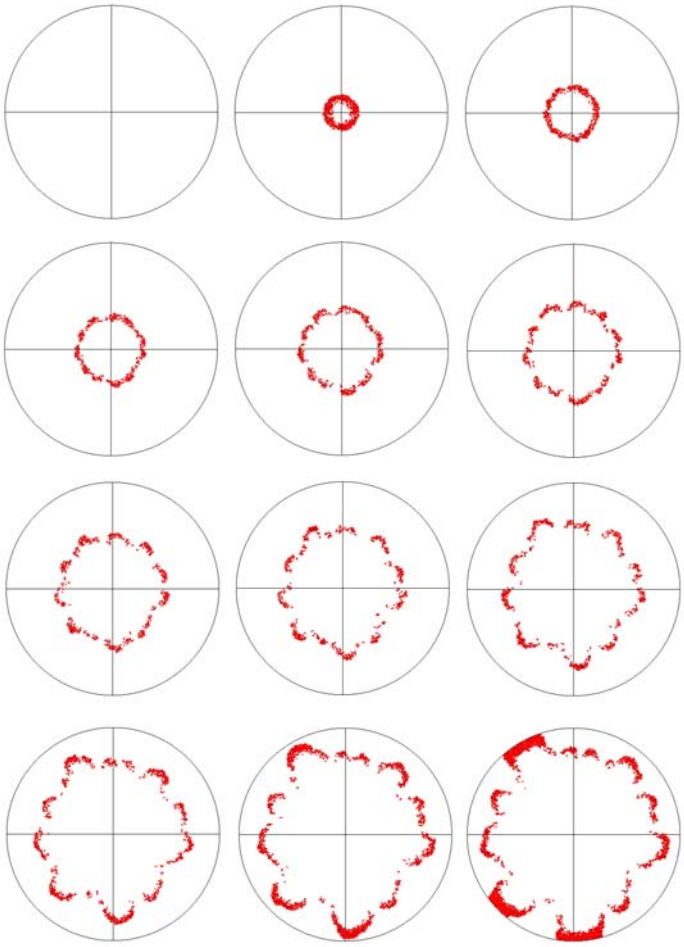

FIG. 2.21 – Living cells are shown in red. Dead cells are removed from the computational domain. The narrow region filled by cells is less stable and propagates with a smaller speed than in the presence of dead cells inside.

of the choice between proliferation and apoptosis. In the beginning cells form, as before, a circular region with living cells outside and the core formed by dead cells. The layer of living cells is narrower than in the previous example. Rather rapidly the layer of living cells becomes disconnected (Figure 2.20, third in the upper row). After that the domain loses its radial symmetry which can be related to an instability with a certain wavenumber. Further growth of the region filled by cells makes the outgrowing parts more pronounced and this region less regular. Finally it reaches the boundary of the domain.

If dead cells are removed from the computational domain, then living cells can form a growing annulus or, when this regime becomes unstable, some narrow region filled by living cells and propagating from the center to the boundary of the domain (Figure 2.21).

2.5 Modelling of Pattern Formation in Bacteria Filament

Filament of bacteria represents a chain of cells connected to each other. They can divide producing identical cells. When the cells in the filament lack nitrogen, some of them differentiate, some other remain in their original form. Differentiated cells do not divide. They are located periodically in the filament being separated by a given number of undifferentiated cells. In the case of anabaena filament, the intracellular regulation which determines cell differentiation is shown in Figure 2.22, [101]. One of the earliest steps of heterocyst differentiation is the accumulation of 2-oxoglutarate (2-OG), which constitutes a signal of nitrogen starvation. It initiates production of the protein HetR which plays a key role in this regulation. First of all, its amplifies its own production. Next, it initiates production of the protein PatS. Finally, when the concentration of HetR becomes sufficiently high, the cell differentiates into heterocyst. On the other hand, PatS suppresses HetR and, as a consequence, cell differentiation. Moreover, PatS can diffuse between the neighboring cells. This competition between HetR and PatS is supposed to determine the pattern of differentiated cells. We emphasize that if a cell differentiates, then PatS prevents differentiation of the neighboring cells but not of the cell itself. So the proposed mechanism should capture this property of the system.

The intracellular concentrations are described by the following system of equations :

$$\begin{cases} \frac{du_i}{dt} = H_u \\ \\ \frac{dG_i}{dt} = H_g \\ \\ \frac{dh_i}{dt} = k_1^{(h)} G_i(t) + k_2^{(h)} h_i^2(t) - k_3^{(h)} p_i(t) h_i(t) \\ \\ \frac{dp_i}{dt} = d(p_{i-1} - p_i) + d(p_{i+1} - p_i) + k_1^{(p)} h_i(t) - k_2^{(p)} p_i(t) \end{cases} \tag{2.31}$$

where u_i denotes the intracellular concentration of the cell division protein, FtsZ, in the i-th cell, G_i is the concentration of 2-oxoglutarate, h_i is the self-enhancing differentiation regulatory protein HetR, p_i is the inhibitor encoded by the gene PatS, which is dependent

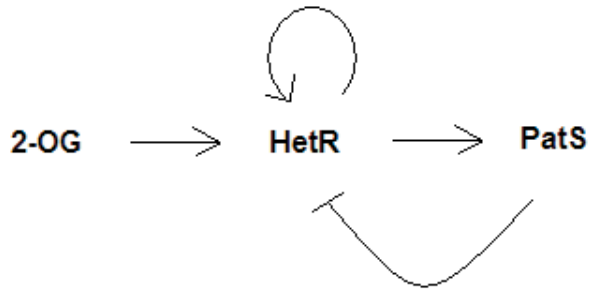

FIG. 2.22 – Intracellular regulation of heterocyst differentiation in anabaena.

on HetR for production. PatS is synthesized in the developing heterocyst and diffuses to the neighboring vegetative cells.

Since the right-hand side in the equation for u_i is constant, then $u_i = H_u t$. If this concentration reaches a critical value u_c, the cell divides. The time of cell proliferation is $\tau_p = u_c/H_u$. During this time, cell grows linearly and becomes twice bigger when its age equals τ_p. The daughter cells are twice as small as the mother cell.

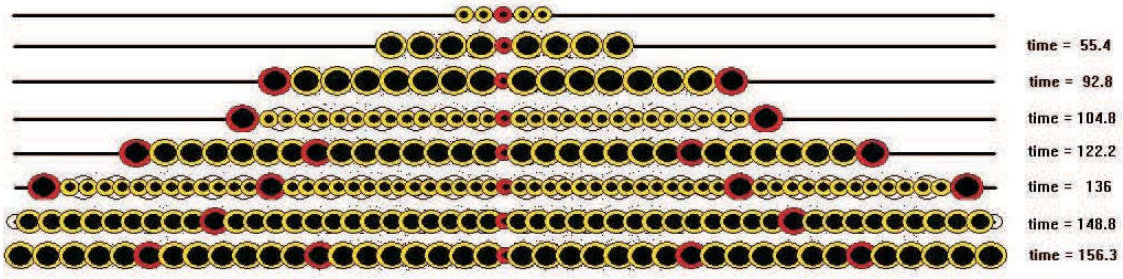

FIG. 2.23 – Anabaena growth. Differentiated cells are red, undifferentiated yellow. The black circle inside cells shows their incompressible part.

Cell differentiation occurs if the concentration of h_i equals some critical value h_c. Therefore, the choice between cell division and differentiation depends on what critical value is reached first. The rate of production of h_i depends on G_i, on h_i itself with quadratic self-acceleration and on p_i which downregulates it. The right-hand side of the equation for p_i contains the flux terms from the surrounding cells which are similar to the discretized diffusion equation, the production term proportional to h_i and the degradation term. After differentiation, the cell does not grow anymore, it cannot divide and it keeps a constant level of p_i.

We need to specify the initial values of the concentrations in a new cell. When a cell divides, the initial conditions in the daughter cells are as follows :

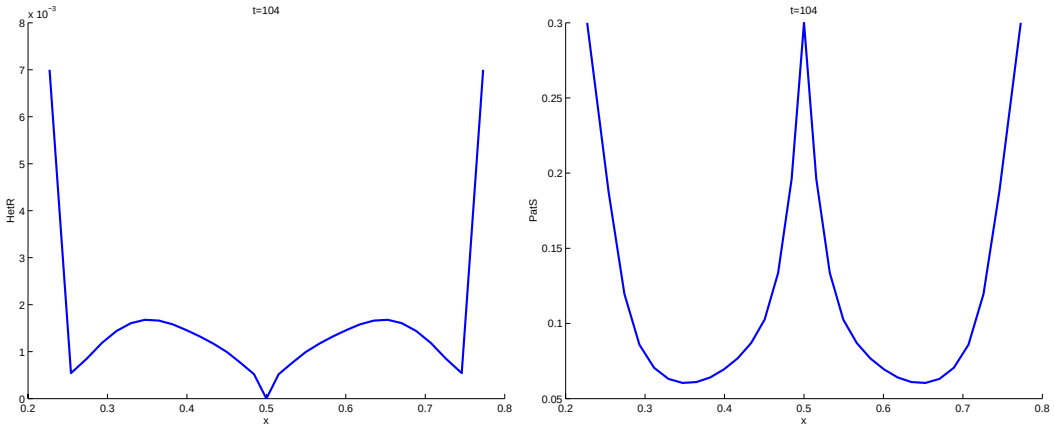

Fig. 2.24 – Concentrations of HetR (left) and of PatS (right) along the filament. Minima of HetR and maxima of PatS correspond to differentiated cells.

$$u_i(t_0) = 0,\ G_i(t_0) = G_0,\ h_i(t_0) = 0,\ p_i(t_0) = \frac{p_i^m}{2} \tag{2.32}$$

where p_i^m quantity of PatS in the mother cell. Hence the initial concentrations of FtsZ and HetR are zero, 2-OG takes on some constant given value, and PatS equals half of the concentration in the mother cell. The latter is important for the pattern of heterocyst differentiation. Indeed, if a cell is located sufficiently close to a differentiated cell, then the concentration of PatS in it is sufficiently high. When it divides, the concentration of PatS in the daughter cell, though two times less, can be sufficient to keep the level of HetR less than the critical level. If the mother cell is located far from differentiated cells, then the initial concentration of PatS in the daughter cell is close to zero, and it cannot prevent growth of HetR up to the critical value which determines differentiation.

An example of numerical simulations is shown in Figure 2.23. We begin with 5 cells, one differentiated cell in the center and two undifferentiated cells from each side. It is also possible to begin with all undifferentiated cells. In this case we need to introduce random perturbations in the production terms for HetR in order to give an advantage to one of the cells to differentiate. Otherwise, if all cells are initially identical, then they will remain identical. Hence, we need to introduce some asymmetry either in initial conditions or in the equations.

Undifferentiated cells begin to grow, then they divide. For $t = 92.8$, the most left and the most right cells differentiate. Undifferentiated cells in between divide once again and after some time a cell at the center of the subpopulation of undifferentiated cells becomes differentiated. The process of growth, division and differentiation continues in the same manner. The number of undifferentiated cells between two nearest differentiated cells is not exactly constant because of the parity due to division. Let us explain this in more detail. At $t = 92.8$ there are 7 undifferentiated cells from each side. After division, there are 14 of them. A new differentiated cell splits them into two groups of 7 and 6 cells. After the next

division, there are 14 and 12 cells. The next differentiation will produce the groups of 7, 6, 6, and 5 cells. Hence, after each cycle, there is a group of undifferentiated cells smaller than previously. At some point, there will be a group small enough such that it will not give a differentiated cell. Then the cells in this group will divide producing a group of cells twice larger.

Figure 2.24 shows the concentrations of HetR and PatS along the filament at $t = 104.8$ (cf. Figure 2.23). The minima of HetR and the maxima of PatS correspond to the differentiated cells. Cells differentiate if the value of HetR is sufficiently high. The values of HetR at the boundary cells is still high because these cells have just differentiated.

Chapitre 3

Hybrid modeling of erythropoiesis

In this part of the work we use a hybrid model to take into account both intracellular and extracellular regulation of erythropoiesis, but also mainly to study the importance of spatial structure of erythroblastic islands in the regulation of erythropoiesis. To our knowledge, this is the first attempt to model erythropoiesis by taking these aspects into account. We focus in particular on the role of the macrophage, by analyzing different situations, with and without macrophage at the center of the island, and actions of the feedback controls, especially regarding the feedback of the macrophage on erythroid cell proliferation and differentiation. The 'classical' structure of the erythroblastic island, with the macrophage at the center and immature erythroid cells surrounding it, will be shown to make the hybrid model stable (so the island can be sustained for an unlimited number of cell cycles) and robust to perturbations due to global and local feedback controls. Following the perturbation, such as an induced anemia, the return to a healthy organism as soon as in experimental data in mice is observed. The hybrid model displays interesting properties to reproduce erythropoiesis in normal and stress situations, considering spatial aspects of this process.

To present multiscale hybrid model, first, we focus on the intracellular scale, detailing regulatory networks considered in this thesis, described by nonlinear ordinary differential equations, and investigating their properties, in particular regarding the existence and stability of steady states associated to cell self-renewal, differentiation and death by apoptosis. Second, we concentrate on the extracellular scale, which consists in erythroid cell populations, possibly a macrophage, bone marrow medium, and is described by a computational model. Interactions between cells and with the surrounding medium are presented. Finally, we justify the coupling of both scales, through global and local feedback controls, and we discuss parameters of the model. In Section 3.2 we present the analysis of the hybrid model. This analysis consists of two parts : first, we consider an erythroblastic island without a macrophage in its center, and investigate the stability of the island and the roles of feedback controls in the stability. Next we study an island consisting of immature erythroid cells surrounding a macrophage, and the roles of feedback controls in its stability. This analysis concludes to the central role of the macrophage in the stability of the erythroblastic island, and consequently of the relevance of considering spatial aspects when modeling erythropoie-

sis. Finally, we confront the results of modelling with experiments on anemia in mice.

3.1 Model

We introduce, in this section, the hybrid model for erythropoiesis used later for in silico experiments. It consists in the coupling of two models, with different space and time scales. The first model describes intracellular dynamics, represented by regulatory networks based on specific protein competition. This intracellular dynamical level can be easily modeled with a continuous approach, namely ordinary differential equations (ODEs) and/or partial differential equations (PDEs). The second model is at cell population level, where discrete cells and events are computed, so that stochasticity due to random events (cell cycle duration, orientation of the mitotic spindle at division) and small population effects plays an important role. Extracellular regulation by growth factors is partially due to continuous models (PDEs). Such discrete-continuous models are usually called hybrid models [19, 51, 83, 88, 90, 102, 111]. We hereafter present how the model is defined at each scale and how the different levels interact.

3.1.1 Intracellular Scale : Mathematical Model

The intracellular scale describes how each erythroid progenitor cell chooses between self-renewal, differentiation and apoptosis. This choice depends on the level of expression of some proteins, involved in a regulatory network.

Ordinary differential equations are used to describe a simplified regulatory network, based on two competing proteins, Erk and Fas. Concentrations of the proteins evolve according to protein-related mechanisms as well as extracellular factor concentrations. A brief analysis of the dynamics of the system (3.1)–(3.2) is performed in order to identify key factors in cell fate choice.

3.1.1.1 ODE System

Precise intracellular regulatory mechanisms involved in erythroid progenitor cell fate are largely unknown. Based on the current knowledge, we decided to focus on a simplified regulatory network based on two proteins, Erk and Fas, responsible respectively for cell self-renewal and proliferation and cell differentiation and apoptosis [28, 37, 79, 99]. These proteins are antagonists : they inhibit each other's expression. They are also subject to external regulation, through feedback loops.

One of these feedback loops is based upon the population of reticulocytes (differentiated erythroid cells). They produce Fas-ligand which is fixed to their exterior cell membrane. Fas-ligand activates Fas, a transmembrane protein, and influences progenitor differentiation and apoptosis. Another feedback control is related to erythrocytes in bloodstream. Their quantity determines the release of erythropoietin and other hormones, called growth factors. Erythropoietin is known to inhibit erythroid progenitor apoptosis [60] and to stimulate

immature erythroid progenitor self-renewal [99, 112]. Other hormones, like glucocorticoids [14, 45, 46, 84], also increase erythroid progenitor self-renewal by activating Erk.

The simplified system of Erk-Fas interactions considered as the main regulatory network for erythroid progenitor fate is then [29]

$$\frac{dE_i}{dt} = (\alpha(Epo, GF) + \beta E_i^k)(1 - E_i) - aE_i - bE_iF_i, \tag{3.1}$$

$$\frac{dF_i}{dt} = \gamma(F_L)(1 - F_i) - cE_iF_i - dF_i, \tag{3.2}$$

where E_i and F_i denote intracellular normalized levels of Erk and Fas, respectively, in the i-th cell (numbering of cells is related to the discrete off-lattice model). Intracellular concentration E_i and F_i are supposed to be uniform inside the i-th cell. They depend on time and independent of space. Their values can be different in different cells. Equation (3.1) describes how Erk level evolves toward maximal value 1 by activation through hormones (function α of erythropoeitin, denoted by Epo, and other growth factors, denoted by GF) and self-activation (parameters β and k). In the meantime, Erk is linearly degraded with a rate a and is inhibited by Fas with a rate bF. Erythropoietin concentration depends only on time.

Equation (3.2) is very similar, only there is no proof for Fas self-activation. Fas is however activitated by Fas-ligand extracellular concentration, denoted by F_L, through the function $\gamma(F_L)$, it is degraded with a rate d and inhibited by Erk with a rate cE. Fas-ligand concentration depends on time and space.

This model simply describes a competition between two proteins (Erk and Fas) through cross-inhibition, self-activation (only for Erk), and activation by extracellular proteins.

In order to explore the parameter space efficiently and observe the possible behaviors of the cell, it is relevant to study the mathematical interpretation of parameters.

3.1.1.2 Brief Analysis : Existence and Stability of Steady States

For fixed values of Epo, GF and F_L, (3.1)-(3.2) is a closed system of ordinary differential equations. In order to analyze the impact of each parameter on the system's behavior, we can derive analytical forms of the zero-lines associated with each equation. The zero-line f associated with equation (3.1) is

$$f(E) = \frac{1}{b}\left(\frac{\alpha}{E} - \beta E^{k-1}(1 - E) - (a + \alpha)\right). \tag{3.3}$$

The zero-line g associated with equation (3.2) is

$$g(E) = \frac{\frac{\gamma}{c}}{\frac{\gamma + d}{c} + E}. \tag{3.4}$$

The shape of the zero-lines depends only on 4 and 2 parameters respectively (α/b, β/b, k and a/b for f, γ/c and d/c for g), the 2 remaining parameters (b and c, related to cross-inhibition) only affecting the absolute and relative speeds of the dynamics along each dimension. The existence of steady states, defined as intersections of the two zero-lines, thus only depends on the former 6 parameters.

Let us stress out that α represents the influence of external factors (erythropoietin, growth factors) on Erk activation, β is related to Erk self-activation, and γ describes the influence of Fas-ligand on Fas activation.

By considering that f can be separated in 3 components, the impact of each parameter can easily be observed. The same can be done for g. Figure 3.1 shows that the variations of the zero-lines are quite constrained, with a central role of α and β for f and γ for g. This will be studied in further detail in the following.

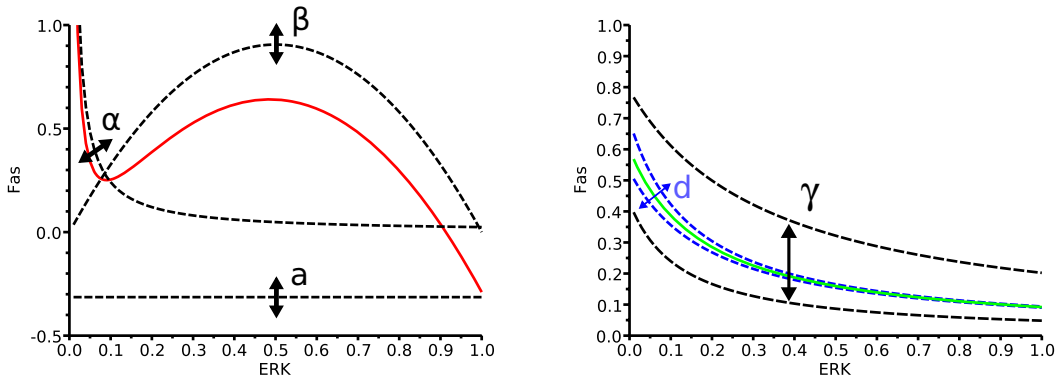

FIG. 3.1 – Zero-lines f and g defined in (3.3) and (3.4). Left panel : the f zero-line (straight red line) and the impact of parameters of equation (3.1). Right panel : the g zero-line (straight green line) and the impact of parameters of equation (3.2).

One may note that the effect of k is not shown here, since $k = 2$ in all experiments. It is however noticeable that increasing k simply decreases the maximum value of the polynomial part of f toward 0 while increasing the value for which it is reached toward 1.

Simple considerations show that the zero-lines can only cross in the $[0, 1] \times [0, 1]$ domain. Furthermore, they intersect at least once, so there is at least one steady state, and there can be only up to three steady states. When there is only one steady state, it is stable. When there are three steady states, the central point is unstable and the two surrounding points are stable [29]. The case with two steady states is singular so it is not really relevant.

Hence, the system exists in two configurations that we will call monostable (one stable state) and bistable (two stable states). The next step is to determine how the system can go from one state to the other one. Thanks to Figure 3.2, two kind of bifurcations can be imagined to achieve this goal.

Let first start with the case where β is large compared to α, this means Erk self-activation rate is stronger than external activators (Epo for instance). In this case, f has two local

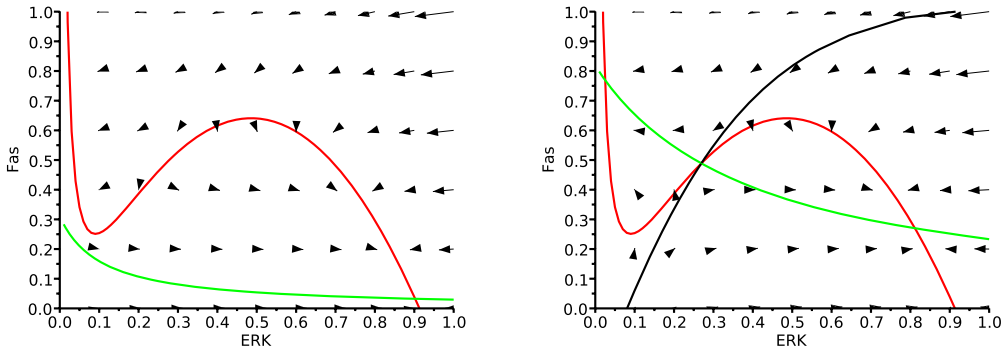

A B

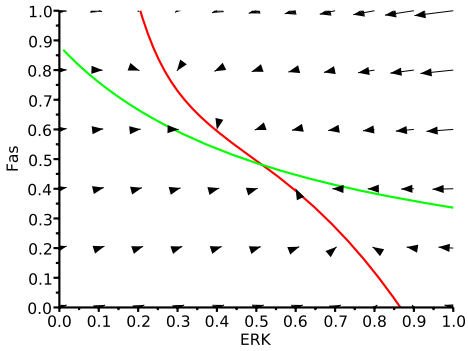

C

Fig. 3.2 – Three possible and characteristic configurations of the system (3.3)–(3.4). The red line represents the f zero-line, the green line the g zero-line. Arrows indicate directions of the solutions of system (3.1)–(3.2) in the (Erk,Fas) phase plane. A : Low value of α, low value of γ. B : Low value of α, medium value of γ (the black curve is the separatrix). C : High value of α compared to β.

extrema (Figure 3.2.A). If γ, which is associated with Fas-ligand, varies then a double saddle-point bifurcation (or fold bifurcation) occurs. For low and high values of Fas-ligand (that is low and high values of γ, respectively), there is only one stable steady state, whereas for medium values of Fas ligand two stable points coexist, a separatrix determining the attractive domain of each point (Figure 3.2.B).

Now consider the case where α is large compared to β. Then f becomes strictly decreasing and, if α is sufficiently large, there will be only one steady state for every value of γ. The system is thus strictly monostable (Figure 3.2.C).

Finally, the system (3.3)–(3.4) exists in two different cases : when α is low it is locally bistable, depending on the value of γ, and when α is high, it is strictly monostable. A kind of fork bifurcation occurs when α increases (approximately around $\alpha = \beta/27$, but exact value depends on other parameters and is quite difficult to obtain).

3.1.1.3 Dynamics of the ODE System

Let us focus on the possible dynamics of the system (3.1)–(3.2). This system must be able to divide the erythroid progenitor cell population into 3 different types : self-renewing, apoptotic and differentiating cells. Differentiation corresponds to low values of Fas and Erk at the end of the cycle, apoptosis to high values of Fas and self-renewal to high values of Erk and reasonable values of Fas.

A simple idea to achieve such a behavior is to introduce two threshold values. The first one, F_{cr}, induces apoptosis when reached. The second one, E_{cr}, determines the choice between self-renewal and differentiation for cells reaching the end of their cycle. So the phase plane of system (3.1)–(3.2) can be divided in three parts : cells having low Erk and Fas values differentiate at the end of their cycle, cells having Erk values greater than E_{cr} self-renew at the end of their cycle and cells reaching Fas values greater than F_{cr} die immediately by apoptosis.

In order to get three robust cell subpopulations, it is necessary to determine how to correctly place these thresholds. Therefore, cases where the system is either strictly monostable or locally bistable have to be considered.

Let us recall that the position of the f zero-line strongly depends on parameters α and β, whereas the position of the g zero-line strongly depends on the parameter γ. Since β denotes the self-activation rate of Erk and α represents a feedback control by global factors (this will be developed later in Section 3.2), then all erythroid progenitor cells will obey the same evolution rule for Erk. On the contrary, γ represents a feedback control by a local factor (Fas-ligand emitted by reticulocytes and acting at short-range, see Section 3.1.2) so all cell positions on the phase-plane will depend on their own exposition to Fas-ligand.

If the system is strictly monostable, then, independently from its starting position in the (E, F)-plane, a cell will converge toward a unique stable state, located on the f zero-line and defined only by its exposition to Fas-ligand (the value of γ). So, at steady-state, if cells are exposed to a continuum of Fas-ligand values, they will be continuously located along the f zero-line, and their level of Erk will not change : there is no real subpopulation. It is

thus quite inefficient to work at steady-state (lack of robustness) to get three subpopulations corresponding to the three possible cell fates.

On the contrary, if the system is locally bistable, cells will still be asymptotically located along the f zero-line, yet a part of it is unstable (roughly speaking the ascending part, see Figure 3.1) so cells will be separated into two subpopulations. In this case, the starting point is important : depending on where it is compared to the separatrix in the bistable domain, a cell will converge either toward the upper or the lower stable branch of f.

Based on these observations, we considered two different initial conditions and dynamics to get the three subpopulations.

The first idea is that, if working at steady-state does not allow to obtain distinct subpopulations, then working out of steady-state may be relevant. Consequently, in a first scenario called the 'out of equilibrium case', all cells are arbitrarily put at the origin (that is $E = 0$ and $F = 0$) at the beginning of their cycle (see Figure 3.3, left) and, before they have reached steady-state, they are forced to take a decision based on Erk and Fas levels.

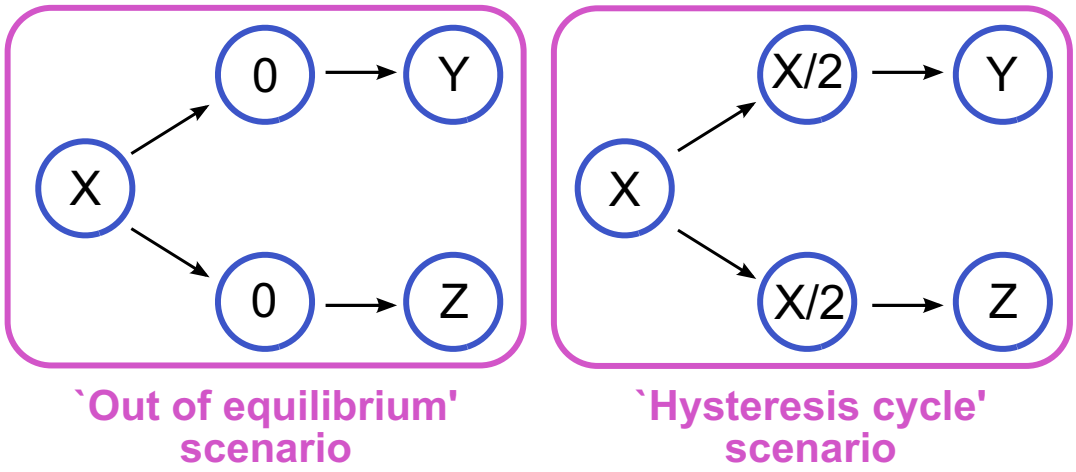

Fig. 3.3 – Schematic representation of the two scenarii considered for distribution of Erk and Fas quantities at cell division. The left panel illustrates the 'out of equilibrium' case, the right panel the 'hysteresis cycle' case. In the 'out of equilibrium' scenario a cell with a level $X = (E, F)$ of Erk and Fas at mitosis gives birth to two daughter cells with no Erk and no Fas ($(E, F) = (0, 0)$). These cells will in turn reach different levels of Erk and Fas at the end of their own cell cycles (provided that they do not die), denoted by Y and Z. In the 'hysteresis cycle' scenario, a cell with a level $X = (E, F)$ of Erk and Fas produces two daughter cells with levels $X/2 = (E/2, F/2)$ which will reach a priori different levels of Erk and Fas at the end of their own cell cycle, due to stochasticity and response to signaling.

In the case where the system is strictly monostable, this solution is nevertheless not satisfactory (no subpopulation appears because cells remain very close to each other). However, when the system is locally bistable, cells will converge either toward the lower stable branch or the upper stable branch of the f zero-line. For a given value of Fas-ligand, the separatrix will cut the origin, so there is a clear threshold between the two states. Even if there is still

a continuum of cells on the phase plane for continuous values of exposition to Fas-ligand, two denser groups appear. In fact, cells exposed to high Fas-ligand values quickly converge toward the top, cells exposed to low Fas-ligand values toward the bottom-right and those exposed to medium values remain trapped near the origin in a 'slow' zone around the separatrix. The latter cells keep low Erk and Fas values, so by introducing the thresholds, three subpopulations are easily obtained (Figure 3.4).

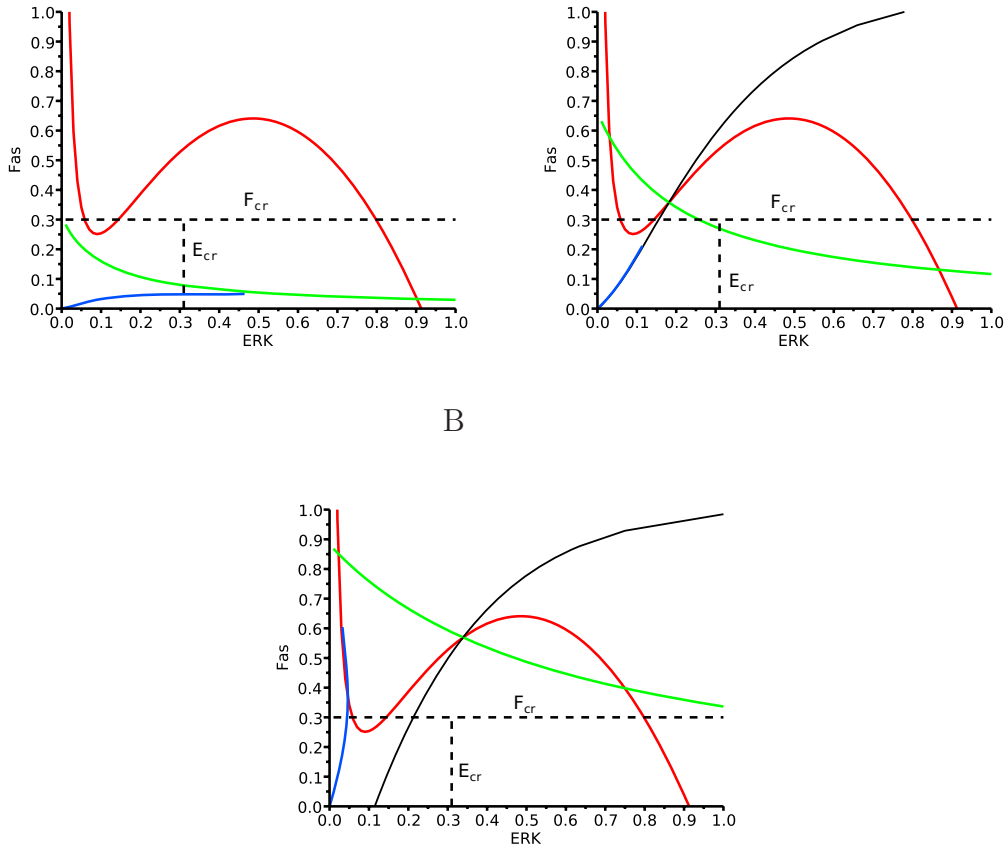

FIG. 3.4 – Illustration of the 'out of equilibrium' hypothesis. All daughter cells are initially placed at the origin of the (Erk,Fas) plane and, depending on the external Fas-ligand value, try to escape the default differentiation zone (bottom left area) into apoptosis (above the dashed F_{cr} line) or self-renewal zone (bottom right area) before the end of their cycle. Trajectories from the origin are illustrated by the straight blue curve. A : Low exposure to Fas-ligand leads to self-renewal. B : Medium exposure to Fas-ligand leads to differentiation. C : High exposure to Fas-ligand leads to apoptosis.

The second idea is that working at steady-state is more robust. When the system is locally bistable, one notices that cells on the lower stable branch are those which will self-renew

(high values of Erk, reasonable values of Fas). If quantities of Erk and Fas are equally divided between the two daughter cells at birth, those exposed to medium values of Fas-ligand will appear near the separatrix and be divided between the upper branch (differentiation/apoptosis) and the lower branch (self-renewal). We thus have a system where cells rapidly take the decision between self-renewal or differentiation/apoptosis. Once the decision is made, cells are trapped on a hysteresis cycle controlled by Fas-ligand, so the decision is hardly reversible. Fas values have to become very high in order to get from the lower branch to the upper branch and conversely, very low in the opposite direction (Figure 3.5).

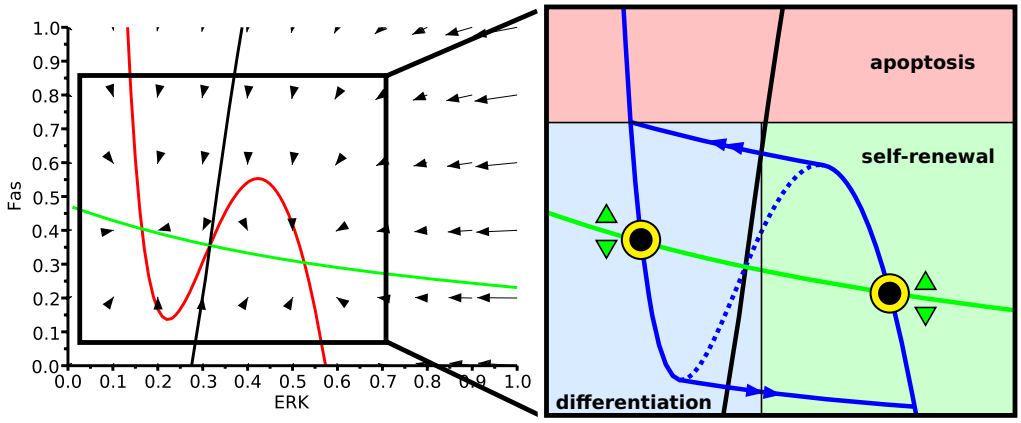

Fig. 3.5 – The 'hysteresis cycle' scenario. Daughter cells initially inherit half of their mother's protein level, 'choose' one of the stable branches depending on their exposition to Fas-ligand, and then move on these branches which form an hysteresis cycle, making the decision hardly reversible. Shown with yellow circles are the two possible positions for newborn cells exposed to exactly the same value of Fas-ligand on the hysteresis cycle. One can see how the initial choice is important : cells whose mother had low Fas values will be located on the lower branch, those whose mother had sufficiently high Fas values will switch to the upper branch.

For this solution, called 'hysteresis cycle case', introducing thresholds in order to determine cell fate is quite simple. The Erk threshold can be situated anywhere between the two branches and the Fas threshold somewhere on the upper branch, cutting into two the cells on this branch and so easily controlling the differentiation/apoptosis ratio.

The 'out of equilibrium' and the 'hysteresis cycle' scenarii are schematically described in Figure 3.3.

3.1.1.4 Feedback Control Role

A key point in system (3.1)–(3.2) is how it reacts to feedback controls. The analysis performed in the previous subsections dealt with the influence of each parameter on the system dynamics, mainly parameters related to feedback controls (α and γ). Let now study how parameters are affected by feedback controls. Erythropoietin (through function α) is expected to decrease apoptosis and enhance self-renewal/differentiation. We also know that,

at a smaller space scale, Fas-ligand induces apoptosis (through function γ) and other growth factors, on the opposite, stimulate self-renewal (through the function α).

In order to validate possible dynamics, the effect of each factor must be checked in both cases, the 'out of equilibrium' and the 'hysteresis cycle' scenarii.

The control exerted by Fas-ligand, which increases the value of Fas reached at steady-state, has already been largely discussed. Simply by existence of the threshold F_{cr}, Fas-ligand plays the expected role. Fas-ligand is linked to the parameter γ, which is actually a function of F_L.

Epo is known to have a direct action on apoptosis [60], independent of Erk pathway [30, 80, 114]. Therefore, a simple idea is to increase F_{cr} with the level of Epo. This clearly reduces apoptosis in favor of differentiation and self-renewal. However, it is also known that Epo, and other growth factors, activate Erk. So erythropoietin and growth factors are supposed to influence the variations of α. It is noticeable that at a local scale, many growth factors are supposed to have similar mechanisms, so α should in fact be a function of many global and local growth factors.

The value of α controls the monostable/bistable bifurcation (Figure 3.1). When the system is locally bistable, α mainly controls the value of the local minimum of the f zero-line. In the case where we work out of equilibrium, α changes the position of the separatrix and of the upper steady states, so when α is increased the separatrix cuts the origin for a higher value of $\gamma(F_L)$ and cells tend to be displaced toward steady-states with lower values of Fas and higher values of Erk. In the case where the hysteresis cycle is used, increasing the local minimum of f reduces the size of the cycle. Cells located on the upper stable branch instantly 'fall' on the lower stable branch, so self-renewal is immediately enhanced and differentiation reduced.

The effect of α is not the same in both dynamics, but finally it is clearly possible to decrease apoptosis in favor of self-renewal/differentiation and the trends for each protein is roughly what is expected biologically. However, it is still necessary to study whether the feedback is as efficient as observed experimentally, when the intracellular scale is coupled to the extracellular one (see Section 3.2).

3.1.2 Extracellular Scale

In the previous section, we focused on the intracellular scale of the hybrid model, based on a system of ordinary differential equations describing competition between two key proteins, Erk and Fas. Concentrations of Erk and Fas induce either cell self-renewal, or differentiation, or death by apoptosis. We now focus on an other layer of the hybrid model, the discrete part, which describes how cells interact and how they influence intracellular parameters which depend on extracellular molecules.

In order to describe the evolution of an erythroid cell population, we chose to use an individual-based model. All cells and their interactions are then numerically computed. The objective being to represent erythroblastic islands, which have a limited size, such an approach takes automatically into account small population effects as well as random effects

(direction of division, cell cycle length).

A population of cells is numerically simulated in a 2D computational domain which is a rectangle. Each cell is a discrete object, an elastic ball, considered to be circular and composed of two parts : a compressible part at the border and a hardly compressible part at the center. All newborn cells have the same radius r_0 and linearly increase in size until the end of their cycle, when they reach twice the initial radius. When a cell divides, it gives birth to two small cells side by side, the direction of division being randomly chosen. The cell cycle duration is itself variable. From a biological point of view, cell cycle proceeds through G_0/G_1, S, G_2 and M phases. Duration of the first G_0/G_1 phase and transitions between phases are controlled by various intracellular and extracellular mechanisms, inducing stochasticity in cell cycle durations [49, 100]. We assumed the duration of G_0/G_1 phase is a random variable with a uniform distribution in some given interval, other phase durations were supposed to be constant.

Under the assumption of small deformations, the force acting between cells can be expressed as a function of the distance between their centers. The force between two particles with centers at x_i and x_j is given by a function $D(d_{ij})$ of the distance d_{ij} between the centers. This function is zero if the distance is greater than the sum of their radii. To describe the motion of a particle, one should determine the forces acting on it from all other particles and possibly from the surrounding medium. The motion of each cell is then described by the displacement of its center by Newton's second law :

$$m\ddot{x} + \mu m\dot{x} - \sum_{j \neq i} D(d_{ij}) = 0, \tag{3.5}$$

where m is the mass of the particle, the second term in left-hand side describes the friction by the surrounding medium, the third term is the potential force between cells. The force between two spherical particles is considered in the form

$$D(d_{ij}) = \begin{cases} K\dfrac{d_0 - d_{ij}}{d_{ij} - d_0 + 2H_1}, & d_{ij} < d_0, \\ 0, & d_{ij} \geq d_0, \end{cases} \tag{3.6}$$

where d_0 is the sum of cell radii, K is a positive parameter, and H_1 accounts for the compressible part of each cell. The force between the particles tends to infinity when d_{ij} decreases to $d_0 - 2H_1$. On the other hand, this force equals zero if $d_{ij} \geq d_0$.

Three cell types are computed. First, erythroblasts, which are immature erythroid cells, also known as erythroid progenitors. They follow the growth rules explained above and their fate is determined as described in Section 3.1.1. They either self-renew and give two cells of the same type, or differentiate and give two differentiated cells (reticulocytes), or die by apoptosis, depending on their exposition to growth factors and Fas-ligand. It is noticeable that no asymmetric division is considered in this model.

Second, reticulocytes. From a biological point of view, reticulocytes are almost mature red blood cells that leave the bone marrow and enter the bloodstream after ejecting their nuclei.

In this individual-based model, they are differentiated cells which stay in the bone marrow a little while after being produced, and leave the bone marrow (computational domain) after a time equal to one cell cycle duration. Contrary to erythroblasts, reticulocytes do not have a choice to make, they only express Fas-ligand, thus influencing the development of surrounding erythroblasts.

Third, macrophages. They are big white blood cells located at the center of erythroblastic islands. They very probably have an active role in the development of blood cells surrounding them. In this model, they express growth factors, driving nearby erythroblasts toward differentiation and self-renewal.

Macrophages express growth factors that are supposed to diffuse in their neighborhood. Reticulocytes express Fas-ligand on their surfaces which does not diffuse in a real bone marrow, yet the expression of Fas-ligand is modeled by short-diffusion. This allows considering several phenomena that are not taken into account in the hybrid model : first, cell motion in the bone marrow is actually more important than computed and, second, there are normally several maturing erythroid subpopulations which increasingly express Fas-ligand, creating a gradient of exposition. Moreover, cells are not circular in reality and this short-range diffusion compensates their inexact representation. Both Fas-ligand (F_L) and growth factor (GF) concentration evolutions are described with the following reaction-diffusion equations,

$$\frac{\partial F_L}{\partial t} = D_{F_L}\Delta F_L + W_{F_L} - \sigma_{F_L}F_L, \tag{3.7}$$

$$\frac{\partial GF}{\partial t} = D_{GF}\Delta GF + W_{GF} - \sigma_{GF}GF, \tag{3.8}$$

where $W_{F_L} = k_{F_L}C_{ret}$ is a source term depending on the number of reticulocytes (C_{ret} denotes the relative volume of reticulocytes in the computational domain) and W_{GF} is a constant source term for growth factor (released by the macrophage) concentration, σ_{F_L} and σ_{GF} are degradation rates, and D_{F_L} and D_{GF} are diffusion rates. If the diffusion coefficient D_{F_L} is sufficiently small, then Fas-ligand is concentrated in a small vicinity of reticulocytes. In this case, Fas-ligand influences erythroid progenitors when they are sufficiently close to reticulocytes. This is the short-diffusion illustrated in this work.

Figure 3.6 shows an example of erythroblastic island in the hybrid model. The big green cell in the center is a macrophage, the green substance surrounding it is the above mentioned growth factors released by the macrophage. At the border, blue cells are reticulocytes emitting Fas-ligand (whose concentration is represented in red). Between them are the erythroblasts, growing in size until they die or divide into two new cells, depending on how they were influenced by the two diffusing proteins.

A fourth cell type, erythrocytes, is considered in this model. Biologically, erythrocytes are mature reticulocytes, circulating in blood and transporting oxygen to the organs. In the model, erythrocytes are reticulocytes that have spent a time equal to one cell cycle in the computational domain and then left it. Hence, erythrocytes are only counted as cells outside the domain (they are not represented on the computational domain) which act, through feedback loops, on the fate of immature cells within the domain. We will assimilate

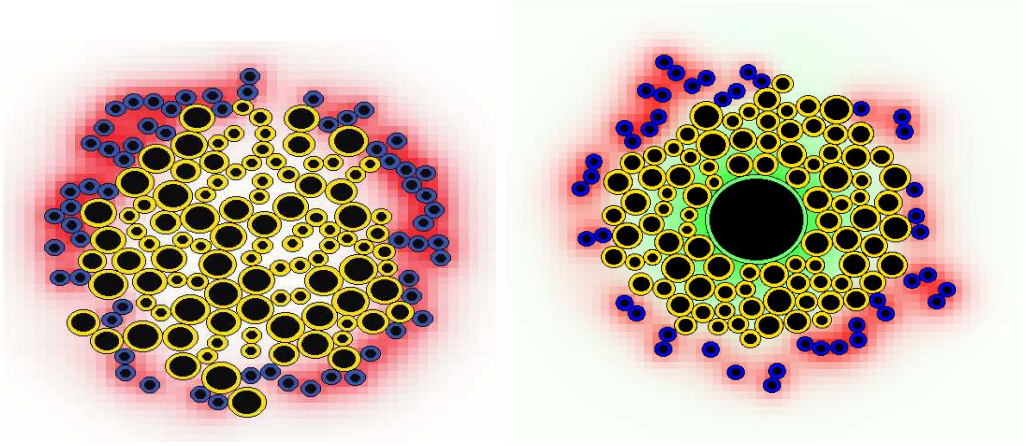

Fig. 3.6 – Screenshots of the software program with and without macrophage. The green cell is a macrophage, yellow cells are immature cells (erythroblasts) and blue cells are differentiated cells (reticulocytes). The green substance is secreted by the macrophage (growth factors) and the red substance by reticulocytes (Fas-ligand). In each cell, the black area represents the incompressible part of the cell.

erythrocytes and red blood cells (RBC) in the following, by considering that RBCs are only erythrocytes (in reality, some reticulocytes usually manage to leave the bone marrow and enter the bloodstream where they end their maturation, so they are also red blood cells). Erythrocytes will be supposed to survive (arbitrarily) during a time corresponding to 3 cell cycle durations (although RBCs do not cycle). This is short, since in mice RBCs have a lifespan of 40 days, yet it allows performing a first feedback test and it can be changed when comparing the model to experimental data.

3.1.3 Coupling Both Scales

Now that both modeling scales have been described and a general picture of the model is accessible, it becomes necessary to detail how the two scales can be linked together. At the highest level, there is a small erythroblastic island formed with two populations of developping red blood cells and, optionally, a central macrophage. The island has a particular topology : the macrophage is at the center, differentiated cells (reticulocytes) at the border and immature cells in between. Both macrophage and differentiated cells emit growth factors continuously controlling intracellular protein concentrations : immature cells at the center are rather exposed to growth factors produced by the macrophage whereas those at the border are rather exposed to Fas-ligand. In addition, immature cells are subject to a feedback control mediated by mature red blood cells circulating in the bloodstream, representing the action of erythropoietin. Concentration of Epo in the computational domain is supposed to be uniform, so all cells are similarly influenced by Epo. This assumption holds true for all external substances acting on cells at a global scale, yet other more sophisticated choices are

possible.

Erythroid progenitors are then exposed to a continuum of erythropoietin Epo, growth factors GF and Fas-ligand F_L. Regarding the intracellular scale, this means that α and γ take continuous values (see (3.1)–(3.2)). Let us remind that high α drives erythroblasts to self-renewal, high γ to death, and intermediate values to differentiation. Hence, the cell population scale influences the intracellular scale through Epo, growth factors and Fas-ligand concentrations, that is through functions α and γ and the critical value F_{cr} of Fas concentration (Epo increases F_{cr} in order to inhibit cell apoptosis).

One can notice that when there is no macrophage, there is only one value of α for all erythroblasts (this value depends on the concentration of Epo which is related to the number of erythrocytes, and is supposed to be the same for all immature cells), so cells are simply situated along a unique f zero-line. It is then convenient to investigate how the value of γ will determine a cell's choice (see Section 3.1.1.4).

As just mentioned, Epo-mediated feedback control simply corrects the critical value for apoptosis F_{cr} and values of α uniformly, so its impact can be easily understood individually by referring to the analysis in Section 3.1.1.4. However, in order to compute this feedback control, the number of erythrocytes in blood circulation must be estimated. This is performed from the reticulocyte population as mentioned at the end of the previous section.

3.2 Results : Stability of Erythroblastic Island and Function of Central Macrophage

In the previous section, the hybrid model has been presented in details. The applicability of such a modeling will be investigated in this part. To do so, we focus on finding conditions (parameter values, that are partially discussed in Appendix 3.3) for the system leading to stable erythroblastic islands (this means the number of cells in the island stays almost constant for a certain time when not facing a perturbation), reacting sensibly to global feedback variables (for example in the case of anemia) and proving to be robust to parameter values variations.

We begin by investigating the case of one erythroblastic island without macrophage in its center. The case of the island with a macrophage is then considered to see how the stability of the island is affected. For these analyses, simple numerical stability and feedback tests were performed to check the validity of hypotheses.

3.2.1 Erythroblastic Island without Macrophage

Consider an island initially composed of 98 erythroid progenitors and 64 reticulocytes surrounding them. Parameters are carefully chosen to optimize stability and response to feedback (see Appendix 3.3).

3.2.1.1 Stability Analysis

Erythroblastic islands are likely to be stable. Indeed, one can expect that, in order to be biologically responsive, an island survives for several cell cycles. It is relevant to determine whether it is mathematically possible to achieve long-lasting stability with the hybrid model or not.

A wide range of parameters has been tested for the two possible dynamics, that is either out of equilibrium or with the hysteresis cycle. At first, the best results look like quite similar (Figure 3.7). In both cases, the island remains approximately stable during some cycles but, due to stochastic variations (cell cycle duration, orientation of the mitotic spindle at division, small size populations), it suddenly dies out or excessively proliferates (it must be noticed that saturation is only due to space limitations). Two questions arise from this fact : why does the system behave this way and is it still biologically relevant ?

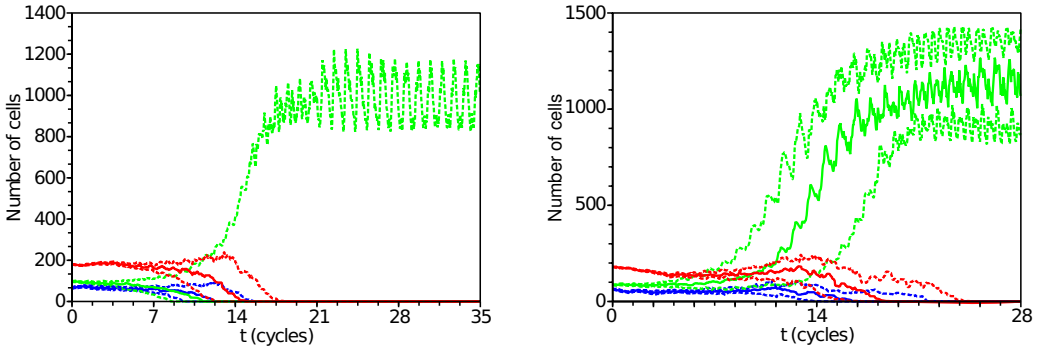

Fig. 3.7 – Illustration of the fate of the most stable erythroblastic islands in the absence of macrophage. Results were obtained out of equilibrium (left) and using the hysteresis cycle (right). Green lines represent the number of erythroblasts, blue lines reticulocytes, red lines estimation of circulating red blood cells produced by the island (thick lines are medians, thin lines quartiles over 40 simulations). Observed saturation is only due to space limitation.

Let's focus first on the mechanisms leading to an island's stability. In the simulations, during each cycle there is a turnover of reticulocytes, in order to replace those which entered bloodstream. These reticulocytes then induce apoptosis and differentiation in the erythroblast population. Within this population, in order to remain stable, the proportion of self-renewing erythroblasts has to be constant. From a geometrical point of view, self-renewing erythroblasts are located at the center of the erythroblastic island, differentiating and dying erythroblasts at the border (Figure 3.6). When a random variation occurs in the size of the island, the amount of the differentiating and dying cells varies like the perimeter of the circle (occupied by reticulocytes which act at constant range), while the amount of self-renewing cells varies like the area of the circle. As a result, the ratio 'differentiating and dying cells' over 'self-renewing cells' does not remain constant. When it derives too far from the initial value, one subpopulation rapidly overgrows the other.

It appears then that it is impossible to find parameter values for which an island would remain at steady-state on a long term. However, this does not imply that results are biologically irrelevant. The fact that islands die in this model is not really surprising since, biologically, there might be a turnover of these structures and erythroid progenitors permanently arise from the differentiation of hematopoietic stem cells, which has been neglected here. Also, proliferation is not as dramatic as it might seem. First, it is possible to turn it down by varying parameters (but sacrificing instead the average lifetime of an island) and also proliferation may not be that simple in a realistic environment. Indeed, there is no obstacle in the computational domain and some particular geometries could clearly reduce variations in the proportion of self-renewing cells. Another point is that when several islands are side-by-side, proliferating islands will collide and be in contact with more reticulocytes than before, which may block their growth (data not shown). Nevertheless, unstable islands revealed hard to control and stability of islands should be expected, as previously mentioned.

Regarding the two possible dynamics, either out of equilibrium or hysteresis cycle, stability of the system at equilibrium (hysteresis cycle) is slightly better (Figure 3.7 right). Moreover, a significant fact arose during experiments when distribution of cell cycle lengths was varied : the dynamics at equilibrium is very robust in this case, whereas the other dynamics becomes clearly biased. Indeed, when cells are placed at the origin at the beginning of their cycle, they start in the differentiating area. When their cell cycle length is short, they do not have enough time to escape this area and differentiate. When cell cycle duration is long, they cannot differentiate. Consequently, some cell fates are only decided because of cell cycle length, independently of the position in the erythroblastic island, and the island structure is quickly lost. In conclusion, since cell cycle length variation may be large [49, 100], it was decided to abandon this 'out of equilibrium' dynamics and to perform further tests with the dynamics using the hysteresis cycle (Figure 3.3, right panel).

3.2.1.2 Feedback Relevance and Relation to Stability

The above-described hybrid system should be clearly influenced by feedback control loops, as expected biologically, and, besides, feedback loops may play a role in the stabilization of erythroblastic islands.

As mentioned in Section 3.1.1, different feedback controls are considered in this model : a local control through Fas-ligand, activating Fas and influencing erythroblast differentiation and death by apoptosis ; two global feedback controls by erythropoietin, one activating Erk through the function α, the second one varying the critical value of Fas, namely F_{cr}, inducing apoptosis. We focus here on the global feedback control mediated by Epo.

It is known that increasing Epo levels in the bloodstream, and consequently in the bone marrow, increases Erk activity and decreases erythroblast apoptosis rate. Hence, an increase of Epo levels induces an increase in the values of both α and F_{cr}. The exact influence of Epo on these two quantities is however not known. Therefore, we began by simply monitoring the behaviour of one island under constant values of these two parameters around the default value (Figure 3.8).

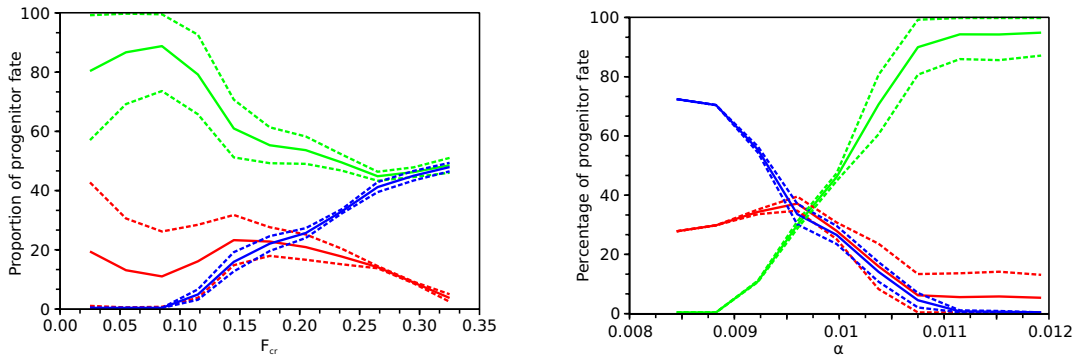

Fig. 3.8 – Effect of feedback controls on progenitor subpopulations in the absence of macrophage in the island. Each curve represents the percentage (means ± standard deviation) of self-renewing (green), differentiating (blue) or apoptotic (red) erythroblasts during the first five cell cycles, as function of F_{cr} (left panel) and α (right panel).

By comparing the proportions of different erythroblast subpopulations (self-renewing, differentiating and apoptotic populations) during the first 5 cycles, it appeared that an increase of F_{cr} (that is, an increase of Epo levels) decreases apoptosis and self-renewal in favor of differentiation. For low values of F_{cr}, there is no differentiation (erythroblasts at the center of the island survive, others die), so the island proliferates by absence of death factors. For higher values, effect on self-renewal can be tuned by modifying parameters controlling the hysteresis cycle. At some point the self-renewing population is not affected anymore and there is simply a transfer from the apoptotic subpopulation to the differentiating subpopulation (the differentiation part of the differentiation/apoptosis branch increases).

Increasing α, on the contrary, mainly acts on the self-renewing population. An increase of α sends all cells on the self-renewing branch of the hysteresis cycle and differentiation/apoptosis disappears. Reducing α increases the size of the apoptosis/differentiation branch. For a constant value of F_{cr}, only the differentiation part of this branch is increased. One thus observes a transfer from the self-renewing branch to the differentiation part of the other branch.

In conclusion, the system's response is qualitatively what is expected. Epo mainly decreases apoptosis in favor of differentiation and stimulates self-renewal. However, the statistics computed above only indicate trends and it is important to see how islands actually react to this feedback.

The next step is then to explicitly include feedback loops in the system's equations to see whether the response is quantitatively correct or not, and if it is possible, through feedback controls, to achieve a better stability than before. Therefore, we assumed a linear variation of both α and F_{cr} with deficiency of red blood cells (RBC), hence implicitly describing the dependency on Epo. Denoting by N_{RBC} the number of circulating red blood cells, and since

a decrease of RBC count induces an increase in Epo levels, one gets

$$\alpha := \alpha(N_{RBC}) = \alpha_0 + k_\alpha(N_{target} - N_{RBC}), \tag{3.9}$$

$$F_{cr} := F_{cr}(N_{RBC}) = F_0 + k_F(N_{target} - N_{RBC}). \tag{3.10}$$

We remind that N_{RBC} is estimated by the number of reticulocytes which have left bone marrow and are supposed to survive during a time equivalent to 3 cell cycles. N_{target} is the number of RBCs in circulation during a typical run before proliferation/extinction of the island. Parameters α_0 and F_0 are 'typical' values of α and F_{cr} (as given in Appendix 3.3). Parameters k_α and k_F are to be estimated.

It must be mentioned that these two feedback controls are not exact from a biological point of view, since one would expect the functions to saturate for low and high values of N_{RBC}, yet they are good approximations when the number of red blood cells is not too far away from the target (for instance, in normal erythropoiesis).

Functions α and F_{cr} in (3.9) and (3.10) were used together with the previous initial conditions (hysteresis cycle case), and it was impossible to achieve better stability than previously mentioned when varying the values of k_α and k_F (data not shown). To be more precise, it was possible with strong feedback controls to stop proliferation, instead the island systematically died out. Other tests, based on simulations of a constant number of red blood cells (N_{RBC}), showed that the effect of feedback controls was not fast enough to deal with the quick proliferation and extinction of erythroblastic islands. The island still lived around 10–15 cycles and, when it began to expand or die out, feedback response came too late or was too strong to bring it back to its ideal size. Therefore, what was observed was only the usual destabilization of the island, feedback being only able to turn proliferation into extinction after some cycles.

As a result, it is very difficult to test feedback reliably on unstable islands. However, the study showed that global feedback loops are inefficient when it comes to controlling local structures, since proliferation or extinction events occur quickly in the model.

In the next section, we consider the addition of a macrophage in the center of the island on the stability of the island and the relevance of feedback controls.

3.2.2 Island with macrophage

In this case, an erythroblastic island is initially composed of one macrophage, 80 erythroid progenitors and 64 reticulocytes (see Figure 3.6, right). As done in the previous section, stability of the island and influences of feedback controls are investigated.

In addition to feedback controls exerted, in the previous section, on erythroblast dynamics by Epo and Fas-ligand, the macrophage in the center of the island is supposed to release growth factors, whose concentration is denoted by GF, which positively act on Erk activation. A number of proteins associated with the proliferation of erythroid progenitors and that could fulfill such a function have been described. This includes Stem Cell factor (SCF), the c-kit ligand, Ephrin-2, the EphB4 ligand, and BMP4, a member of the TGFβ family ([95] and

references therein). All those growth factors are assumed to diffuse around the macrophage as developed in Section 3.1.2 (Equation (3.8)). They trigger erythroblast self-renewal through the function α : the more growth factors, the higher α. Function α now becomes

$$\alpha := \alpha(N_{RBC}, GF) = \alpha_0 + k_\alpha(N_{target} - N_{RBC}) + k_{GF}GF. \tag{3.11}$$

Meaning of parameters α_0, k_α and N_{target} is identical to the ones defined for (3.9). Values are also the same, except for α_0 that had to be decreased to compensate the addition of the term $k_{GF}GF$. Parameter k_{GF} was set accordingly (influence of these parameters are discussed below). Default values are $\alpha_0 = 0\,h^{-1}$ and $k_{GF} = 3\,h^{-1}$.molecule^{-1}.

3.2.2.1 Stability Analysis

Stability of the hybrid system is first investigated without considering global feedback controls (that is, $k_\alpha = 0$ in (3.11) and $k_F = 0$ in (3.10)). Results are illustrated in Figure 3.9.

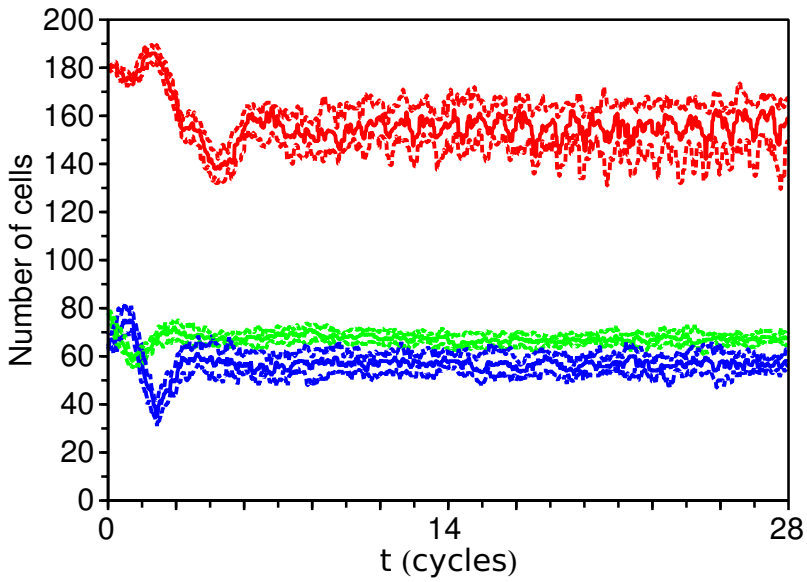

Fig. 3.9 – Number of erythroid cells in the presence of a macrophage in the center of the island. Results were obtained using the hysteresis cycle. Green lines represent the number of erythroblasts, blue lines reticulocytes, red lines estimation of circulating red blood cells produced by the island (thick lines are medians, thin lines quartiles over 40 simulations). After addition of a macrophage, islands automatically stabilize for previously chosen parameters.

For a large range of parameter values, the system quickly converges toward a steady-state. The number of self-renewing and differentiating cells (and thus circulating RBC) can be precisely controled by parameter values, as will be detailed in the next subsection. There is a first phase where the size of subpopulations oscillates (because of lack or abundance of

death factors) yet steady-state is always quickly reached (within a few cycles), even though inherent stochastic oscillations are always present.

The macrophage completely controls the island. If α_0 is sufficiently low, a cell will not be able to self-renew without external growth factors. Therefore, the default behaviour of an isolated cell is differentiation. On the other hand, a cell in contact with the macrophage will be exposed to a very high concentration of growth factors and will always self-renew, since it is generally not exposed to death factors. In the vicinity of the macrophage, there is a competition between growth factors and death factors, which will eventually determine the size of the island. If α_0 or k_{GF} gets higher, growth factors will reach further erythroblasts, thus the size of the final island will increase.

3.2.2.2 Feedback Relevance and Relation to Stability

Now that erythroblastic islands are stable, due to the presence of the macrophage, it is not necessary to be limited to a period of 5 cycles to compare the subpopulations of the island, as was done in the previous case (Section 3.2.1.2). Rather, it becomes relevant to see how the size of the island and the production of RBC could evolve on a long term.

Similarly to what has been done in the previous case, we once again simulated the expected consequences (in terms of steady state value) of feedback control by running simulations under constant values of α and F_{cr}. Results are shown in Figure 3.10.

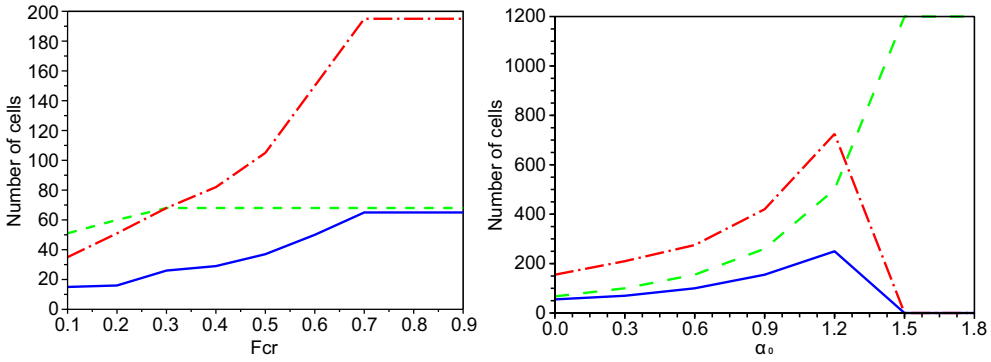

FIG. 3.10 – Impact of feedback controls on steady-state values when the erythroblastic island contains a macrophage. Left panel : Influence of F_{cr} variations ; Right panel : Influence of α variations. Green dash lines represent erythroblast counts, blue solid lines reticulocyte counts and red dash-dot lines RBC counts.

When F_{cr} increases, both the number of reticulocytes and RBC increases, as the differentiation part of the differentiation/apoptosis branch increases. For high values of F_{cr}, there is no apoptosis anymore. The number of erythroid progenitors seems to be rather independent of the value of F_{cr}.

When α increases, which can be seen as an increase of the ground level of global 'surviving factors' (here Epo and macrophage-emitted growth factors), the size of the island increases mainly due to the increase of the self-renewing population. As a result, reticulocytes, situated

all around the island, also increase in number, as does the amount of RBC. However, for very high values of α, surviving signals are so strong that almost all erythroblasts self-renew (the macrophage has no effect anymore) and the island is made only of proliferating cells, reticulocyte and RBC counts vanish. Such high values of α may only be reached in extreme stress situations and mainly create a pool of cells which may afterwards differentiate and substantially increase the number of RBC at once (but this implies that another mechanism has to lower the value of α at some point). In any case, these values of α may else be avoided by adding a saturation effect on the feedback loop.

In each case, a substantial increase of RBC production (about 3-fold and 4-fold respectively) is observed. As the two mechanisms are largely independent, they can be combined and thus the overall production rate can be greatly increased, in magnitudes comparable to what can be observed biologically [27, 95, 107]. This seems to indicate that the reaction of the system with macrophage to feedback controls is more efficient, relevant and easy to observe compared to the case without macrophage, again in good agreement with biological evidences [95].

3.3 Parameter Estimation

We discuss here the parameter values used when investigating stability of the hybrid model in Section 3.2. Some parameters are clearly related to the discrete macroscopic model while some others are related to intracellular dynamics.

Choosing individual-based modelling creates many implicit parameters. Most of them can be chosen quite easily (cell radius, parameters of motion, etc.) and are not essential in the results of simulations. However, other parameters clearly change the overall cell behavior and have to be set carefully.

Let first consider parameters associated with extracellular dynamics (mainly growth factor release and action). Exact quantities of Fas-ligand, Epo and growth factors released by the macrophage are not fundamental, because their effect will be normalized at the intracellular scale (intracellular parameters controlling the sensitivity to these molecules). More important are the diffusion coefficients, for both Fas-ligand and growth factors released by the macrophage. These parameters are chosen in order to describe a short range action of Fas-ligand, and to locate growth factors around the macrophage. It is important that the range of diffusion is set according to the size of the cells in order to have a realistic short-diffusion for instance. The distribution of cell cycle lengths is also really important : it changes how the island expands, how cell cycles are locally correlated and plays a role in the fate of immature cells when we work out of equilibrium. Parameter values are shown in Table 3.1.

Intracellular parameters are chosen in order to optimize robustness of the system. It is noticeable that no experimental data is available to set values of these parameters, only the expected behavior is accessible. Parameters b and c of system (3.1)–(3.2) control the relative and absolute speeds of the reactions. They are set first. The magnitude of the hysteresis cycle can then be tuned by choosing carefully α/b and β/b (these ratios control its height,

Parameter	Value	Unit
Cell cycle length	24	h
Cell cycle variations	4/3	h
r_0	0.01	L
m	1	M
μ	3.10^5	h^{-1}
K	9.10^5	$M.h^{-2}$
D_{F_L}	3.10^{-4}	$L^2.h^{-1}$
k_{F_L}	3.10^{-3}	molecules.cell^{-1}.h^{-1}
σ_{F_L}	0.6	h^{-1}
D_{GF}	3.10^{-3}	$L^2.h^{-1}$
W_{GF}	3.10^{-2}	molecules.$L^{-2}.h^{-1}$
σ_{GF}	0.3	h^{-1}

TAB. 3.1 – Extracellular parameters (M is an arbitrary mass unit, L an arbitrary length unit)

Parameter	Value	Unit
α	0.01	h^{-1}
β	1.5	$h^{-1}.NU^{-2}$
k	2	-
a	0.12	h^{-1}
b	0.414	$h^{-1}.NU^{-1}$
k_γ	0.009	$h^{-1}.NU^{-1}$.molecule^{-1}
c	0.0828	$h^{-1}.NU^{-1}$
d	0.006	h^{-1}
E_{cr}	0.31	NU
F_{cr}	0.3	NU

TAB. 3.2 – Internal parameters when cells begin at the origin ('out of equilibrium' case). NU is a normalized quantity unit for the intracellular molecules (maximum possible quantity is 1).

Parameter	Value	Unit
α	1.62	h^{-1}
β	60	$h^{-1}.NU^{-1}$
k	2	-
a	15.9	h^{-1}
b	1.8	$h^{-1}.NU^{-1}$
k_γ	0.9	$h^{-1}.NU^{-2}$.molecule^{-1}
c	3	$h^{-1}.NU^{-1}$
d	1.5	h^{-1}
E_{cr}	0.3	NU
F_{cr}	0.6	NU

Tab. 3.3 – Internal parameters when cells are on the hysteresis cycle. NU is a normalized quantity unit for the intracellular molecules (maximum possible quantity is 1).

their absolute values its width). Parameter a controls the offset of the cycle and is set such that it is located in the $[0,1] \times [0,1]$ domain. Parameter d mainly controls how a cell goes from a stable branch of the cycle to the other : the higher the value of d, the higher the change in Fas quantity.

In equation (3.2), the function γ explicitly describes the influence of Fas-ligand. This function has been taken as $\gamma = k_\gamma F_L$, where k_γ is the sensitivity of progenitors to Fas-ligand. This linear dependency is chosen for simplicity, in order to avoid introduction of additional parameters. It is a good approximation if the variation of Fas-ligand is small.

Finally, α and F_{cr} also depend on extracellular molecules. However, in what follows we will first consider the case when feedback loops are not included, so α and F_{cr} will be constants first.

When Erk and Fas levels are supposed to be zero when the cell starts its cycle, the speeds of reactions are very important : some cells have to remain trapped near the origin at the end of their cycle in order to observe differentiation. The values of b and c are thus very constrained. The others simply define a large hysteresis cycle which aims at separating the different cell subpopulations as far as possible from each other. See Table 3.2 for values.

When Erk and Fas values are initially on the hysteresis cycle, then b and c are allowed to vary more largely. It has been decided to put quicker dynamics than in the first case in order to get rapid variations along the cycle. The width of the hysteresis cycle was also reduced, so values for α and β are higher. See Table 3.3 for values.

Finally, an initial size for the island has to be set and the number of islands that will be simulated must be chosen. An initial size of 144 cells with central macrophage or 162 cells without macrophage was chosen, and parameters were adjusted to keep the size of the island roughly constant. Therefore, we only simulated one island at the beginning, but once reasonable parameters are found, it is possible to put several islands side-by-side and see how they interact. Preliminary experiments have been performed in this direction (not

shown here), see the end of Section 3.2.1.1.

3.4 Responsiveness of the system to stress situations

We now investigate a response of erythroblastic island to different feedback mechanisms in the case of anemia. Anemia is one of the more common blood disorders, characterized by low levels of healthy red blood cells (RBCs) in the body or less than normal quantity of hemoglobin in the blood. Anemia can be caused either by blood loss, by excessive destruction of RBCs or by decreased or faulty red blood cell production. It can also be either due to a disease or induced.

The nature of induced anemia can be very different, according to the method used to urge it. In the experiment, done by M. Koury [1], the mice were bled 15 microliters of blood per gram of body weight for three consecutive days. After the bleeding on day 3, the mice were allowed to recover. Then 20 microliter samples were taken each day on days 4 to 16 that were tested for hematocrit percentages. Three mice were used in this experiment.

RBCs count is determinant for the release of various growth factors. Erythropoietin production is increased in response to anemia. We consider both erythropoietin influence on erythroid progenitor self-renewal capacity through function $\alpha(N_{RBC})$, and on apoptosis protection through function $F_{cr}(N_{RBC})$. The functions $F_{cr}(N_{RBC})$ and $\alpha(N_{RBC})$ are supposed to be linear (see (3.10)-(3.11)). Parameters k_{alpha} and k_F are chosen to obtain the qualitative correct response to anemia.

To model an anemia we take the erythrocyte count at day 0 that is lower than its equilibrium value. First, we run the test simulations to find out erythropoietin feedback sensitivity of the system to anemia through the function $\alpha(N_{RBC})$ and $F_{cr}(N_{RBC})$ separately. We assume that the lifespan of erythrocyte is 2 days, cell cycle length of progenitors and reticulocytes is assumed to be 16 ± 3 hours. Feedback control parameters are given in Table 3.4. Extracellular and internal parameters are given in Tables 3.5 and 3.6. At the beginning of the numerical computations the hematocrit is 23% of its equilibrium. For the normal mouse the value of hematocrit is 46 %. We present here the results of system response through the function $\alpha(N_{RBC})$ (Figure 3.11). The return to the equilibrium state on day 4 is observed in Figure 3.11a. With excessive growth of k_F feedback becomes too strong with strong oscillations and results in the disappearance of the cell population (Figure 3.11b,c).

Next, to compare the results of the simulations with existing experimental data on mice, according to the average lifespan in mice, we increase erythrocyte lifespan to 40 days. The lifespan of progenitors is assumed 24±6 hours. In normal conditions in mice, maturation age of reticulocytes is about 2–4 days. It was shown that residence time of reticulocytes in bone marrow decreases in stress situations in mammalians [44, 50]. It was demonstrated that reticulocytes in mice are released early from bone marrow in phlebotomy-induced anaemia [52]. We carried out the simulations under assumption that lifespan of reticulocytes equal to 24±6 hours or equal to 12±6 hours. The count of erythrocytes in blood was decreased to

[1] Private communication, work in progress

Parameter	Value	Unit
α_0	0.6	h^{-1}
k_α	0	h^{-1} / reticulocyte
k_{GF}	6	h^{-1} / GF molecules
N_{target}	70	reticulocyte
N_0	42	reticulocyte
F_0	0.6	NU

Tab. 3.4 – Feedback control parameters. NU is a normalized quantity unit for the intracellular molecules (maximum possible quantity is 1).

Parameter	Value	Unit
Cell cycle length	12	h
Cell cycle variations	3	h
r_0	0.01	L
m	1	M
μ	6.10^5	h^{-1}
K	$3.6.10^6$	$M.h^{-2}$
D_{F_L}	6.10^{-4}	$L^2.h^{-1}$
k_{F_L}	6.10^{-3}	F_L molecules / reticulocyte / h
σ_{F_L}	1.2	h^{-1}
D_{GF}	6.10^{-3}	$L^2.h^{-1}$
W_{GF}	6.10^{-2}	GF molecules / L^2 / h
σ_{GF}	0.6	h^{-1}

Tab. 3.5 – Extracellular parameters : M is an arbitrary mass unit, L an arbitrary length unit

Parameter	Value	Unit
β	120	$h^{-1}.NU^{-1}$
k	2	-
a	31.8	h^{-1}
b	3.6	$h^{-1}.NU^{-1}$
k_γ	1.8	$h^{-1}.NU^{-2}$ / F_L molecule
c	6	$h^{-1}.NU^{-1}$
d	3	h^{-1}
E_{cr}	0.3	NU
F_{cr}	0.4	NU

Tab. 3.6 – Internal parameters when cells are on the hysteresis cycle. NU is a normalized quantity unit for the intracellular molecules (maximum possible quantity is 1).

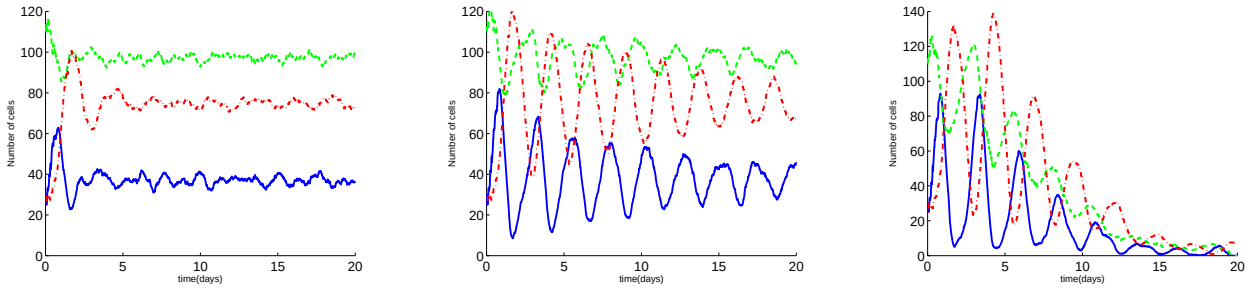

(a) k_F=0.002 (b) k_F=0.004 (c) k_F=0.005

FIG. 3.11 – Feedback by Epo. Cell cycle length is 16 ± 3 hours. Anemia conditions were created by suddenly lowering the number of cells in blood to 23%. Red dash-dot curve corresponds to the number of RBCs in the blood, green dash curve represents the number of progenitors and the blue solid one is the number of reticulocytes.

23% of its equilibrium level. To improve the overall production of RBCs we combine both feedback mechanisms, erythropoietin promotes self-renewal and downregulates apoptosis. Parameters of function k_{alpha} and k_F are chosen to obtain the correct response to anemia (Table 3.7). Other model parameters are presented in Tables 3.1, 3.3. The first measurement in the experiments is made before the first bleeding, and the second measurement is made one day after the bleeding. We compare numerical simulations with the experimental data beginning from the moment when the system starts to respond to anemia increasing the number of erythrocytes. The model in this work provide only erythrocyte count and not hematocrit. The hematocrit is defined by

$$H(t) = \frac{vN_{RBC}(t)}{vN_{RBC}(t) + \text{PlasmaVolume}}, \tag{3.12}$$

where vN_{RBC} represents the volume of erythrocytes in the blood. As in [28] we assume that the plasma volume is not modified during experiments in comparison with normal hematocrit. Considering normal hematocrit H^* (assumed to equal 46%) and erythrocyte count N^*_{RBC} we obtain

$$H^* = \frac{vN^*_{RBC}}{vN^*_{RBC} + \text{PlasmaVolume}}, \tag{3.13}$$

which provides

$$\text{PlasmaVolume} = \frac{1 - H^*}{H^*} vN^*_{RBC}. \tag{3.14}$$

Consequently, hematocrit can be deduced from the erythrocyte count,

$$H(t) = \frac{N_{RBC}(t)}{N^*_{RBC} + H^*(N_{RBC}(t) - N^*_{RBC})}. \tag{3.15}$$

Following the anemia, erythrocytes count quickly increases and reaches the equilibrium value after 6 days as fast as observed in the experiments (Figure 3.12). Simulation results and experimental data are in the best agreement under the assumption that the residence time of reticulocytes in bone marrow is decreased to 12±3 hours (Figure 3.12b).

Parameter	Value	Unit
α_0	0.3	h^{-1}
k_α	$3.3.10^{-4}$	h^{-1} / reticulocyte
k_{GF}	3	h^{-1} / GF molecules
N_{target}	4250	reticulocyte
N_0	1490	reticulocyte
k_F	0.0029	NU / reticulocyte
F_0	0.6	NU

Tab. 3.7 – Feedback control parameters. NU is a normalized quantity unit for the intracellular molecules (maximum possible quantity is 1).

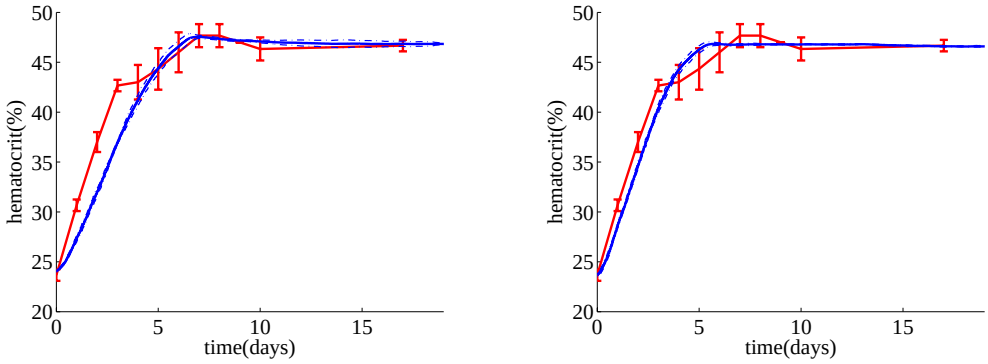

(a) Lifespan of progenitors and reticulocytes is 24±6 hours; k_α=$3.9.10^{-4}$.

(b) Lifespan of progenitors is 24±6 hours. Lifespan of reticulocytes is 12±3 hours; k_α=$3.3.10^{-4}$.

Fig. 3.12 – Evolution of hematocrit. Red curve corresponds to experimental results on mice with standard deviation lines on either side of the mean. Blue curve corresponds to the simulation results (thick line is mean values, thin line is the standard deviation over 20 simulations).

3.5 Discussion

We proposed a new model for erythropoiesis modeling based on the coupling of two relevant scales, the intracellular scale consisting of protein regulatory networks and the extracellular scale focusing on cell movement and interactions as well as growth factor distribution

in the medium. Description of the competition between two proteins within erythroid progenitors has been performed with continuous models (ordinary differential equations) whereas cells have been studied as discrete objects on an off-lattice model, so the whole system can be named 'hybrid model', for it consists in the coupling of continuous and discrete systems. Applied to normal erythropoiesis in the bone marrow, in particular to the regulation of erythroblastic islands, the model suggests an important role of macrophages in the stability of islands. In the absence of macrophages, erythroblastic islands very quickly lose their stability, meaning they either die out or abnormally proliferate (with overproduction of erythroid progenitors). They survive only for the equivalent of about ten cell cycles. On the contrary, when the erythroblastic island is built around a central macrophage, assumed to release growth factors sustaining erythroid progenitor survival and proliferation (like SCF, Ephrin-2 or BMP-4 [95]), then the island is a very robust structure, able to produce continuously erythrocytes while keeping a steady structure (that is an almost constant ratio of reticulocytes over progenitors).

This control of the production of differentiated red blood cells by the macrophage at the level of the erythroblastic island may first appear in contradiction with usual knowledge of erythropoiesis. It is indeed well known that during a response to a stress, erythropoiesis is a very intense process, large amounts of cells being produced in a short time, so the whole process is expected to possess the ability to overcome its usual production, in particular the ratio of reticulocytes over progenitors should not stay constant. The hypothesis we propose is that the macrophage, inside the erythroblastic island, controls the explosiveness of erythropoiesis and that, contrary to other hematopoietic lineages (white cells, platelets), this control is necessary because stress erythropoiesis must deal with very large amounts of cells and otherwise the stability of the process could be lost. It is moreover noticeable that getting more stability with the central macrophage does not decrease responsiveness of the model. For instance, the island reacts to perturbations simulating anemia (sudden loss of mature red blood cells), returning quickly to 'normal' values of the different erythroid populations, progenitors, reticulocytes and erythrocytes (not shown here). Hence the gain of stability is not compensated by a loss in the system's reactivity. Simulation of stress erythropoiesis (anemia) confirm that the macrophage plays a relevant role in the stability of erythropoiesis.

Some comments may however be made on the behavior of an island without macrophage in its center. Although it is clear that this system cannot lead to a stable island (this can be explained by considering that fluctuations automatically lead to proliferation or extinction), it is nevertheless possible to imagine a system working with such islands. For instance, if islands are put side-by-side, proliferation is made difficult (islands cannot expand due to confinement) and extinction can be compensated by the birth of new islands. Moreover, other assumptions, based on a better knowledge of erythroblastic islands, could lead to more stability (geometry of bone marrow and islands,...), even though all scenarii cannot and were not tested. However, the lack of stability makes it hard to have a clear view on how feedback controls act on one single island, and as far as we know of, studying erythropoiesis models (or hematopoiesis models, in a wide sense) without considering feedback controls does not make sense. Hence, searching for island stability appeared relevant in this study. At

a global scale, it is still possible that island stability is not necessary and can be compensated between proliferation and extinction. When looking at one single island however, the fact that feedback controls do not work correctly on an unstable island is somewhat compelling.

Stability of the erythroblastic island including a central macrophage was obtained by considering two scenarii (see Figure 3.3) for the distribution of Erk and Fas quantities in daughter cells, following mitosis and mother cell's division. In the first one, initial values of Erk and Fas in newborn cells were set to zero, and cell fate was decided depending on the evolution of concentrations through the cell cycle duration (this is the 'out of equilibrium' assumption). This scenario was shown to lead to results strongly dependent on the length of cell cycle. The second scenario, called the 'hysteresis cycle case', which is more biologically relevant, consisted in dividing values of Erk and Fas of the mother cell at mitosis into two, so both daughter cells are located on a hysteresis cycle in the Erk-Fas plane at birth. Combining the hysteresis cycle scenario with a structure including a local feedback on the island (the macrophage) gave relevant results and appears very promising. Parameter values which were obtained through mathematical analysis appear to be very robust and the system exhibits qualitatively the same behavior for a wide range of parameters. The stability of the island allows a better control of its size and its subpopulations and, as a result, gives much more satisfying results on feedback tests.

Regarding parameter values used to study the model and check different scenarii (with or without macrophage in the center of the island, distribution of initial quantities of Erk and Fas), one must note that most of these values are mainly not accessible through experiments. Some others, such as for instance the time of survival of RBC, are however rather quite arbitrary and not necessarily in agreement with usual knowledge on erythropoiesis. Yet, results show that the behaviour may be satisfying from a biological point of view. Since a wide range of parameters is allowed, this system can fit experimental data and numerically reproduce certain stress behavior.

Chapitre 4

Pharmacokinetics-Pharmacodynamics model of leukemia treatment

In this chapter we use the hybrid model to study normal and leukemic red blood cell production, and treatment of leukemia. Normal cells are supposed to have a circadian rhythm, that influences their cell cycle durations, whereas leukemic cells, appart from being characterized by excessive proliferation and insufficient differentiation and apoptosis, are supposed to escape circadian rhythms. We consider a treatment based on periodic administration of Ara-C, an anti-cancer agent targeting cells in DNA synthesis. A pharmacodynamic/pharmacokinetic model of Ara-C is then proposed, and used to simulate the treatment. Influences of the period of the treatment and the day delivery time on the outcome of the treatment are investigated and stress the relevance of considering chronotherapeutic treatments to cure leukemia.

4.1 Mathematical model

4.1.1 Intracellular and extracellular regulation of normal erythropoiesis

In this chapter, in order to focus ourself on leukemia treatment we consider two types of cells, erythroid progenitors and reticulocytes. Reticulocytes produce Fas-ligand which diffuses into extracellular matrix and influences erythroid progenitors. Erythroid progenitors are also influenced by the hormone erythropoietin. Its production depends on the number of erythrocytes in blood. Finally, we will introduce pharmacokinetics of Ara-C, a drug used for chemotherapy of acute myeloblastic leukemia.

Intracellular regulation We focus our attention on two key intracellular proteins, Erk and Fas, which are involved in cell fate decision (high levels of Erk induce cell self-renewal, whereas high levels of Fas induce either cell differentiation or apoptosis). Evolution of the

concentrations of these proteins inside an erythroid progenitor is described by a system of two ordinary differential equations [29],

$$\begin{cases} \dfrac{dE_i}{dt} &= (\alpha(Epo) + \beta E_i^k)(1 - E_i) - aE_i - bE_iF_i, \\ \dfrac{dF_i}{dt} &= \gamma(FasL)(1 - F_i) - cE_iF_i - dF_i, \end{cases} \tag{4.1}$$

where E_i and F_i are the concentrations of Erk and Fas, respectively, in the i-th cell.

Here, we do not consider the feedback by erythropoietin. The concentration of Epo is assumed to be constant, so the function α in (4.1) will be considered as a positive parameter. For this study, we focus only on the feedback control exerted on progenitor cells by reticulocytes through Fas-ligand (see the next paragraph *Extracellular regulation*).

As we already discussed above, this system of equations can have between one and three stationary points [29], depending on parameter values. The choice of parameters is an important issue when describing intracellular regulatory networks. In most cases, there are no experimental data on the reaction rates of involved proteins. So the criterion when choosing parameter values is to describe the normal behavior of the whole system with approximately correct proportion between self-renewing, differentiating and apoptotic cells and the correct response of the system to stimulation by the hormones. The set of parameters satisfying these conditions may not be unique. A detailed discussion of the choice of parameters is presented in previous chapter. Here, parameter values are chosen in such a way that the system has three steady states, and values are given in Table 4.1. In this case, the system exhibits bistability, with one unstable steady state, and two stable ones.

Let us recall that the intracellular regulation scheme described above concerns erythroid progenitors but not reticulocytes. Indeed, reticulocytes are differentiated cells. Similar to mature red blood cells, they do not proliferate. However, reticulocytes produce Fas-ligand, which influences intracellular regulation of erythroid progenitors (the second equation in system (4.1) depends on Fas-ligand). For large values of Fas-ligand, trajectories of the system move towards greater values of F_i and to smaller values of E_i. If during the cell cycle, the value of Erk becomes greater than a given critical value E_c, then the cell will self-renew : at the end of the cell cycle, it will divide and give rise to two daughter cells that are identical to the mother cell. During the same cell cycle, if the value of Fas becomes greater than a given critical value, F_c, then the cell immediately dies by apoptosis. If none of these conditions are satisfied, then the cell will differentiate : when the cell cycle is finished, the cell divides and gives birth to two more mature cells, that are reticulocytes.

Once produced, a reticulocyte remains in the computational domain during a time equal to one cell cycle, during which it produces Fas-ligand, and then becomes a mature erythrocyte. At the end of their development, reticulocytes leave the bone marrow and enter the bloodstream as red blood cells. In the framework of our model, reticulocytes that have performed one cell cycle are removed from the computational domain.

We note finally that the duration of cell cycle for each cell is considered as a random variable with the uniform distribution in the interval $[T_c - \tau, T_c + \tau]$, where T_c is the mean cell cycle time and $\tau < T_c$ is a parameter accounting for variability of the cell cycle duration.

Extracellular regulation Reticulocytes interact with erythroid progenitors by direct cell-cell contact. As previously mentioned, reticulocytes produce Fas-ligand, which binds to the Fas receptors located on the surface of erythroid progenitors, and stimulates apoptosis and differentiation. For convenience, Fas-ligand distribution in space is modelled with a reaction-diffusion equation (3.7),

$$\frac{\partial FasL}{\partial t} = D\Delta FasL + W - \sigma FasL,$$

where W is a source term proportional to the concentration of reticulocytes. If the diffusion coefficient is sufficiently small, Fas-ligand is concentrated in a small vicinity of reticulocytes. [31]. In this case, Fas-ligand influences erythroid progenitors when they are sufficiently close to reticulocytes. This is the situation illustrated in this work.

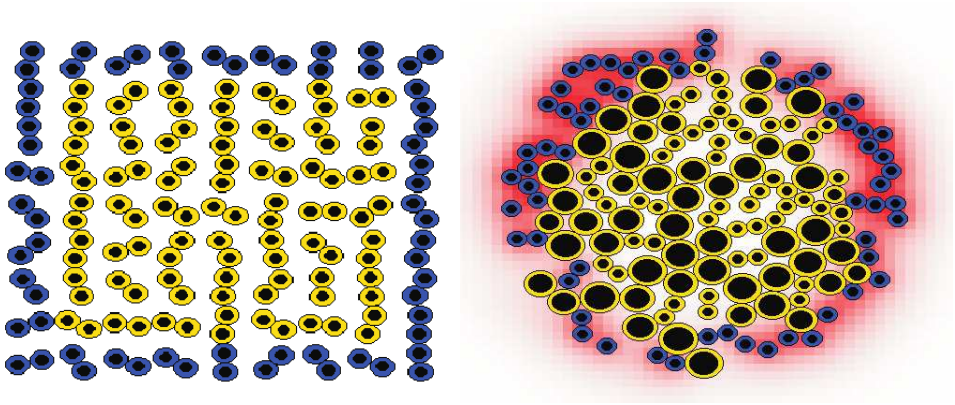

Fig. 4.1 – Erythroblastic island : yellow cells in the center are erythroid progenitors, blue cells at the border are reticulocytes producing Fas-ligand (in red). The initial cell distribution is on the left panel, the typical configuration of the island after several cell cycles on the right panel.

Let us recall that the source term W in equation (3.7) is distributed in space since cells have a finite size. In numerical simulations, local concentration of reticulocytes is computed as the total cell area in each box of the numerical grid (see Section 2.1). The concentration of Fas-ligand depends both on space and time. It enters the second equation in (4.1) with the value $FasL(x_i, t)$, where x_i is the center of the i-th cell.

Figure 4.1 shows the evolution of an erythroblastic island, by considering only the influence of Fas-ligand (Epo concentration is fixed). The left panel represents the initial cell configuration with immature progenitors inside and more mature reticulocytes outside. The right panel shows the typical structure of the island several cell cycles later. Extracellular Fas-ligand concentration (shown in red color) is higher near reticulocytes. Fas-ligand stimulates intracellular production of Fas in erythroid progenitors : if an erythroid progenitor is close to a reticulocyte, then the extracellular concentration of Fas-ligand and, as a consequence, the intracellular concentration of Fas in the progenitor can be sufficiently high to induce its

apoptosis. Progenitors located at some distance from reticulocytes can have an intermediate value of intracellular Fas. Such cells will preferentially differentiate into reticulocytes. Finally, progenitors located far from reticulocytes mostly self-renew.

4.1.2 Ara-C kinetics

One of the most common and effective chemotherapeutic agents against acute myelogenous leukemia is cytosine arabinoside, also known as Ara-C. Our aim is to apply a treatment with Ara-C to a population of erythroid cells formed with normal and leukemic cells, using the hybrid model described in the previous paragraphs. We describe hereafter the pharmacokinetics and pharmacodynamics of Ara-C.

Once introduced intravenously in the organism, Ara-C penetrates cell membranes by a mechanism based essentially on the human equivibrative nucleoside transporter-1 (hENT1), which can be considered as facilitated diffusion. This process does not need energy and goes in accordance with the gradient of concentration up to the equilibrium between the intracellular and extracellular concentrations of Ara-C.

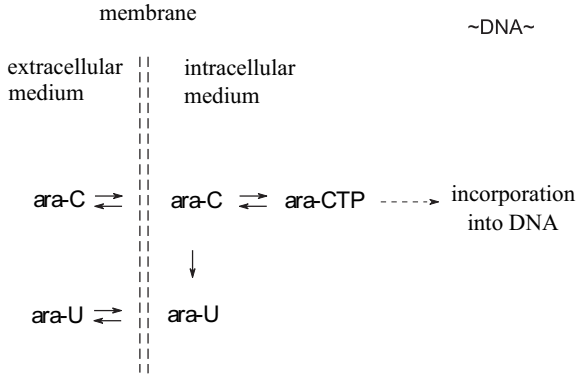

FIG. 4.2 – Metabolism of Ara-C (adapted from [78]). Schematical representation of Ara-C pharmacokinetics : Ara-C crosses cell membrane, it is phosphorylated becoming Ara-CTP. Ara-CTP is used for DNA replication instead of nucleotide C. Besides, Ara-C can be transformed in Ara-U.

Inside cells, part of Ara-C is phosphorylated into its active form, Ara-CTP, which arrests DNA synthesis and induces cell apoptosis. The rest, about 70%, of Ara-C is deaminated into its inactive form Ara-U. Ara-CTP, in turn, can be dephosphorylated back to Ara-C. We take into account these three reactions in order to model the intracellular kinetics of Ara-C and Ara-CTP (see Figure 4.2). We describe them by Michaelis-Menten mechanisms. The phosphorylation rate of Ara-C, denoted by r_p, is given by

$$r_p = \frac{V_k}{1 + \frac{K_m K_a}{w_i}},$$

where w_i is the Ara-C concentration inside the i-th cell, K_m is the Michaelis-Menten constant, K_a accounts for additional effects and V_k is the kinase activity.

Denote by w_i^a the Ara-CTP concentration in the i-th cell. Ara-CTP dephosphorylation rate, r_{dp}, is given by

$$r_{dp} = \frac{V_{dp}}{1 + \frac{\alpha^1 K_{dp}}{w_i^a}},$$

with V_{dp} the enzyme activity, α^1 accounts for additional effects, K_{dp} is the Michaelis-Menten constant.

Finally, deamination of Ara-C follows similar kinetics, with r_{da} the rate of deamination,

$$r_{da} = \frac{V_{da}}{1 + \frac{K_{da}}{w_i}},$$

and V_{da} is the enzyme activity and K_{da} the Michaelis-Menten constant.

The kinetics of intracellular Ara-C concentration in the i-th cell is then described by the following equation,

$$\frac{dw_i}{dt} = k_1(w - w_i(t)) - k_2 w_i(t) - (r_p - r_{dp} + r_{da}), \tag{4.2}$$

where w is the extracellular concentration of Ara-C in the bone marrow, supposed to be uniformly distributed in the bone marrow, yet varying with time ($w = w(t)$); In fact, cells are infused in Ara-C for two hours, then Ara-C is removed (or washed out). The constant k_1 is related to the rate of membrane penetration, k_2 accounts for degradation of Ara-C. There is no extracellular degradation of Ara-C.

The balance equation for the intracellular concentration of Ara-CTP is

$$\frac{dw_i^a}{dt} = k_\alpha(r_p - r_{dp}). \tag{4.3}$$

Ara-CTP exerts a cytotoxic effect on all dividing cells, arresting DNA synthesis and inducing apoptosis. Evolution of the quantity p_i of Ara-CTP in DNA is described with the following equation,

$$\frac{dp_i}{dt} = k_\beta w_i^a, \tag{4.4}$$

with k_β the rate of conversion of Ara-CTP. When p_i overcomes a critical value p_{cr}, then it is assumed the cell dies by apoptosis. Above equations and parameters (Table 4.1) for Ara-C metabolism are derived from Morrison et al. [78].

4.1.3 Organization and duration of cell cycle

Generally speaking, cell cycle proceeds through G_1, S, G_2 and M phases, and cells can also enter a quiescent state, named G_0 phase. Duration of this resting phase and transition to cell cycle are controlled by various intracellular and extracellular mechanisms. Erythroid progenitors are believed to be basically in the cell cycle with a short or inexisting G_0 phase. Taking this into account, we consider a single G_0/G_1 phase, whose duration varies randomly

TAB. 4.1 – Parameter values (N.U. means "no unit", min is for "minute")

Parameter		Value	Unit
	Force between two cells		
H_1	Cell compressible part	1.75	μm
K	Positive parameter	1000	
	Intracellular regulation		
α	Epo-dependent Erk activation rate	0.0003472	min^{-1}
k	Erk self-activation power	2	N.U.
β	Erk self-activation rate	0.05	min^{-1}
a	Erk degradation rate	0.004	min^{-1}
b	Erk inhibition constant	0.0138	min^{-1}
k_γ	Fas-ligand-dependent Fas activation rate	0.0002	min^{-1}
c	Fas inhibition rate	0.00138	min^{-1}
d	Fas degradation rate	0.0001	min^{-1}
E_c	Erk critical level	0.4	N.U.
F_c	Fas critical level	0.2	N.U.
	Extracellular regulation		
D	Fas-ligand diffusion coefficient	$1e^{-5}$	$\mu\text{m}^2.\text{min}^{-1}$
σ	Fas-ligand degradation rate	0.02	min^{-1}
W	Source term	0.0001	min^{-1}
	Metabolism of AraC		
k_1	Membrane penetration rate	0.0116	min^{-1}
k_2	Ara-C degradation rate	0	min^{-1}
V_k	Kinase activity	1.28	$\mu\text{M.min}^{-1}$
K_m	Michaelis-Menten constant	27.0	μM
K_a	Additional effects constant	16	N.U.
V_{dp}	Enzyme activity	300	$\mu\text{M.min}^{-1}$
K_{dp}	Michaelis-Menten constant	900	μM
α^1	Additional effects constant	44.4	N.U.
V_{da}	Enzyme activity	16.45	$\mu\text{M.min}^{-1}$
K_{da}	Michaelis-Menten constant	1011.7	μM
k_α	Metabolism constant	0.8	N.U.
k_β	Ara-CTP conversion rate	1	N.U.
p_{cr}	Critical value of Ara-CTP in DNA	40	μM
	Circadian rhythm		
c_x	Constant characterizing the circadian clock	$\in [0, 1]$	N.U.
θ	Phase shift	5	hours

in some given interval. Denote by $G_0/G_{1_{min}}$ and $G_0/G_{1_{max}}$ the minimal and maximal values, respectively, of the G_0/G_1 phase and assume that duration of this phase is a random variable with a uniform distribution between them.

This assumption corresponds to biological observations [100]. From the modelling point of view, variation in the G_0/G_1 phase duration, and consequently in cell cycle duration, allows cells to desynchronize. This is essential for correct modelling of Ara-C pharmacodynamics and treatment of leukemia. Figure 4.3 shows two simulations of the complete model with $G_0/G_{1_{min}} = 0$ and different values of $G_0/G_{1_{max}}$. In the case $G_0/G_{1_{max}} = 7$ hours, after approximately 7 cell cycles the proportion of cells in the S phase becomes almost constant. For shorter cell cycle durations, $G_0/G_{1_{max}} = 3$ hours, the proportion of cells in S phase is strongly oscillating, even after several cell cycles, so cells are mainly not desynchronized.

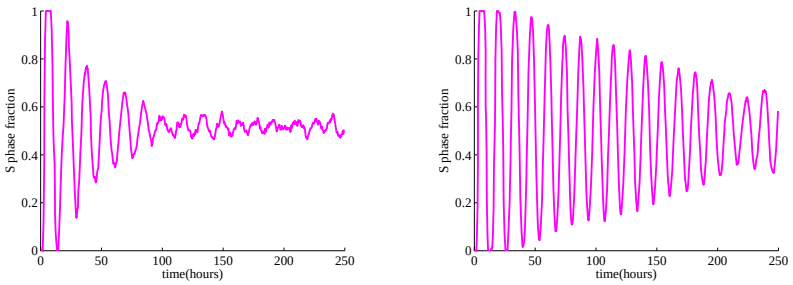

(a) $G_0/G_{1_{max}}$=7 hours (b) $G_0/G_{1_{max}}$=3 hours

Fig. 4.3 – Proportion of cells in phase S, with $G_0/G_{1_{min}} = 0$.

4.1.4 Circadian rhythm in the cell cycle

Circadian rhythms can influence proportion of cells in the S phase [110]. Their ratio with the total number of cells is not constant during the day. Therefore efficiency of drug administration can also depend on time [10]. In order to describe circadian rhythms, we introduce a variable x that describes the concentration of cyclin-D1, a circadian clock control protein, whose activity is required for cell cycle G_1/S transition. Let us assume that this value x is in the interval $[0, x_{max}]$, where x_{max} is a threshold value at which the cell enters S phase. At the time of cell division (cell birth) t_0 we prescribe $x(t_0) = x_0$, where the initial concentration of the protein x_0 is a random variable uniformly distributed in $[0, x_{max}]$.

Since the corresponding gene is controlled by the circadian rhythm, the cyclin-D1 protein concentration is determined by the time of the day. This is reflected in the following equation for the concentration of the protein,

$$\frac{dx}{dt} = 1 + c_x \sin(f(t - \theta)), \tag{4.5}$$

where $f = \frac{2\pi}{24}$, $c_x \in [0, 1]$ and θ is a phase shift chosen to reproduce circadian timing of cell

division in humans. Solution to (4.5) is given by the formula :

$$x(t) = x_0 + (t - t_0) + \frac{c_x}{f}\cos(f(t_0 - \theta)) - \frac{c_x}{f}\cos(f(t - \theta)), \tag{4.6}$$

Assume that $\tau = t - t_0$, where τ is the time spent in phase G_0/G_1. Then we have

$$x(t_0 + \tau) = x_0 + \tau + \frac{c_x}{f}\cos(f(t_0 - \theta)) - \frac{c_x}{f}\cos(f(t_0 + \tau - \theta)), \tag{4.7}$$

If $x(t_0 + \tau) = x_{max}$, the concentration of the protein attains the G_1/S transition threshold value, and the cell enters the S phase. That way, G_0/G_1 phase duration τ is a random variable distributed in $[0, \tau_{max}]$, and τ is also modulated by the circadian clock. The maximal value of τ, τ_{max}, corresponds to the threshold x_{max}.

4.2 Results

In this section, we numerically simulate the hybrid model presented in Section 4.1 and the action of Ara-C on cell populations, considering a population formed with normal or leukemic erythroid progenitors, and reticulocytes. Each progenitor cell is characterized by proteins concentrations evolving according to the properties presented in Section 4.1.1. In particular, cell fate of the i-th cell depends on the values of Erk and Fas concentrations, E_i and F_i : during a cell cycle, if Erk concentration reaches the critical value E_c then the cell will self-renew at the end of its cycle, if Fas concentration reaches its critical value F_c then the cell will die by apoptosis immediately, in the other case the cell will differentiate in reticulocytes. These latter cells play an active role in progenitor fate, by releasing Fas-ligand, which induces Fas concentration increase. Since the feedback control by Fas-ligand is the only one considered for the simulations of this model, cell fate depends exclusively on the distance between progenitors and reticulocytes (Fas-ligand diffuses in the domain, according to equation (3.7)).

We recall that Ara-C acts both on normal and leukemic proliferative cells. Hence, optimization of chemotherapy implies killing all leukemic cells and preserving maximum of normal cells. In this section we study action of Ara-C on normal cells and on leukemic cells.

First, we focus on the effect of treatment on proliferation and survival of normal cells (Section 4.2.1). We investigate the respective influences of the period of treatment and the starting hour of treatment with respect to the cell cycle duration. We show that relation between cell cycle duration and periodicity of treatment can drastically influence cell population dynamics.

Second, we simulate the effect of a chronomodulated treatment with Ara-C (Section 4.2.2), in the situation where normal cells are subject to circadian rhythm ($c_x = 0.5$ in (4.7)) whereas leukemic cells do not exhibit circadian rhythm dependency ($c_x = 0$). We will see that population dynamics of normal cells depends on the time of the day when Ara-C is administered according to the proportion of cells in the S-phase. This allows us to make a difference between normal and leukemic cells in the treatment by Ara-C. We have

deliberately chosen to consider normal and leukemic cells with the same properties except for circadian rhythms. In this case we obtain a more precise response about the influence of circadian rhythms on the results of chemotherapy.

In both cases, the cell population is first simulated from an initial state until it reaches a satisfactory state, in which the erythroblastic island is large enough and cells are well mixed (see Figure 4.1, right panel). Then numerical experiments start with Ara-C treatment. Consequently, time $t = 0$ in every picture must be understood as the time of the beginning of the numerical experiments and not as the beginning of erythroblastic island simulations.

4.2.1 Treatment protocol depending on cell cycle duration

We first consider a population of erythroid cells, composed with two types of cells : immature progenitors and reticulocytes, and using the hybrid model previously presented we perform a simulation of treatment by Ara-C injections (all cells in the domain are in contact with Ara-C, which does not degrade in the extracellular medium and is uniformly distributed in the domain, for 2 consecutive hours, then Ara-C is removed). We investigate the relevance of taking cell cycle durations into account when treating with Ara-C.

Because the cytotoxic effect of Ara-C is related to DNA synthesis, time periodic drug administration killing cells in the S phase will influence consecutive cell generations. This can result in so-called resonance effect, first discussed in [35]. If the periodicity of treatments is close to the duration of the cell cycle or to its multiples, then cells that are not in the S phase during one administration will be unlikely to be in S phase at subsequent administrations. These cells will divide resulting in growth of cell population.

Numerical simulations of erythroid cell populations with an average duration of cell cycle equal to 31 hours and with different protocols of drug administration are shown in Figure 4.4. For the same total amount of injected Ara-C, the cell population can either disappear (Figure 4.4a) or grow (Figure 4.4b,c) if the period of drug injections is far or close to multiples of cell cycle duration.

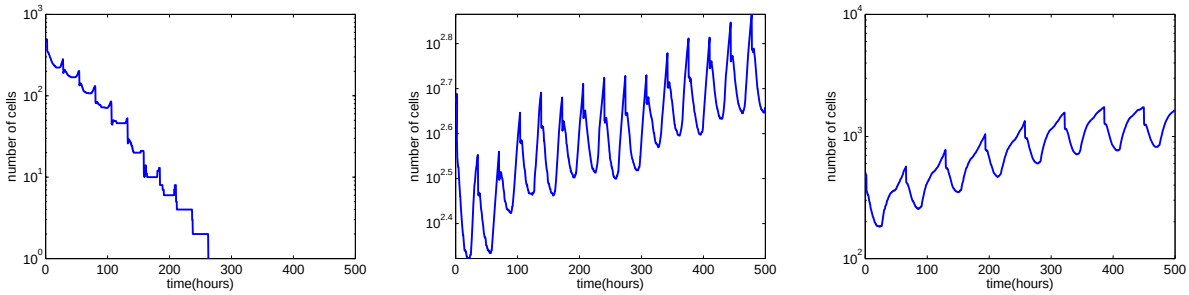

(a) Injection of *AraC* every 26 hours.

(b) Injection of *AraC* every 34 hours.

(c) Injection of *AraC* every 64 hours.

Fig. 4.4 – Evolution of erythroid cell population under treatment with Ara-C. Number of progenitors in cell population.

Cell population growth or decay is approximately exponential with periodic modulations due to the action of the treatment. Considering that cell population evolves proportionally to $e^{\lambda t}$, where λ is the growth exponent (either positive or negative), Figure 4.5 shows the value λ as a function of the period of treatment T for two different values of cell cycle duration. In the first case, the duration of the G_0/G_1 phase is random and uniformly distributed between $G_0/G_{1_{min}} = 5$ hours and $G_0/G_{1_{max}} = 31$ hours, the duration of the S phase is 10 hours and of G_2/M phases is 3 hours. Hence the average cell cycle duration T_c is 31 hours, and the variation ± 13 hours. In the second case, T_c is 33.5 hours and the variation is ± 15,5 hours. The function $\lambda(T)$ in the left panel has a peak at approximately 33 hours close to the average cell cycle duration. The second maximum is much wider but corresponds to approximately twice the duration of cell cycle. Similar results are presented in the right picture for another value of cell cycle duration. The first peak is at 38 hours, close to the average cell cycle.

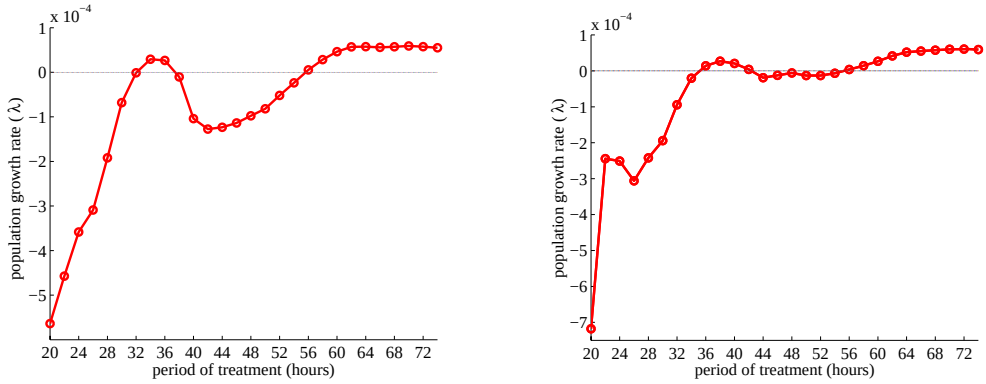

(a) $G_0/G_{1_{max}}$=31 hr (b) $G_0/G_{1_{max}}$=36 hr

FIG. 4.5 – Growth exponent λ as a function of the treatment period T.

These first results of numerical simulations with hybrid models confirm that the search for an optimal treatment period is relevant within the context of erythroid cell populations. Depending on the period of the treatment with Ara-C, compared to the average cell cycle duration, the progenitor population can either grow or decay.

4.2.2 Optimal administration of Ara-C related to circadian rhythm

Most cytotoxic drugs used in chemotherapy are not specific to malignant cells. They affect both normal and leukemic cells. However, in leukemia, downregulation of circadian clock genes is often observed [118]. Malignant cells can even escape circadian control. Thus, treatment protocol should take into account this difference in normal and leukemic cells in order to reduce undesirable effects of chemotherapy and to increase its efficacy.

Let us consider two different populations of cells. The first one consists of erythroid progenitors that follow circadian rhythms with a certain synchronization in their DNA synthesis activity [109]. This population is characterized by a coefficient $c_x = 0.5$ in equation (4.7).

The second population consists of leukemic cells that do not obey the circadian control. Consequently, this population is characterized by a coefficient $c_x = 0$ in (4.7).

We first simulate cell population dynamics, considering a duration of $S/G_2/M$ phases equal to 13 hours and a duration of G_0/G_1 phase varying according to circadian rhythms between $G_0/G_{1_{min}} = 5$ and $G_0/G_{1_{max}} = 31$ hours. The fraction of erythroid progenitors in the S phase is then maximal around 1 p.m. and minimal between midnight and 1 a.m. (see Figure 4.6), in agreement with clinical observations [110].

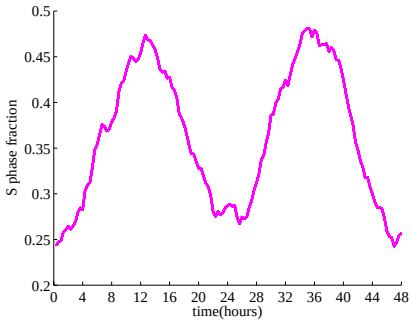

Fig. 4.6 – Fraction of cells in the S phase.

Second, we simulate the chronomodulated administration protocol of Ara-C with intervals ranging from 8 hours to 65 hours. The total dose of Ara-C administered is conserved, and day time delivery t_0 of the treatment is taken every hour, between 1 :00 and 24 :00 (Figure 4.7a). Outcomes of the model, chosen here to be measurements of the growth rate λ, are then functions of only the period of treatment and the initial time t_0.

As expected, the most important variations of growth rate as a function of t_0 together with the best values of the growth rate are observed for periods of treatment equal to 24 hours (Figure 4.7b, zoom in of Figure 4.7a) and 48 hours (Figure 4.7c, zoom in of Figure 4.7a). Apart from these periods, the delivery time does not appear to modify the outcome of the simulations (Figure 4.7a). Low values (black) indicate bad treatment outcomes and high values (white) indicate good treatment. It is noticeable, however, that if period of treatment is slightly larger (or less, resp.) than 24 hours or 48 hours, then the time of first delivery t_0 should be advanced (or delayed, resp.) to produce an equivalent outcome. This dependence is more brightly expressed at 48 hours (Figure 4.7c) [16]. It should be noticed that the white area between 30 and 40 hours (Figure 4.7a) corresponds to periodicity of the drug administration close to the average duration of the cell cycle and the reason of its appearance is the same as for the first peak in Figure 4.5a, discussed in the Section 4.2.1.

The timing of a 24-periodic treatment (Figure 4.8a) and 48-periodic treatment (Figure 4.8b) affects the treatment toxicity. If Ara-C is administered at 1 a.m., when the lowest fraction of cells are in the S-phase (see Figure 4.6), the total cell number decreases slowly (upper curve). If Ara-C is introduced at 1 p.m., when more cells are in the S-phase (Figure 4.6), then the cell population decreases faster (lower curve). With the periodicity of treatment 48 hours and the time of first delivery 1 a.m., the population of cells decreases more slowly

than with periodicity of treatment 24 hours and the same time of first delivery (Figure 4.7). As mentioned above, it is the population of normal cells that do obey the circadian control. So, it can be deduced, that a treatment with 48 hours period administered at the better time t_0 gives less toxicity, than the same administration with a 24-periodic treatment. Moreover, the worst treatment is at 1 p.m. with a 48-periodic treatment, and the best time to treat is at 1 a.m.

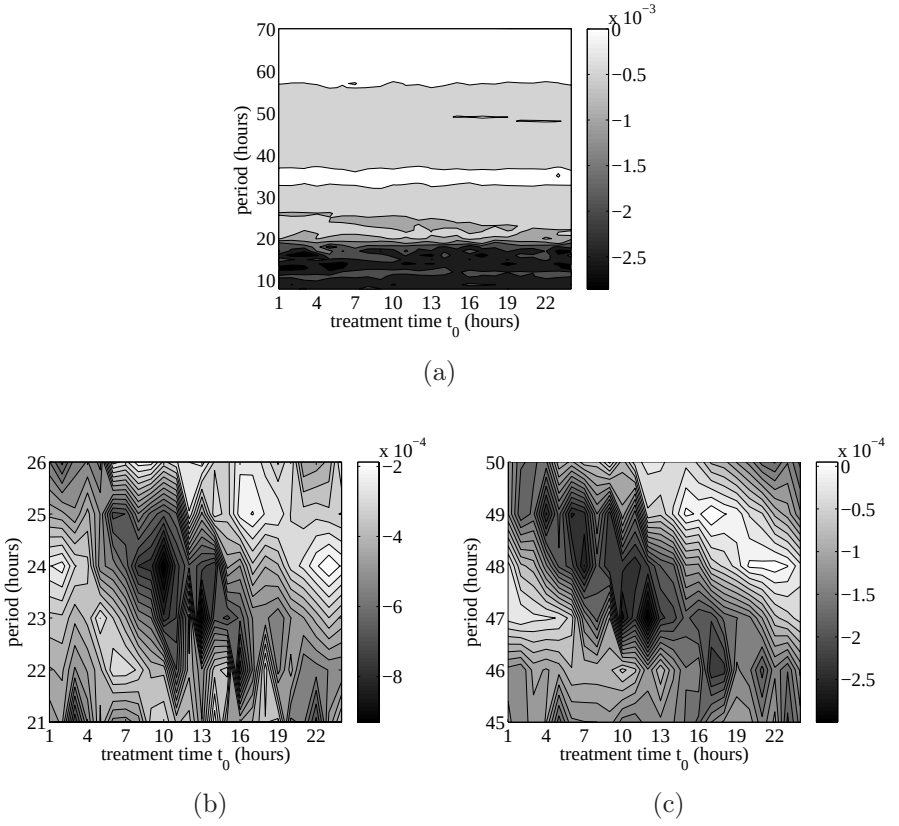

FIG. 4.7 – Treatment outcomes. The gray scale shows the value of λ as a function of the first day delivery time t_0 and the period T between two consecutive drug administrations. Panel (a) represents the growth exponent λ for t_0 ranging from 1 a.m. to midnight, and T ranging between 8 and 65 hours. Panel (b) and (c) show a specific region around period T=24 hours and T=48 hours, respectively. All three panels correspond to the same numerical simulations.

Next, we compare the response to treatment of normal cells, which follow circadian rhythm, and of leukemic cells, which escape it. Populations of normal (green line) and leukemic cells (red line), subjected to 48 h interval treatment at different times t_0, are presented in Figure 4.9. The population of normal cells remains approximately constant while the population of leukemic cells dies when t_0 is 1 a.m. (Figure 4.9a). On the contrary, the population of normal cells dies even faster than the population of leukemic cells if first time delivery is at 1 p.m. when the toxicity of the drug is extremely large (Figure 4.9b).

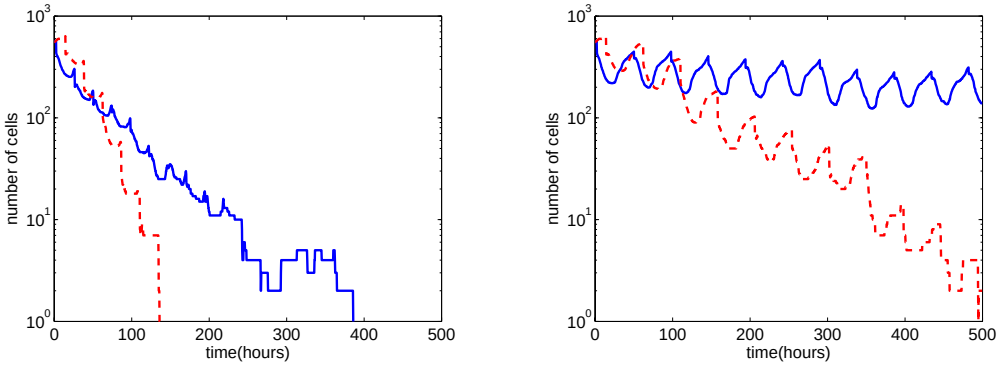

(a) (b)

Fig. 4.8 – Evolution in time of the total number of cells with Ara-C administered at 1 a.m. (upper curve) or at 1 p.m. (lower curve). Left : Interval between administrations is 24 hours. Right : Interval between administrations is 48 hours.

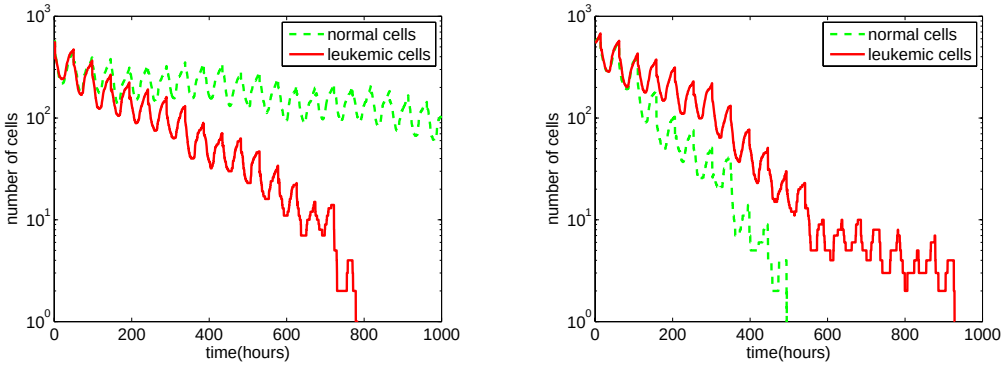

(a) (b)

Fig. 4.9 – Evolution in time of the total number of normal cells (green line) and leukemic cells (red line) with Ara-C administered every 48 hours at 1 a.m. (left) and at 1 p.m. (right).

4.3 Comparison with clinical data of leukemia treatment

The complete model described in the previous section includes cell dynamics, intracellular and extracellular regulations, pharmacokinetics of Ara-C and circadian rhythms. In this section, we will use a simplified model, which consists of cell dynamics and pharmacokinetics, in order to describe clinical data on leukemia treatment. We will not consider here intracellular and extracellular regulations but we will have to describe leukemic hematopoiesis, that is different types of leukemic cells.

We will reproduce here with numerical simulations the number of blasts in blood due to chemotherapy of acute leukemia [76]. The protocol applied in [76] was tested on a patient with acute myeloblastic leukemia who was unresponsive to conventional chemotherapy. Ara-

C was given as two hours continuous i.v. infusion for 5 times over a total duration of 34 hr with 6-hr interval between infusions. The reason why the current mode of administration was chosen is as follows. Since Ara-C produces its cytotoxic effects during two hours, the duration of each infusion should not be more than 2 hours in order to avoid overaccumulation and undesired toxic effects. As the duration of phase S (T_s) of human leukemic cells is about 10 hours, so the interval of administrations should be less than 10 hours. It is also known that it takes leukemic cells from about 6 to 8 hours to recover their capacity to synthesize DNA. The level of Ara-C in plasma was 10 to 20 μm. After application of this protocol 99% reduction in the leukemic blast cells in the blood was observed.

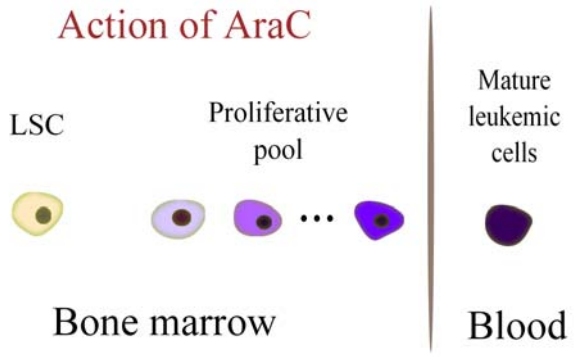

FIG. 4.10 – Leukemic hematopoiesis starts with leukemic stem cells. After several divisions with differentiation, mature leukemic cells leave the bone marrow to blood.

In order to describe the clinical data, we have tested different schemes of leukemic hematopoiesis. The minimal model includes leukemic stem cells (LSC), proliferative leukemic cells and mature leukemic cells (MLC) in blood (Figure 4.10). Apoptotic rate of LSCs is assumed to be zero. With probability 0.5 leukemic stem cell after its division gives a birth to two cells with higher degree of maturity or one LSC and one differentiated cell. These more mature cells, named here proliferative leukemic cells, represent the second type of cells in the model. Proliferative leukemic cells at different stages of maturation are also located in bone marrow. Similar LSCs, these cells do not die by apoptosis without medical treatment. After their division, they give two daughter cells with higher maturity. We assume here seven stages of their maturity. The cells of eighth stage of maturation form the third type of cells, so called post mitotic almost mature leukemic cells (MLC), which are released from the bone marrow into the blood (see Figure 4.10). These assumptions are consistent with biological and clinical observations.

It was chosen to start simulation with 162 leukemic stem cells initially. Then, first of all we run the simulation without application of treatment. After eight days of computing we

have the population of about 7.10^3 leukemic cells of different maturity [48, 58], Figure 4.11. Then, the protocol described above is applied.

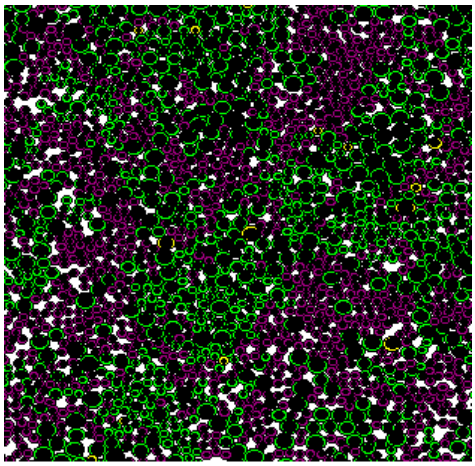

Fig. 4.11 – Three types of cells in the simulation : leukemic stem cells (yellow), leukemic proliferative cells (green), mature leukemic cells (magenta).

Duration of each cell phase of leukemic stem cells is as follows. Duration of phase T_{G_1} is a random variable with a uniform distribution between 5 hours and 31 hours, T_S is 10 hours and T_{M/G_2} is 3 hours. So, $T_{G_1} + T_M + T_{G_2}$ of leukemic stem cells is equivalent to or less than 34 hours and the maximal T_c is 44 hours. This corresponds to estimates from [76] which is similar to some of the T_c values reported for human leukemic cells. We make the assumption that T_{G_1} of proliferative leukemic cells is reduced and varies between 5 hours and 12 hours, T_S is 10 hours and T_{M/G_2} is 3 hours. From the experimental data in [76] we can conclude that the survival half-life of post mitotic mature leukemic cells in blood is about 12 hours. It was implemented into the model by forcing post mitotic MLC to take a decision every 12 hours to die or to survive with probability 0.5.

Over the last years, the evidence that AML is initiated and propagated by leukemic stem cells, a very small population when compared with mature cancer cells, has grown. Conceivably, these most immature leukemia cells are more resistant to therapy and subsequently initiate relapse. Even a small proportion of the leukemic stem cells ($\sim 1/10^6$) in acute myeloid leukemia can seed tumor growth [55]. Therefore, the number of leukemic stem cells which considered in the model before application of treatment should be less than number of mature leukemic cells. The proportion 1 to 60 was assumed. Ara-C targets all cells during DNA synthesis (S-phase of the cell cycle), so it does not act on post mitotic leukemic cells. Result of Ara-C therapy on the number of myeloblastic leukemic cells in blood is shown in Figure 4.12.

We note that extracellular regulation is not considered in the model. There are no extracellular signaling molecules (like Fas-ligand for erythroid progenitors) which influence cell fate. The concentration of Ara-C is supposed to be everywhere the same. This means that the space variable is not explicitly present in the model. On one hand, this simplifies the

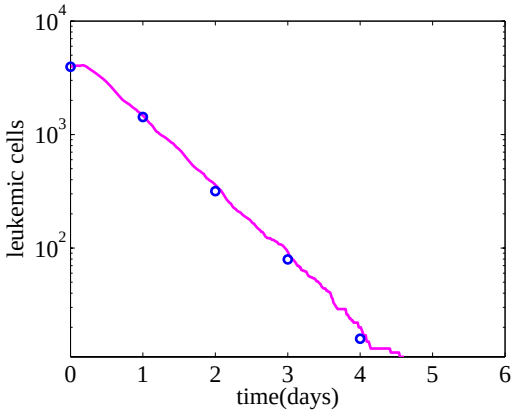

FIG. 4.12 – Effect of araC therapy on the number of leukemic cells in the blood. Magenta curve represents simulation results. Blue points correspond to the clinical data. 10 μm of araC was given as a 2-hr continuous i.v. infusion for 5 times over a total duration 34 hr with 6-hr interval between the 2-hr of Ara-C infusions.

modelling since we do not have to remove mature leukemic cells from the computational domain and to introduce two different compartments, one for bone marrow and another one for blood. On the other hand, we should explain why the space distribution is not important here. Indeed, since leukemic cells are not sensitive to normal regulatory mechanisms, we assume that they make their choice between self-renewal and differentiation according to their internal properties and independently of the surrounding cells. If this is the case, then the question is why to introduce a relatively complex hybrid model and not to work with a simpler model, for example ordinary differential equations. First of all, we need to note that this should be a cell population structured with respect to intracellular drug concentrations. Therefore, it should be transport equations with time dependent coefficient and not ordinary differential equations. Second, since we introduce stochasticity in the problem, then we would have to study stochastic transport systems of equations which are not simpler than hybrid models. They do not admit analytical solution and should be solved numerically. Let us finally note that in a more complete model we need to take into account both normal and leukemic cells which compete for space. In this case, introduction of space distributions can have a crucial importance.

4.4 Discussion

In this chapter, we applied this approach to study treatment of acute myeloblastic leukemia (AML) with Ara-C, one of the main chemotherapeutic drugs used for AML patients. Since Ara-C kills both normal and leukemic cells, one of the main questions in chemotherapy is to choose optimal patient adapted treatment protocol which allows elimination of all leukemic cells and preservation of maximum of normal cells. Our results indicate that chronotherapy, which takes into account circadian rhythms of normal cells, can improve the

result of treatment.

It can be noted that leukemic cells are practically irresponsive to intracellular and extracellular regulation. From the modelling point of view developed in this work, this means that the regulation described in Section 4.1.1 does not influence leukemic cells. Hence the analysis of pharmacokinetics and pharmacodynamics of leukemic cells, which was one of the main objectives of this work, is applicable not only for erythroleukemia but also for all types of acute leukemia. On the other hand however, when analyzing the influence of chemotherapy on normal cells, we need to take into account their regulation.

Regarding the chronomudulated treatment, it should be noted that resonance is observed in the simplified model while the real *in vivo* situation can be much more complex. First of all, cell lineages with different durations of cell cycle can coexist. Moreover, treatment itself can change duration of cell cycle, delaying the process of DNA duplication [78]. To our knowledge, resonance effect has not yet been observed *in vivo*.

One would have noticed that, in order to use hybrid models and methods in cancer modelling and treatment, development of several submodels are required. First, rather sophisticated computational tools or frameworks must be developed, including : a) cells as individual objects that can divide, move, change their type (differentiation), die (disappear from the computational domain), interact with each other and with the surrounding medium mechanically and chemically ; b) intracellular regulatory networks described, for instance, by ordinary differential equations ; c) extracellular bio-chemical species, whose evolution can be described by partial differential equations. Second, detailed knowledge of intracellular and extracellular regulations are needed. Extracellular regulation can include local regulation due to cell communication in the tissue or global feedback through hormones or other signaling molecules produced in other organs. Intracellular and extracellular regulations can influence each other in a complex way. Third, pharmacokinetics of medical treatment, treatment protocol, some particular biological or medical aspects of the problem under consideration, like for instance resonance and chronotherapy in this work, must be modeled.

There are two major obstacles in the development of this approach : values of parameters and availability of clinical data. Some values of parameters can be found in the literature. In many cases, however, reaction rates in intracellular protein cascades are completely unknown. Moreover, a "complete" reaction scheme can contain hundreds of interacting proteins, genes, and other factors. So we need to simplify the model preserving its most essential features. The values of parameters should be adjusted in order to obtain biologically realistic functioning of the system : correct proportion of each cell type, correct response to various control parameters, and so on. The uncertainty of the choice of parameters will nevertheless often remain. Pharmacokinetical parameters are taken from [78].

Beyond the question of access to the existing clinical data, which is not straightforward, the main difficulty when trying to compare simulations to existing data, and possibly suggest an improved treatment protocol, is related to the extreme complexity of *in vivo* processes. Intra-specific variation, which has a crucial importance from the evolutionary point of view, complicates even more treatment optimization for individual patients.

In spite of these difficulties, we can expect that hybrid models will be used in biological

experiments and clinical practice. These models allow one to take simultaneously into account spatial effects, intracellular and extracellular regulation, stochasticity, mechanical properties of cells and of the surrounding medium. Conventional continuous models based on ordinary and partial differential equations either cannot describe ensemble of these effects at all or can do it in an empiric way hardly possible to justify rigorously. Moreover, they can become excessively complex even for numerical simulations.

Chapitre 5

From hybrid to continuous models

The present chapter deals with asymptotic analysis of the diffusion-discrete absorption (DDA) equation. This differential-difference equation describes the steady state diffusion with the pointwise absorption. Such a model corresponds, for example, to a chain of cells (points) absorbing some substance ; between the cells a steady diffusion process takes place. The discrete sorption corresponds to the term that is a sum of large number of δ-functions multiplied by the unknown function (concentration). The main result of of this part of thesis is the homogenization (continualisation) of this equation when the small parameter is the distance h between two neighboring cells (in the equilibrium state). This homogenization leads to a purely differential equation describing the macroscopic field. The error estimates are proved for the difference of the exact solution of the DDA equation and the solution of the homogenized differential equation.

Up to our knowledge the existence and uniqueness of solution of the DDA equation was not studied earlier. That is why we prove the existence of solution of the DDA equation. The theoretical results are confronted to the numerical study. This comparison confirms a good accuracy of the asymptotic approximation.

The present chapter continues a set of works devoted to an asymptotic analysis of the discrete models, in particular, in the atomistic mechanics. Some first results in this direction can be found in the book [23]. The idea of an asymptotic derivation of the continuous mechanics from the atomistic description has been revisited in a vast literature [62]. This approach is close in some sense to the justification of difference schemes for the partial differential equations, when the difference scheme plays part of the initial model and the corresponding PDE is the limit model. That is why the homogenization of difference schemes could be also considered in the frame of the passage from discrete to continuous models [13, 61, 82, 87]. The discrete homogenization has been developed in [24]. Finally, the hybrid partially discrete and partially continuous models has been considered in [17, 21, 22, 43, 85, 86].

5.1 Formulation of the problem.

Let R be a positive number, $f_1 \in C([0,1])$, $f_2 \in C([-R,R])$, y be a monotone (increasing) function $[0,1] \to [a,b]$, such that

$$\begin{cases} y''(x) &= f_1(x), x \in (0,1) \\ y(0) &= a, \\ y(1) &= b. \end{cases} \tag{5.1}$$

$-R < a < b < R$; denote by y^{-1} the inverse function to y,

$$\chi_{[a,b]}(x) = \begin{cases} 1, & x \in [a,b], \\ 0, & \text{otherwise.} \end{cases}$$

Consider the problem

$$\begin{cases} u''(x) - h\sum_{j=0}^{k} \alpha\delta(x - y(jh))u(x) &= f_2(x), \quad x \in (-R,R), \\ u'(-R) &= 0, \\ u(R) &= 0. \end{cases} \tag{5.2}$$

where $\alpha, h > 0$, α is the absorption coefficient, $hk = 1$ and k is integer.

Let us introduce the Sobolev space : $H^1_{0R} = \{\varphi \in H^1(-R,R) |\ \varphi(R) = 0\}$. Define a solution of (5.2) as a function $u \in H^1_{0R}$, such that $\forall \varphi \in H^1_{0R}$,

$$-(\int_{-R}^{R} u'(x)\varphi'(x)dx + \sum_{j=0}^{k} \alpha h u(y(jh))\varphi(y(jh))) = \int_{-R}^{R} f_2(x)\varphi(x)dx \tag{5.3}$$

Theorem 5.1.1 Problem (5.3) admits a unique solution.

Proof

Consider a linear functional : $\Phi : H^1_0 \to R$, such that $\Phi(\varphi) = -\int_{-R}^{R} f\varphi dx$. This functional Φ is continuous in L_2 : $| -\int_{-R}^{R} f\varphi dx | \leq \|f\|_{L_2}\|\varphi\|_{L_2}$ and Φ is also continuous in the norm $\|\varphi'\|_{L_2}$ due to the Poincaré-Friedrichs inequality. Let us introduce a new scalar product :

$$(u,v) = \int_{-R}^{R} u'v'dx + \alpha h \sum_{j=0}^{k} u(y_j)\varphi(y_j)$$

and, respectively, the norm

$$\|u\|^2 = \|u'\|^2_{L_2} + \alpha h \sum_{j=0}^{k} u^2(y_j). \tag{5.4}$$

We have

$$u(y_j) = -\int_{y_j}^{R} u'(x)dx,$$

so

$$|u(y_j)| \le \sqrt{2R}\|u'\|_{L_2},$$

and

$$\|u\|^2 \le (1 + 2\alpha R)\|u'\|^2_{L_2},$$

because $hk = 1$. So, the norm (5.4) is equivalent to the norm H^1_{0R}.

Due to the Riesz theorem, there exists a unique solution $u \in H^1_{0R}$ such that $\forall \varphi \in H^1_{0R}$

$$\Phi(\varphi) = \int_{-R}^{R} u'v'dx + \alpha h \sum_{j=0}^{k} u(y_j)\varphi(y_j)$$

Here and below, $y_j = y(jh)$. Then, there exists a unique $u \in H^1_{0R}$ such that $\forall \varphi \in H^1_{0R}$

$$-(\int_{-R}^{R} u'\varphi'dx + \alpha h \sum_{j=0}^{k} u(y(jh))\varphi(y(jh))) = \int_{-R}^{R} f\varphi dx$$

The theorem is proved.

□

The goal of this work is to justify the closeness of problem (5.1)-(5.2) and the macroscopic differential equation :

$$\begin{cases} \overline{u}''(x) - \alpha\overline{u}(x)(y^{-1}(x))'\chi_{[a,b]}(x) &= f_2(x), x \in (-R, R) \\ \overline{u}'(-R) &= 0, \\ \overline{u}(R) &= 0. \end{cases} \tag{5.5}$$

The existence and uniqueness of its solution is well known.

5.2 Comparison of the discrete and continuous models.

Let us prove that the solution of problems (5.1)-(5.2) and (5.5) satisfy the estimate with a constant c independent of h. To this end, compare the integral

$$I_1 = \int_{-R}^{x} h \sum_{j=1}^{k} \alpha\overline{u}(z)\delta(z - y(jh))dz$$

and

$$I_2 = \int_{-R}^{x} \alpha\overline{u}(z)(y^{-1}(z))'dz$$

We have

$$I_1 = h\sum_{j:y(jh)\le x} \alpha\overline{u}(y(jh)) = h\sum_{j:jh\le y^{-1}(x)} \alpha\overline{u}(y(jh)) = \int_0^{y^{-1}(x)} \alpha\overline{u}(y(\theta))d\theta + r_h$$

where

$$r_h = \sum_{j:j\le\frac{y^{-1}(x)}{h}} \int_{jh}^{jh+h} \alpha[\overline{u}(y(jh)) - \overline{u}(y(\theta))]d\theta + \int_{y^{-1}(x)}^{(j_0+1)h} \alpha\overline{u}(y(\theta))d\theta,$$

where

$$j_0 = [\frac{y^{-1}(x)}{h}]$$

Applying the Lagrange theorem, we get

$$|\overline{u}(y(jh)) - \overline{u}(y(\theta))| \le \sup_{\theta\in[0,1]} |\overline{u'}(y(\theta)||\theta - jh| \le \sup_{x\in[-R,R]} |\overline{u'}(x)| \sup_{\theta\in[0,1]} |y'(\theta)|h$$

$$|\int_{y^{-1}(x)}^{(j_0+1)h} \alpha\overline{u}(y(\theta))d\theta| \le |\alpha| \sup_{x\in[-R,R]} |\overline{u}(x)|h$$

Hence,

$$|r_h| \le Mh,$$

where

$$M = \alpha(\sup_{x\in[-R,R]} |\overline{u'}(x)| \sup_{\theta\in[0,1]} |y'(\theta)| + \sup_{x\in[-R,R]} |\overline{u}(x)|) \tag{5.6}$$

Making change, $t = y(\theta)$, in the integral $\int_0^{y^{-1}(x)} \alpha\overline{u}(y(\theta))d\theta$, we get

$$\int_0^{y^{-1}(x)} \alpha\overline{u}(y(\theta))d\theta = \int_a^x \alpha\overline{u}(t)(y^{-1}(t))'dt$$

Integrating equations (5.5) and (5.2), we get

$$\begin{cases} u'(x) - \int_{-R}^{x} h\sum_{j=0}^{k} \alpha u(\theta)\delta(\theta - y(jh))d\theta = \int_{-R}^{x} f_2(\theta)d\theta, \\ u(R) = 0. \end{cases} \tag{5.7}$$

$$\begin{cases} \overline{u}'(x) - \displaystyle\int_{-R}^{x} \alpha\overline{u}(\theta)(y^{-1}(\theta))'\chi_{[a,b]}(\theta)d\theta = \int_{-R}^{x} f_2(\theta)d\theta, \\ \overline{u}(R) = 0. \end{cases} \tag{5.8}$$

Denote $w = \overline{u} - u$. Then, subtracting (5.7) from (5.8), we get

$$w'(x) - \int_{-R}^{x} h\sum_{j=0}^{k} \alpha w(\theta)\delta(\theta - y(jh))d\theta + I_1 - \int_{-R}^{x} \alpha\overline{u}(\theta)(y^{-1}(\theta))'\chi_{[a,b]}(\theta)d\theta = 0$$

On the other hand,

$$I_1 - \int_{a}^{x} \alpha\overline{u}(t)(y^{-1}(t))'\chi_{[a,b]}(\theta)d\theta = r_h.$$

Therefore,

$$\begin{cases} w'(x) - \displaystyle\int_{-R}^{x} h\sum_{j=0}^{k} \alpha w(\theta)\delta(\theta - y(jh))d\theta + r_h &= 0, \\ w(R) &= 0. \end{cases} \tag{5.9}$$

Multiply (5.9) by φ' where $\varphi \in H^1_{0R}(-R, R)$, and integrate, we get

$$\int_{-R}^{R} w'\varphi' dx - \int_{-R}^{R}\int_{-R}^{x} h\sum_{j=0}^{k} \alpha w(\theta)\delta(\theta - y(jh))d\theta\varphi'(x)dx + \int_{-R}^{R} r_h(x)\varphi'(x)dx = 0$$

$$\int_{-R}^{R} w'\varphi' dx + h\sum_{j=0}^{k} \alpha w(y(jh))\varphi(y(jh)) = -\int_{-R}^{R} r_h(x)\varphi'(x)dx$$

Setting $\varphi = w$, we have

$$\|w'\|^2_{L_2} + h\sum_{j=0}^{k} \alpha w^2(y(jh)) \le \|r_h\|_{L_2}\|w'\|_{L_2}$$

$$\|w'\|_{L_2} \le \|r_h\|_{L_2}$$

Applying the Poincaré-Friedrichs inequality, we get

$$\|w\|_{H^1} \le \sqrt{2R^2 + 1}\|r_h\|_{L_2}$$

Let us estimate constant M (see (5.6)). We have

$$y(x) = \int_0^x \int_0^t f_1(\theta) d\theta dt + a - x \int_0^1 \int_0^t f_1(\theta) d\theta dt + (b-a)x \tag{5.10}$$

therefore,

$$y'(x) = \int_0^x f_1(\theta) d\theta + (b-a) - \int_0^1 \int_0^t f_1(\theta) d\theta dt$$

then,

$$\max_{0 \le x \le 1} \|y'(x)\| \le |b-a| + 2\|f_1\|_{L^1} \tag{5.11}$$

For $\overline{u}$ we get

$$\|\overline{u}'\|_{L^2}^2 + \alpha \int_{-R}^{R} \overline{u}^2(x)(y^{-1}(x))' dx = -\int_{-R}^{R} f_2 \overline{u} dx$$

hence,

$$\|\overline{u}'\|_{L^2} \le \|f_2\|_{L^2} R\sqrt{2} \tag{5.12}$$

$$\|\overline{u}\|_{L^\infty} = \|\int_x^R \overline{u}'(t) dt\|_{L^\infty} \le \sqrt{2R}\|\overline{u}'\|_{L^2} \le 2R^{\frac{3}{2}}\|f_2\|_{L_2} \tag{5.13}$$

Let

$$K_0 = \min_{x \in [0,1]} \int_0^x f_1(\theta) d\theta + (b-a) - \int_0^1 \int_0^t f_1(\theta) d\theta dt > 0 \tag{5.14}$$

Then,

$$\overline{u}' = \alpha \int_{-R}^{x} \overline{u}(t)(y^{-1}(t))' dt + \int_{-R}^{x} f_2(t) dt$$

therefore,

$$\|\overline{u}'\|_{L^\infty} \le \alpha \|\overline{u}\|_{L^\infty} 2R \max_{t \in [a,b]} (y^{-1}(t))' + \|f_2\|_{L_1} \le 4\alpha R^{\frac{5}{2}} \frac{1}{K_0} \|f_2\|_{L^2} + \|f_2\|_{L^1} \tag{5.15}$$

And so, finally,

$$M = \alpha((4\alpha R^{\frac{5}{2}} \frac{1}{K_0} \|f_2\|_{L^2} + \|f_2\|_{L^1})(|b-a| + 2\|f_1\|_{L^1}) + 2R^{\frac{3}{2}}\|f_2\|_{L_2}) \tag{5.16}$$

Theorem 5.2.1 The estimate holds :

$$\|u - \overline{u}\|_{H^1} \le \sqrt{2R^2+1}\sqrt{2R} M h$$

This theorem justifies the homogenized continuous models (5.5).

5.3 Numerical experiments

Below we compare the solution of problems (5.1),(5.2) and (5.5), solved numerically. To this end we consider a one-dimensional lattice of points $x_i = R + ih_1$, $i = 0, \ldots, N_1$, where the mesh-step $h_1 = 2R/N_1$, $h_1 \ll h$ is a small positive parameter ($N_1 >> 1$). Discretized form of equation (5.2) corresponds the following finite-difference equation :

$$\frac{u_{i+1} - u_i}{h_1} - h\alpha \sum_{j:y(jh)\le x_i} (\theta_j u_{i(j)} + (1-\theta_j) u_{i(j)+1})) = \int_{-R}^{x_i} f_2(x_i), \;\; i = 1, ..., N_1 - 1, \;\; u_1 = u_0, \; u_{N_1} = 0, \tag{5.17}$$

where for any j $x_{i(j)}$, $x_{i(j)+1}$ are the neighboring nodes of $y(jh)$. and θ_j is defined from relation $y(jh) = \theta_j x_{i(j)} + (1 - \theta_j) x_{i(j)+1}$. We solve (5.17) with shooting method [12].

To compute a numerical approximation for the solution of equation (5.5) we apply the second order difference scheme :

$$\frac{u_{i+1} - 2u_i + u_i}{h_1^2} - \alpha u_i((y^{-1})'(x_i)))\chi_{[a,b]} = f_2(x_i), \;\; i = 1, ..., N_1 - 1, \;\; u_1 = u_0, \; u_{N_1} = 0, \tag{5.18}$$

and we solve this equation with the "balayage" method (known also as the "Thomas algorithm") [12].

3.1. We consider the following data : a=1, b=5, $f_2 = 1$, $\alpha = 0.2$. Let us consider the function y satisfying $y'' = 0$, i.e. $y = 4x + 1$, $(y^{-1})' = 1/4$.

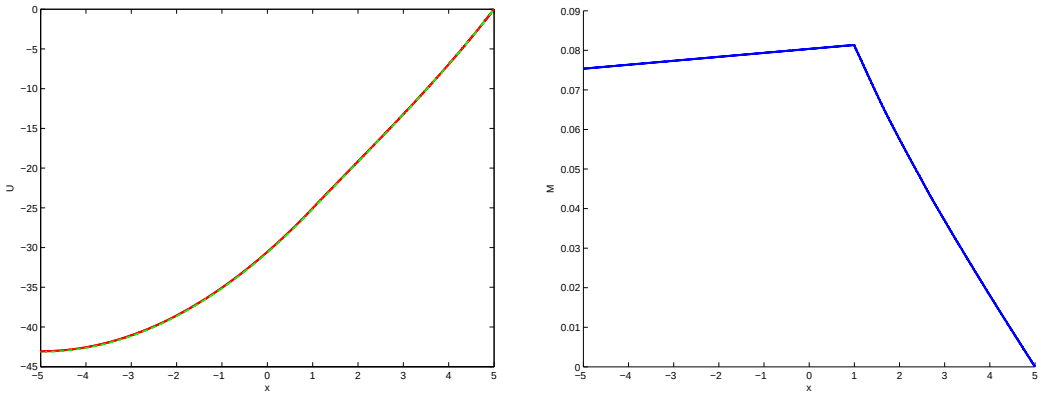

(a) $h = 0.01$, $h_1 = 0.001$ (b) $h = 0.01$, $h_1 = 0.001$

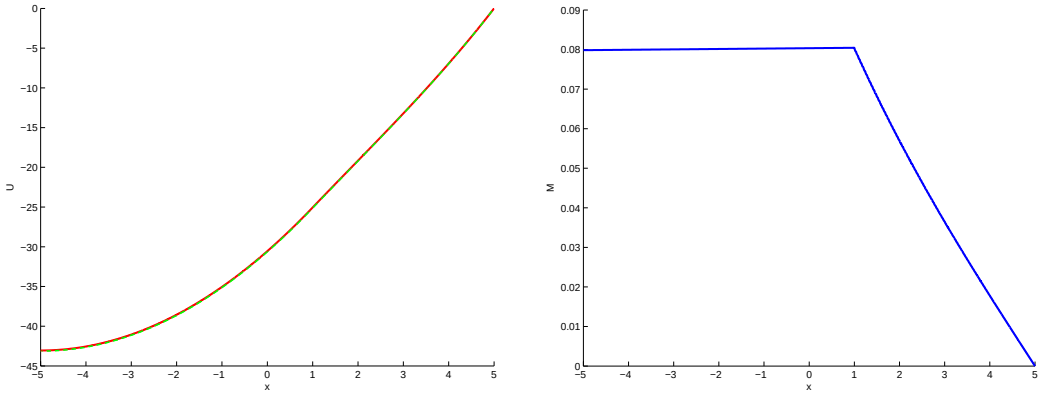

(c) $h = 0.01$, $h_1 = 0.0001$ (d) $h = 0.01$, $h_1 = 0.0001$

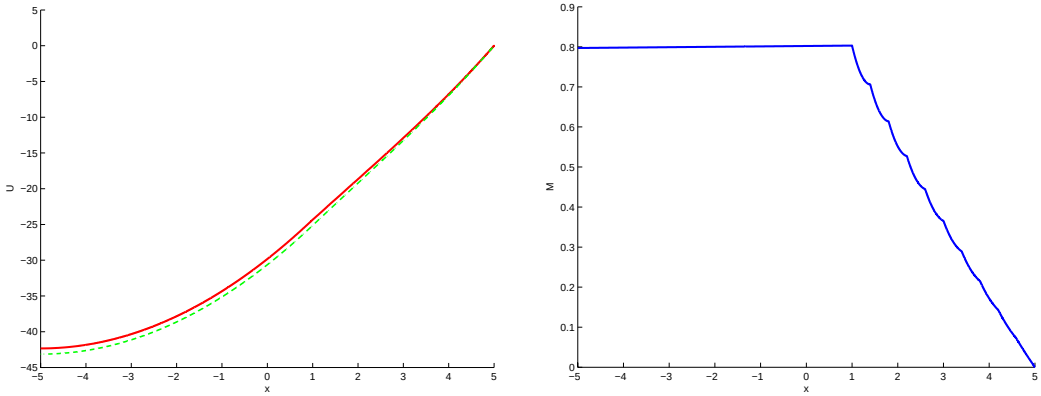

(e) $h = 0.1$, $h_1 = 0.001$ (f) $h = 0.1$, $h_1 = 0.001$

FIG. 5.1 – Left : red (solid) and green (dash) curves correspond to the numerical solution of (5.2) and (5.5), respectively. Right : blue curve is the difference between these two solutions.

3.2. Now let us consider the function y satisfying $y'' = 1$, i.e. $(y^{-1})' = \frac{2}{\sqrt{41+8x}}$.

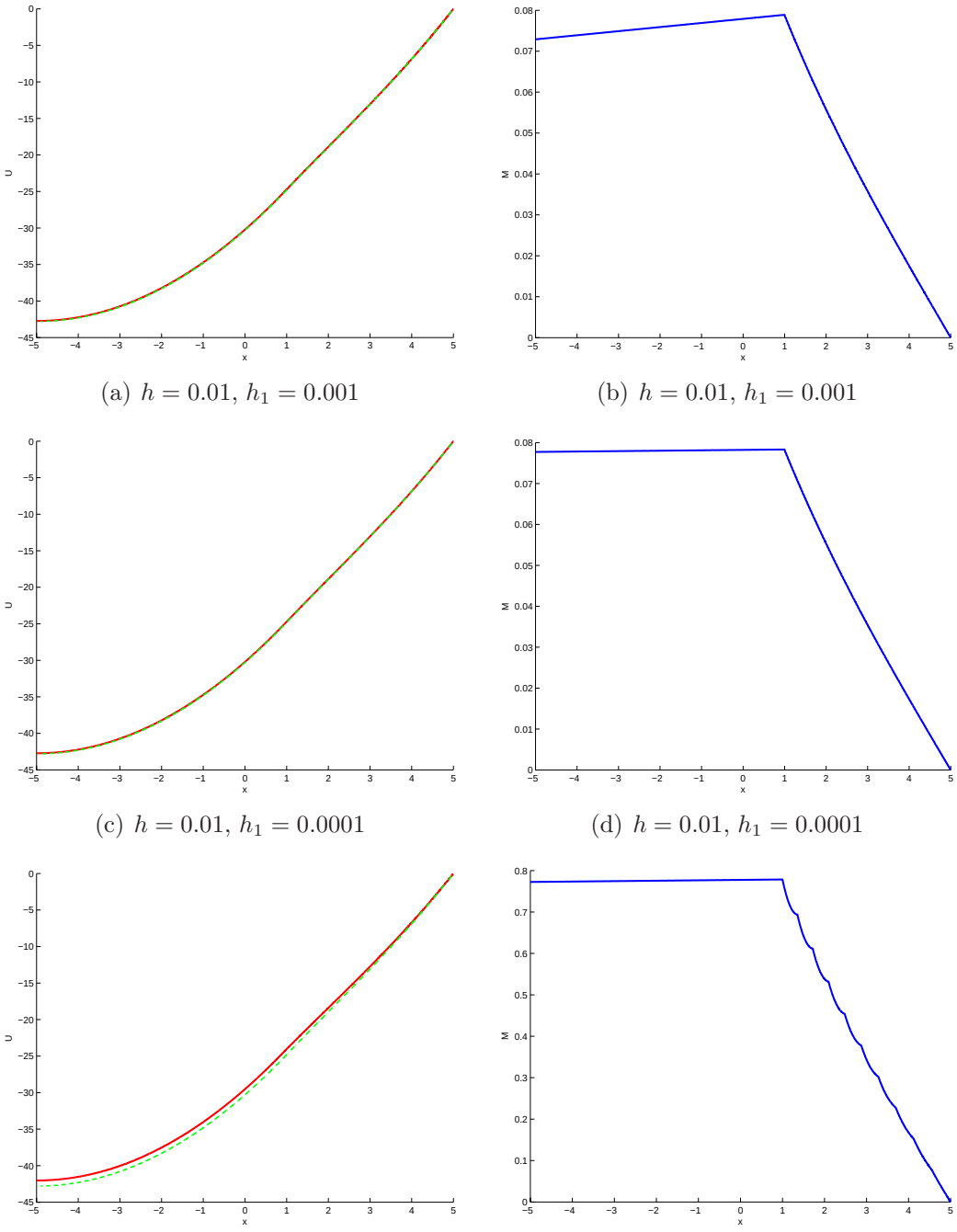

(a) $h = 0.01$, $h_1 = 0.001$ (b) $h = 0.01$, $h_1 = 0.001$

(c) $h = 0.01$, $h_1 = 0.0001$ (d) $h = 0.01$, $h_1 = 0.0001$

(e) $h = 0.1$, $h_1 = 0.001$ (f) $h = 0.1$, $h_1 = 0.001$

FIG. 5.2 – Left : red (solid) and green (dash) curves correspond to numerical solution of (5.2) and (5.5), respectively. Right : blue curve is the difference between two solutions.

Conclusions and Perspectives

Conclusions. This thesis is devoted to off-lattice discrete-continuous hybrid modeling applied to hematopoiesis and blood diseases, such as leukemia and anemia. The main results of the dissertation are as follows :

- Hybrid models with off-lattice cell dynamics were introduced and studied. Cells are considered as individual object. Intracellular regulation determine cell fate, that is their self-renewal, differentiation and apoptosis. Therefore, we do not impose the corresponding rates as parameters but obtain them as a result of modeling. This is one of the main achievements of this work.
- Model examples of hybrid models which describe biological processes such as the competition between cell proliferation and apoptosis, between proliferation and differentiation and between cell cycling and quiescent state were presented.
- Biological pattern formation with hybrid models and its application to bacteria filament is discussed.
- A new model of red blood cell production considering the intracellular scale (protein regulation, cell fate decision) and the cell population scale (cell-cell interactions, influence of feedback controls) was proposed.
- The numerical simulation of an erythroblastic island were carried out. Our results brought new information on the role of the macrophage and the erythroblastic island in the production and regulation of red blood cells, the macrophage was shown to play a key role in the stability and robustness of the production process.
- Using experimental data on anemia in mice, we investigate the roles of different feedback mechanisms in response to stress situations.
- Hybrid models was applied to leukemia modeling and its treatment. A Physiologically Based Pharmacokinetics-Pharmacodynamics (PBPKPD) model of leukemia treatment with AraC drug and the relevance of considering chronotherapeutic treatments to control leukemia was examined.
- The passage from a hybrid model to a continuous model in the 1D case was carried out :
  - Comparison between particle dynamics flow and the corresponding equations of continuum mechanics was done. Numerical simulations confirm a good agreement between these approaches
  - Comparison of diffusion-discrete absorption equation that describes the steady state diffusion with the pointwise absorption equation and its homogenized form that

leads to continuous differential equation shows a good accuracy of the asymptotic approximation.

Perspectives. We propose and study the model of normal and leukemic erythropoiesis which give some insight in the way how erythroid cell proliferation and differentiation can be controlled, *in vitro* and *in vivo*. Nevertheless, further developments could be considered :

- The regulatory network can be completed by introduction of additional proteins, for example, such as GATA-1, which involved in erythroid progenitor differentiation [2, 107].
- Influx of BFU-E and CFU-E from HSC can be considered in the further work.
- Both erythropoietin's influence on erythroid progenitor self-renewal capacity and on apoptosis protection were taken as linear functions of the number of circulating red blood cells. Saturation effects should be envisaged when confronting the model to strong perturbations (for instance, a severe anemia), in order to be closer to the reality where responses of the organism to a loss of red blood cells have shown to be nonlinear [28, 29].
- In this work focus was made on the behavior of one single erythroblastic island and on feedback controls at global and local scales. However, particular geometries, with obstacles or describing the porous aspect of the bone marrow can be investigated.
- The hybrid model was numerically simulated in two dimensions. The case of simulations in three dimensions has not been developed. Qualitatively, such a change is not expected to modify the results, it should nevertheless be tested.
- Moreover, in this work, we focus our attention on red blood cell lineage. Study of haematopoiesis should be improved by taking into account development of different blood cells lineages, lymphopoiesis and myelopoiesis.
- In the modeling of leukemic erythropoiesis and its treatment, in order to predict the outcome of treatment in a more realistic situation, we need to introduce :
  - different proliferation rates for normal and leukemic cells
  - different lineages of leukemic cells
  - resistance to treatment
- Next important step in the modeling of leukemia treatment will be directed to optimization of the AML treatment by taking into account individual variability of patients. To achieve this goal the malignant cells from individual patients should be analyzed in order to determine pharmacokinetics-pharmacodynamics parameters.

We intend to study these questions in the subsequent works.

Annexe A

Addition to chapter 3 and 4

A.1 Computational algorithm

Programming is done in C++. The algorithm is shown schematically in Figure (A.1). We present here its short description.

1. Generate an initial configuration of cells. Each cell of the list is parameterized by cell's coordinate, speed, radius, age, duration of cell's phases, its type and intracellular concentrations. Initial intracellular concentration in the cells are prescribed to be zero.
2. Update boxes. To economize computational time space domain was devised into square boxes with size $4r \times 4r$ where r is the radius of cell. Force between two cells is zero is zero if the distance is greater than the sum of their radii. Therefore, each cell can communicate only with cells from the same and neighboring boxes.
3. Find the total force F_i acting on the i-th cell from all other cells, $F_i = \sum_{j \neq i} f_{ij}$, in the same and the neighboring cells.
4. Compute cell movement due to Newton's second law.
5. Calculate cell growth with respect that cell should reach twice of its initial radius at the end of the cell cycle.
6. Interpolate extracellular values from the grid to the cell position and update the intracellular variables by an explicit scheme.
7. Check for

   I *progenitors :*

   (a) if Erk concentration reaches the critical value E_c then the cell self-renews at the end of its cycle.

   (b) if Fas concentration reaches its critical value F_c then the cell dies by apoptosis immediately.

   (c) otherwise, cell differentiates in reticulocytes.

   II *reticulocytes :*

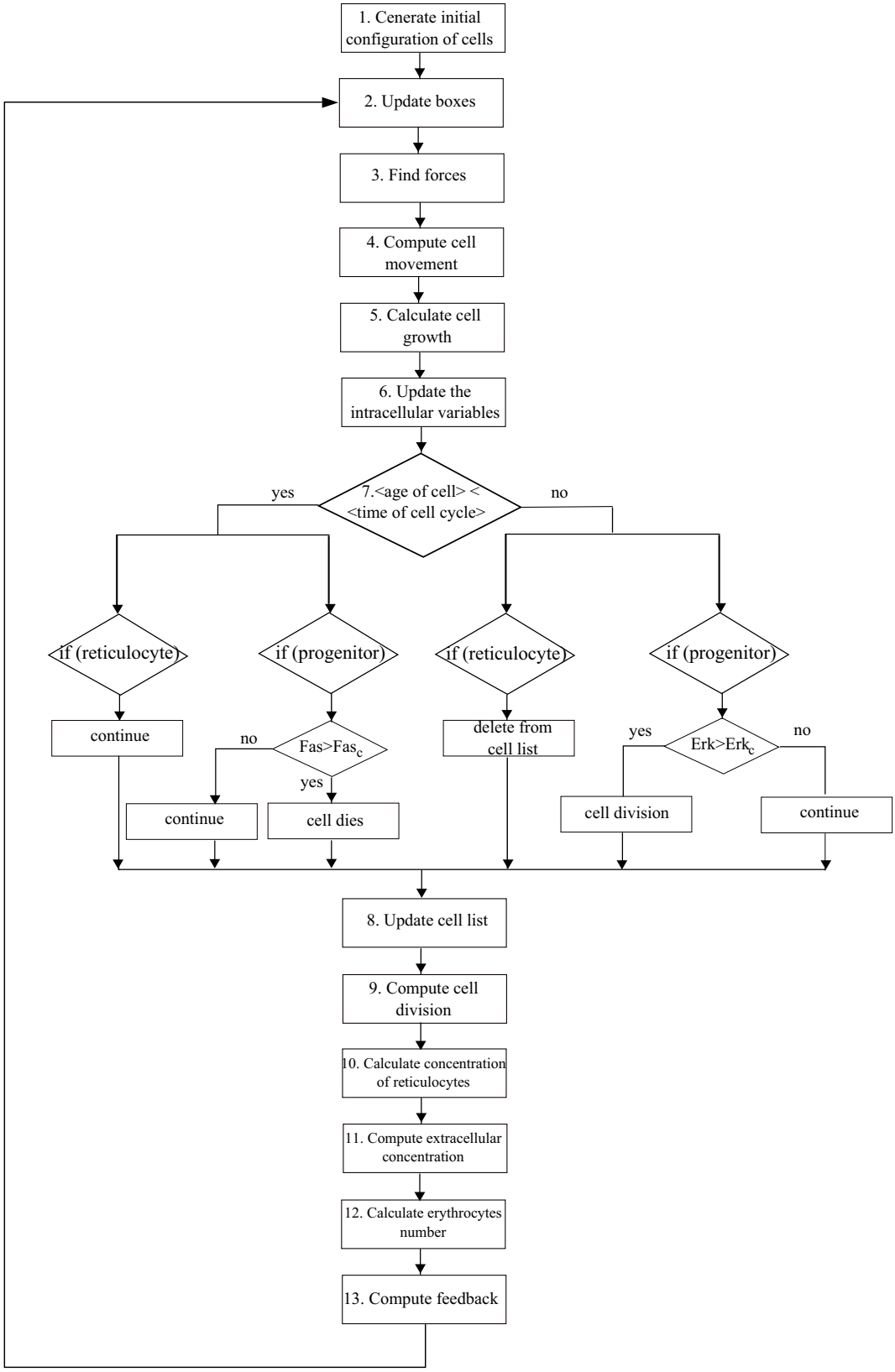

FIG. A.1 – Schematic representation of the computational algorithm.

(a) if reticulocyte age is more than one cycle we assume that it become erythrocyte and we delete reticulocyte from computational domain.

8. Update cell list.
9. Compute cell division, by replacing mother cell with two daughter cells. Orientation of the mitotic spindle at division is chosen randomly.
10. Calculate concentration of reticulocytes in each square grid of space to transfer the secreted Fas-ligand to the grid.
11. Solve equations of extracellular concentrations of Fas-ligand, produced by reticulocytes, and growth factors (in case with macrophage) on a regular grid, using an alternating direction implicit method for the partial differential equations.
12. Calculate the number of circulating erythrocytes. They are counted as cells outside the domain which live during a time corresponding to certain cycle durations.
13. Compute feedback from erythrocytes, which act through feedback loops, on the fate of immature cells within the domain.
14. Continue with step (2).

In computational algorithm of leukemia treatment we also calculate pharmacokinetics of AraC in each cell in step 6. Next, in step 7 we check if intracellular concentration of AraCTP in DNA reached its critical value. In this case cell dies by apoptosis and is deleted from the cell list.

Alternating direction implicit method. Consider the diffusion equation in two dimensions :

$$\begin{cases} \dfrac{\partial u}{\partial t} = \dfrac{\partial^2 u}{\partial x^2} + \dfrac{\partial^2 u}{\partial y^2}, \quad 0 \le x, y \le 1, \quad 0 \le t \le T \\ u(x, y, 0) = \psi(x, y), \quad 0 \le x, y \le 1 \\ u(x, y, t) \mid_D = G \end{cases} \tag{A.1}$$

in the square domain $0 \le x, y \le 1$ with the boundary D. We chose the grid $(x_i, y_j, t_p) = (ih, jh, pt)$, $i = 1, 2, ..., N_x$ and $h_1 = 1/N_x$, $j = 1, 2, ..., N_y$ and $h_2 = 1/N_y$. The problem (A.1) can be written in the following form :

$$\begin{cases} \dfrac{\partial u}{\partial t} = \dfrac{1}{2}(\dfrac{\partial^2 u}{\partial x^2} + \dfrac{\partial^2 u}{\partial y^2}) + \dfrac{1}{2}(\dfrac{\partial^2 u}{\partial x^2} + \dfrac{\partial^2 u}{\partial y^2}), \quad 0 \le x, y \le 1, \quad 0 \le t \le T \\ u(x, y, 0) = \psi(x, y), \quad 0 \le x, y \le 1 \\ u(x, y, t) \mid_D = G \end{cases} \tag{A.2}$$

Next, we split the first equation of (A.2) in two sub-steps and chose the following finite difference scheme :

$$\begin{cases} \dfrac{u_{i,j}^{p+1/2}-u_{ij}^{p}}{\Delta t/2}=\dfrac{u_{i-1,j}^{p+1/2}-2u_{i,j}^{p+1/2}+u_{i+1,j}^{p+1/2}}{h^2}+\dfrac{u_{i,j-1}^{p}-2u_{i,j}^{p}+u_{i,j+1}^{p}}{h^2}, \\ \dfrac{u_{i,j}^{p+1}-u_{ij}^{p+1/2}}{\Delta t/2}=\dfrac{u_{i-1,j}^{p+1/2}-2u_{i,j}^{p+1/2}+u_{i+1,j}^{p+1/2}}{h^2}+\dfrac{u_{i,j-1}^{p+1}-2u_{i,j}^{p+1}+u_{i,j+1}^{p+1}}{h^2}, \end{cases} \tag{A.3}$$

To calculate u^{p+1} using the scheme above, first of all for each fixed j we should solve the first equation of (A.3) for $u^{p+1/2}$. Next, we should solve the second equation relative u^{p+1}. Let us start with the first equation :

$$\frac{u_{i,j}^{p+1/2}-u_{ij}^{p}}{\Delta t/2}=\frac{u_{i-1,j}^{p+1/2}-2u_{i,j}^{p+1/2}+u_{i+1,j}^{p+1/2}}{h^2}+\frac{u_{i,j-1}^{p}-2u_{i,j}^{p}+u_{i,j+1}^{p}}{h^2},$$

$$\underbrace{\frac{1}{h^2}}_{a_{ij}}u_{i-1,j}^{p+1/2}+\underbrace{(-\frac{2}{h^2}-\frac{1}{\Delta t/2})}_{b_{ij}}u_{i,j}^{p+1/2}+\underbrace{\frac{1}{h^2}}_{c_{ij}}u_{i+1,j}^{p+1/2}=\underbrace{-\frac{u_{i,j}^{p}}{\Delta t/2}-\frac{u_{i,j-1}^{p}-2u_{i,j}^{p}+u_{i,j+1}^{p}}{h^2}}_{f_{ij}},$$

Therefore, the first equation of the system can be written in the following form :

$$a_{ij}u_{i-1,j}^{p+1/2}+b_{ij}u_{i,j}^{p+1/2}+c_{ij}u_{i+1,j}^{p+1/2}=f_{ij}^{p},$$

for each fixed j, $j=1,2,...,N_y-1$ we solve the equation :

$$a_iu_{i-1}^{p+1/2}+b_iu_i^{p+1/2}+c_iu_{i+1}^{p+1/2}=f_i^p,\quad \forall i=1,...,N_x-1 \tag{A.4}$$

with the boundary conditions $u_{i=0}^{p}=g_1$, $u_{i=N_x}^{p}=g_2$.

We can solve equation (A.4) using the Thomas algorithm. For that we can write equation $u_{i=0}^{p}=g_1$ in the following form :

$$u_0=L_{1/2}u_1+K_{1/2},$$

where $L_{1/2}=0$ and $K_{1/2}=g_1$. From equation

$$a_1u_0+b_1u_1+c_1u_2=f_1,$$

that correspond to equation (A.4) with $i=1$, represent u_1 :

$$u_1=L_{3/2}u_2+K_{3/2}, \tag{A.5}$$

where we denote by $L_{3/2}=\frac{-c_1}{b_1}$, $K_{3/2}=\frac{a_1g_1-f_1}{-b_1}$. From equation

$$a_2u_1+b_2u_2+c_2u_3=f_2,$$

that correspond to equation (A.4) with $i = 2$, using (A.5) we represent u_2 :

$$u_2 = L_{5/2}u_3 + K_{5/2}.$$

We continue this process for $i = 3, 4, ...$

Substitute

$$u_{i-1} = L_{i-1/2}u_i + K_{i-1/2}$$

into equation

$$a_i u_{i-1} + b_i u_i + c_i u_{i+1} = f_i,$$

we have

$$u_i = \frac{-c_i}{b_i + a_i L_{i-1/2}} u_{i+1} + \frac{f_i - a_i K_{i-1/2}}{b_i + a_i L_{i-1/2}}$$

or

$$u_i = L_{i+1/2}u_{i+1} + K_{i+1/2} \tag{A.6}$$

We see that the coefficients $L_{i+1/2}$ and $K_{i+1/2}$ obtained due to the method described above can be calculated with following recurrent formulas

$$L_{i+1/2} = \frac{-c_i}{b_i + a_i L_{i-1/2}}, \tag{A.7}$$

$$K_{i+1/2} = \frac{f_i - a_i K_{i-1/2}}{b_i + a_i L_{i-1/2}}. \tag{A.8}$$

For $i = N - 1$ we obtain

$$u_{N-1} = L_{N-1/2}u_N + K_{N-1/2}.$$

As $u_N = g_2$, we can calculate

$$u_{N-1} = L_{N-1/2}g_2 + K_{N-1/2}.$$

After that we can obtain the values of u_{N-2}, u_{N-3}, ..., u_1 by formula (A.6). Therefore, the Thomas algorithm consists of the forward sweep with calculating $L_{i+1/2}$ and $K_{i+1/2}$ with recurrent formulas (A.7)-(A.8). The solution is obtained by the backward sweep with formula (A.6).

Thereby, we found $u^{p+1/2}$. Analogically, we find u^{p+1} from the second equation of system (A.3).

Bibliographie

[1] A.S Ackleh, K. Deng, K. Ito, J. Thibodeaux, *A structured erythropoiesis model with nonlinear cell maturation velocity and hormone decay rate*, Math. Bios. 204, (2006), pp. 21–48.

[2] G.R. Aispuru, M.V. Aguirre, J.A. Aquino-Esperanza, C.N. Lettieri, J.A. Juaristi, N.C. Brandan, *Erythroid expansion and survival in response to acute anemia stress : the role of EPO receptor, GATA-1, Bcl-xL and caspase-3*, Cell Biol. Int. 32 (8), (2008), pp. 966–78.

[3] E. Afenya, *Acute leukemia and chemotherapy : A modeling viewpoint*, Original Research Article Mathematical Biosciences 138 (2), (1996), pp. 79–100.

[4] T. Alarcón, H.M. Byrneb, P.K. Mainia, *A cellular automaton model for tumour growth in inhomogeneous environment*, J. Theor. Biol. 225, (2003), pp. 257–274.

[5] A.R.A. Anderson, M.A.J. Chaplain, *Continuous and discrete mathematical models of tumor-induced angiogenesis*, Bull. Math. Biol. 60 (5), (1998), pp. 857–99.

[6] A.R.A. Anderson, M.A.J. Chaplain, K.A. Rejniak, *The cellular Potts model and its variants*, Single-Cell-Based Models in Biology and Medicine, (2007).

[7] A.R.A. Anderson, K.A. Rejniaka, P. Gerleea, V. Quaranta, *Modelling of Cancer Growth, Evolution and Invasion : Bridging Scales and Models*, Math. Model. Nat. Phenom. 2 (3), (2007), pp. 1–29.

[8] A.R.A. Anderson, *A hybrid multiscale model of solid tumour growth and invasion : Evolution and the microenvironment*, Single Cell Based Models in Biology and Medicine, Mathematics and Biosciences in Interaction, (2007), pp. 3–28.

[9] A. Altinok, F. Lévi and A. Goldbeter, *Identifying mechanisms of chronotolerance and chronoefficacy for the anticancer drugs 5-fluorouracil and oxaliplatin by computational modeling*, Eur. J. Pharm. Sci. 36, (2009), pp. 20–38.

[10] A. Altinok, F. Lévi and A. Goldbeter, *A cell cycle automaton model for probing circadian patterns of anticancer drug delivery*, Adv. Drug Deliv. Rev. 59, (2007), pp. 1036-1053.

[11] R. Apostu, M.C. Mackey, *Understanding cyclical thrombocytopenia : A mathematical modeling approach*, J. Theor. Biol. 251, (2008), pp. 297–316.

[12] N.S. Bakhvalov, *Méthodes Numériques*, Edition Mir, Moscow, (1973).

[13] N.S. Bakhvalov, *Averaging of partial differential equations with rapidly oscillating coefficients*, Doklady Acad. Nauk SSSR 224 (2), pp. 351–355, 1975.

[14] A. Bauer, F. Tronche, O. Wessely, C. Kellendonk, H.M. Reichardt, P. Steinlein, G. Schutz, and H. Beug, *The glucocorticoid receptor is required for stress erythropoiesis*, Genes Dev. 13 (22), (1999), pp. 2996–3002.

[15] S. Bernard , J. Bélair, M.C. Mackey *Oscillations in cyclical neutropenia : New evidence based on mathematical modeling* J. Theor. Biol. 223, (2003), pp. 283–298, doi :10.1016/S0022-5193(03)00090-0.

[16] S. Bernard, B. Cajavec Bernard, F. Lévi and H. Herzel, *Tumor growth rate determines the timing of optimal chronomodulated treatment schedules*, PLoS Comput. Biol. 6, (2010), e1000712.

[17] N. Bessonov, V. Volpert, *Dynamic models of plant growth.*

[18] N. Bessonov , F. Crauste, S. Fischer, P. Kurbatova, V. Volpert, *Application of Hybrid Models to Blood Cell Production in the Bone Marrow*, in press Math. Model. Nat. Phenom., submitted.

[19] N. Bessonov, P. Kurbatova, V. Volpert, *Particle dynamics modelling of cell populations*, Proc. Conf. JANO, Mohhamadia, 2008. Math. Model. Nat. Phenom. 5 (7), (2010), pp. 42–47.

[20] N. Bessonov, L. Pujo-Menjouet, V, Volpert. *Cell modelling of hematopoiesis.* Math. Model. Nat. Phenom. 1 (2), (2006), pp. 81–103.

[21] X. Blanc, C. Le Bris, P.L. Lions, *Atomistic to continuum limits for computatioal materials science* , Laboratoire Jacques-Louis Lions, (2005).

[22] X. Blanc, C. Le Bris, F. Legoll, *Analysis of a prototypical multiscale method coupling atomistic and continuum mechanics*, Mathematical Modelling and Numerical Analysis 39 (4), (2005), pp. 797–826.

[23] M. Born, K. Huang, *Dynamical Theory of Crystal Lattices*, Oxford U. P., London, (1954).

[24] D. Caillerie, A. Muorad, A. Raoult, *Discrete hohmogenization in graphene sheet modeling*, Journal of Elasticity 84, (2006), pp. 33–68.

[25] C. Colijn and M.C. Mackey, *A mathematical model of hematopoiesis – I. Periodic chronic myelogenous leukemia*, J. Theor. Biol. 237, (2005), pp. 117–132.

[26] C. Colijn and M.C. Mackey, *A mathematical model of hematopoiesis – II. Cyclical neutropenia*, J. Theor. Biol. 237, (2005), pp. 133–146.

[27] J.A. Chasis and N. Mohandas, *Erythroblastic islands : niches for erythropoiesis*, Blood 112, (2008).

[28] F. Crauste, L. Pujo-Menjouet, S. Génieys, C. Molina, O. Gandrillon, *Adding Self-Renewal in Committed Erythroid Progenitors Improves the Biological Relevance of a Mathematical Model of Erythropoiesis*, J. Theor. Biology 250, (2008), pp. 322–338 .

[29] F. Crauste, I. Demin, O. Gandrillon, V. Volpert, *Mathematical study of feedback control roles and relevance in stress erythropoiesis* J. Theor. Biology 263, (2010), pp. 303–316.

[30] S.H. Chapel, P. Veng-Pedersen, R.L. Schmidt, J.A. Widness, *A pharmacodynamic analysis of erythropoietin-stimulated reticulocyte response in phlebotomized sheep*, J. Pharmacol. Exp. Ther. 295 (1), (2000), pp. 346–351.

[31] R. Cheong, A. Bergmann, S. L. Werner, J. Regal, A. Hoffmann and A. Levchenko, *Transient IκB Kinase Activity Mediates Temporal NF-κB Dynamics in Response to a Wide Range of Tumor Necrosis Factor-αDoses*, The Journal of Biological Chemistry, 281 (5), (2006), pp. 2945–2950.

[32] John C. Dallon, *Models with lattice-free center-based cells interacting with continuum environment variables*, Single Cell Based Models in Biology and Medicine, Mathematics and Biosciences in Interaction, III., (2007), pp. 197–219

[33] J.C. Dallon and H.G. Othmer, *A discrete cell model with adaptive signalling for aggregation of Dictyostelium discoideum*, Philos. Trans. R Soc. Lond B Biol Sci. 352 (1351), (1997), pp. 391–417.

[34] A. Deutsch, *Lattice-gas cellular automaton modeling of developing cell systems* , Single-Cell-Based Models in Biology and Medicine, Mathematics and Biosciences in Interaction, (2007), pp. 29–51.

[35] B.F. Dibrov, *Resonance effect in self-renewing tissues*, J. Theor. Biol. 192, (1998), pp. 15–33.

[36] S. Dazy, F. Damiola, N. Parisey, H. Beug and O. Gandrillon, *The MEK-1/ERKs signaling pathway is differentially involved in the self-renewal of early and late avian erythroid progenitor cells*, Oncogene 22, (2003), pp. 9205–9216.

[37] I. Demin, F. Crauste, O. Gandrillon and V. Volpert, *A multi-scale model of erythropoiesis*, Journal of Biological Dynamics 4 (2010), pp. 59–70.

[38] R. Dillon, M. Owen, and K. Painter, *A single-cell-based model of multicellular growth using the immersed boundary method*, AMS Contemp. Math. 466, (2008), pp. 1–15.

[39] D. Drasdo, *Center-based single-cell models : An approach to multi-cellular organization based on a conceptual analogy to colloidal particles*, Single Cell Based Models in Biology and Medicine, Mathematics and Biosciences in Interaction, (2007), pp. 171–196

[40] S. Dormann and A. Deutsch, *Modeling of self-organized avascular tumor growth with a hybrid cellular automaton*, In Silico Biol., (2002), pp. 393–406.

[41] J. Eller , I. Gyori, M. Zollei, F. Krizsa, *Modelling Thrombopoiesis Regulation - I Model description and simulation results*, Comput. Math. Appli 14, (1987), pp. 841–848.

[42] E.H. Estey, *Treatment of acute myeloid leukemia*, Haematologica, 94 (2009), pp. 10–16

[43] M. Betoue Etoughe, G. Panasenko, *Partial homogenization of discrete models*, Applicable Analysis 87 (12), (2008) pp. 1425–1442.

[44] K.J. Freise, J.A. Widness, R.L. Schmidt, P. Veng-Pedersen, *Pharmacodynamic analysis of timevariant cellular disposition : reticulocyte disposition changes in phlebotomized sheep*, J. Pharmacokinet. Pharmacodyn. 34, (2007), pp. 519–547.

[45] O. Gandrillon, *The v-erbA oncogene. Assessing its differentiation-blocking ability using normal chicken erythrocytic progenitor cells*, Methods Mol. Biol. 202, (2002), pp. 91–107.

[46] O. Gandrillon , U. Schmidt, H. Beug, J. Samarut, *TGF-beta cooperates with TGF-alpha to induce the self-renewal of normal erythrocytic progenitors : evidence for an autocrine mechanism*, Embo J. 18, (1999), pp. 2764–2781.

[47] C. Giverso, M. Scianna, L. Preziosi, N. Lo Buono and A. Funaro, *Individual Cell-Based Model for In-Vitro Mesothelial Invasion of Ovarian Cancer*, Math. Model. Nat. Phenom. 5 (1), (2010), pp. 203-223.

[48] D.F. Gluzman, V.A. Nadgornaya, L.M. Sklyarenko, T.S. Ivanovskaya, L.Yu. Poludnenko, N.I. Ukrainskaya, *Immunocytochemical markers in acute leukemias diagnosis*, Exp. Oncol., (2010).

[49] A. Golubev, *Random discrete competing events vs. dynamic bistable switches in cell proliferation in differentiation*, J. Theor. Biol. 267 (3), (2010), pp. 341–354.

[50] R.S. Hillman, *Characteristics of marrow production and reticulocyte maturation in normal man in response to anemia*, J. Clin. Invest. 48, (1969), pp. 443–453.

[51] S. Hoehme, D. Drasdo, *A cell-based simulation software for multi-cellular systems*, Bioinformatics 26 (20), (2010), pp. 2641–2642.

[52] N.H. Al-Huniti, J.A. Widness, R.L. Schmidt, P. Veng-Pedersen, *Pharmacodynamic analysis of changes in reticulocyte subtype distribution in phlebotomyinduced stress erythropoiesis*, J. Pharmacokinet. Pharmacodyn. 32, (2005), pp. 359–376.

[53] J. Jeon, V. Quaranta, and P. T. Cummings, *An Off-Lattice Hybrid Discrete-Continuum Model of Tumor Growth and Invasion*, Biophys. J. 98 (1), (2010), pp. 37–47.

[54] M. Karttunen, I. Vattulainen, A. Lukkarinen, *A novel methods in soft matter simulations*, Springer, Berlin, (2004).

[55] P. N. Kelly, A. Dakic, J. M. Adams, S. L. Nutt, and A. Strasser, *Tumor Growth Need Not Be Driven by Rare Cancer Stem Cells*, Science, 317 (5836), (2007), p. 337.

[56] W. Kern, E. H. Estey, *High-dose cytosine arabinoside in the treatment of acute myeloid leukemia* Cancer 107, (2006), pp. 116–124.

[57] Y. Kim, M.A. Stolarska, H.G. Othmer, *A hybrid model for tumor spheroid growth in vitro, I : theoretical development and early results*, Math. Models Methods Appl. Sci. 17, (2007), pp. 1773–1798.

[58] H.P. Koeffler, *Induction of differentiation of human acute myelogenous leukemia cells : therapeutic implications*, Blood 62 (4), (1983), pp. 709–721.

[59] A. Kowal-Vern, F.M. Mazzella, J.D. Cotelingam, M.A. Shrit, J.T. Rector and H.R. Schumacher, *Diagnosis and characterization of acute erythroleukemia subsets by determining the percentages of myeloblasts and proerythroblasts in 69 cases*, Am. J. Hematol. 65, (2000), pp. 5–13.

[60] M. J. Koury and M.C. Bondurant, *Erythropoietin retards DNA breakdown and prevents programmed death in erythroid progenitor cells*, Science 248, (1990), pp. 378–381.

[61] S.M. Kozlov, *Averaging of difference schemes*, Math. USSR Sb. 57, (1987), pp. 351–369.

[62] I.A. Kunin, *Media with Microstructure*, Spring-Verlag, Berlin, New-York, I (26), (1982) ; Spring-Verlag, Berlin, New-York, II (44), (1983).

[63] F. Lévi, *Circadian chronotherapy for human cancers* The Lancet Oncology 2 (5), (2001), pp. 307 – 315.

[64] F. Lévi, C. Focan, A Karaboué, de la Valette V, D. Focan-Henrard, B. Baron, F. Kreutz, S. Giacchetti, *Implications of circadian clocks for the rhythmic delivery of cancer therapeutics*, Adv. Drug Deliv. Rev. 59, (2007), pp. 1015–1035.

[65] T.L. Lincoln, P.F. Morrison, J. Aroesty, and G. Carter, em Computer simulation of leukemia therapy : combined pharmacokinetics, intracellular enzyme kinetics, and cell kinetics of the treatment of l1210 leukemia by cytosine arabinoside, Cancer Treat. Rep. 60, (1976), pp. 1723–1739.

[66] A. Madan, C. Lin, Z. Wang and P.T. Curtin, *Autocrine stimulation by erythropoietin in transgenic mice results in erythroid proliferation without neoplastic transformation*, Blood Cells, Molecules and Diseases, 30 (2003), pp. 82–89.

[67] J.M. Mahaffy, J. Belair, M.C. Mackey, em Hematopoietic model with moving boundary condition and state dependent delay : applications in erythropoiesis, J. Theor. Biol. 190, (1998), pp. 135–146.

[68] F.M. Mazzella, C. Alvares, A. Kowal-Vern and H.R. Schumacher, *The acute erythroleukemias*, Clin. Lab. Med. 20, (2000), pp. 119–37.

[69] M.C. Mackey, *Unified hypothesis of the origin of aplastic anaemia and periodic hematopoïesis*, Blood 51, (1978), pp. 941–956.

[70] M.C Mackey, *Dynamic hematological disorders of stem cell origin*, In : G. Vassileva-Popova and E. V. Jensen, Editors. Biophysical and Biochemical Information Transfer in Recognition, Plenum Press, New York., (1979), pp. 373–409.

[71] M.C. Mackey, R. Rudnicki, *A new criterion for the global stability of simultaneous cell replication and maturation processes*, J. Math. Biol. 38, (1999), pp. 195–219.

[72] S.R. McDougall, A.R.A. Anderson, M.A.J. Chaplain and J.A. Sherratt, *Mathematical modelling of flow through vascular networks : Implications for tumour-induced angiogenesis and chemotherapy strategies*, Bulletin of Mathematical Biology 64 (4), (2002), pp. 673–702.

[73] F. Michor, T.P. Hughes, Y. Iwasa, S. Branford, N.P. Shah, et al. *Dynamics of chronic myeloid leukaemia*, Nature 435 (7046), (2005), pp. 1267–1270.

[74] F. Michor, *Quantitative approaches to analyzing imatinib-treated chronic myeloid leukemia*, Trends Pharmacol. Sci. 28 (5), (2007), pp. 197–199.

[75] F. Michor, *Mathematical models of cancer stem cells*, J. Clin. Oncol. 26 (17), (2008), pp. 2854–1861.

[76] R.L. Momparler, *A Model for the Chemotherapy of Acute Leukemia with 1-β-D-Arabinofuranosylcytosine*, Cancer Research 34, (1974), pp. 1775–1787.

[77] M.C. Mormont and F. Lévi, *Cancer chronotherapy : principles, applications, and perspectives*, Cancer 97, (2003), pp. 155–69.

[78] P.F. Morrison, T.L. Lincoln and J. Aroesty, *The disposition of ara-c and its metabolites : a pharmacokinetic simulation*, Cancer Chemother. Rep. 59, (1975), pp. 861–876.

[79] R. De Maria, U. Testa, L. Luchetti, A. Zeuner, G. Stassi, E. Pelosi, R. Riccioni, N. Felli, P. Samoggia and C. Peschle, *Apoptotic Role of Fas/Fas Ligand System in the Regulation of Erythropoiesis*, Blood 93, (1999), pp. 796–803.

[80] Y. Nagata, N. Takahashi, R.J. Davis, K. Todokoro, *Activation of p38 MAP kinase and JNK but not ERK is required for erythropoietin-induced erythroid differentiation* Blood 92, (1998), pp. 1859–1869.

[81] H. G. Othmer, K. Painter, D. Umulis,C. Xue, *The Intersection of Theory and Application in Elucidating Pattern Formation in Developmental Biology*, Math. Model. Nat. Phenom. 4 (4), (2009), pp. 3–82.

[82] R. Orive, E. Zuazua, *Finite difference approximation of homogenization problems for elliptic equations*, Multi-scale Methodes and Simulation 4, (2005), pp. 36–87.

[83] J.M. Osborne, A. Walter, S.K. Kershaw, G.R. Mirams, A.G. Fletcher, P. Pathmanathan, D. Gavaghan, O.E. Jensen, P.K. Maini and H.M. Byrne, *A hybrid approach to multi-scale modelling of cancer*, Phil. Trans. R. Soc. A 368, (2010), pp. 5013–5028.

[84] B. Pain, C.M. Woods, J. Saez, T. Flickinger, M. Raines, H.J. Kung, et al. *EGF-R as a hemopoietic growth factor receptor : The c-erbB product is present in normal chicken erythrocytic progenitor cells and controls their self-renewal*, Cell 65, (1991), pp. 37–46.

[85] G. Panasenko, *Multi-scale Modeling for Structures and Composites*, Springer, (2005).

[86] G. Panasenko, *Partial homogenization : continuous and discrete versions*, Math. Maodels and Methods in Applied Sciences 17 (8), (2007), pp. 1183–1209.

[87] A. Piatnitski, E. Rémy, *Homogenization of elliptic difference operators*, SIAM J. Math. Anal., (2001), pp. 53–83.

[88] A.A. Patel, E.T. Gawlinsky, S.K. Lemieux and R.A. Gatenby, *A Cellular Automaton Model of Early Tumor Growth and Invasion : The Effects of Native Tissue Vascularity and Increased Anaerobic Tumor Metabolism*, J. Theor. Biol. 213, (2001), pp. 315–331.

[89] A. Plesa, G. Ciuperca, V. Louvet, L. Pujo-Menjouet, S. Génieys, C. Dumontet, X. Thomas and V. Volpert, *Diagnostics of the AML with immunophenotypical data*, Math. Model. Nat. Phenom. 1 (2), (2006), pp. 104–123.

[90] I. Ramis-Conde, M.A. Chaplain, A.R. Anderson, D. Drasdo, *Multi-scale modelling of cancer cell intravasation : the role of cadherins in metastasis*, Phys. Biol. 6 (1), (2009) : 016008.

[91] I. Ramis-Conde, D. Drasdo, Alexander R. A. Anderson, and Mark A. J. Chaplain, *Modeling the Influence of the E-Cadherin-SS-Catenin Pathway in Cancer Cell Invasion : A Multiscale Approach*, Biophys. J., 95 (1), (2008), pp. 155–165.

[92] G. Rivard, C. Infante-Rivard, C. Hoyoux, J. Champagne, *Maintenance chemotherapy for childhood acute lymphoblastic leukaemia : better in the evening*, Lancet 2 (8467), (1985), pp. 1264-1266.

[93] S. M. Reppert, D. R. Weaver *Coordination of circadian timing in mammals* Nature 418, pp. 935–941.

[94] K. A. Rejniak, *An immersed boundary framework for modelling the growth of individual cells : An application to the early tumour development*, J. Theor. Biol. 247 (1), (2007), pp. 186–204.

[95] M.M. Rhodes, P. Kopsombut, M.C. Bondurant, J.O. Price, M.J. Koury. *Adherence to macrophages in erythroblastic islands enhances erythroblast proliferation and increases erythrocyte production by a different mechanism than erythropoietin*, Blood 111, (2008).

[96] I. Roeder, *Quantitative stem cell biology : computational studies in the hematopoietic system*, Curr. Opin. Hematol. 13, (2006), pp. 222–228.

[97] S. I. Rubinow and J. L. Lebowitz, A mathematical model of the acute myeloblastic leukemic state in man, Biophys. J. 16, (1976), pp. 897–910.

[98] S. I. Rubinow and J. L. Lebowitz, A mathematical model of the chemotherapeutic treatment of acute myeloblastic leukemia, Biophys. J. 16, (1976), 1257–1271.

[99] C. Rubiolo, D. Piazzolla, K. Meissl, H. Beug, J.C. Huber, A. Kolbus and M. Baccarini, *A balance between Raf-1 and Fas expression sets the pace of erythroid differentiation*, Blood 108, (2006), pp. 152–159.

[100] D.A. Rew, G.D. Wilson, I. Taylor and P.C. Weaver, *Proliferation characteristics of human colorectal carcinomas measured in vivo*, Br J Surg. 78, (1991), pp. 60-66.

[101] S. Sakr, R. Jeanjean, C.-C.Zhang, and T. Arcondeguy, *Inhibition of Cell Division Suppresses Heterocyst Development in Anabaena sp. Strain PCC 7120*, Journal of Bacteriology 188 (4), (2006), pp. 1396–1404.

[102] I. Salazar-Ciudad, J. Jernvall, *A computational model of teeth and the developmental origins of morphological variation*, Nature 464 (7288), (2010), pp. 583–586.

[103] M. Santillan, J.M. Mahaffy, J. Belair, M.C. Mackey, *Regulation of platelet production : The normal response to perturbation and cyclical platelet disease*, J. Theor. Biol. 206, (2000), pp. 585–603.

[104] S.T. Sawyer, S.M. Jacobs-Helber, *Unraveling distinct intracellular signals that promote survival and proliferation : study of erythropoietin, stem cell factor, and constitutive signaling in leukemic cells*, J. Hematother. Stem Cell Res. 9, (2000), pp. 21–29.

[105] M. Scianna, R. M. H. Merks, L. Preziosi and E. Medico, *Individual cell-based models of cell scatter of ARO and MLP-29 cells in response to hepatocyte growth factor*, J. Theor. Biol. 260 (1), (2009), pp. 151–160.

[106] V. Shenoy, R. Miller, E.B. Tadmor, D. Rodney, R. Philips, M. Ortiz, *An adaptive finite element approach to atomistic-scale mechanics - The Quasi-Continuum Method*, J. Mech. Phys. Solids 47, (1999), pp. 611–642.

[107] M. Socolovsky, *Molecular insights into stress erythropoiesis*, Current opinion in hematology 14 (3), (2007), pp. 215–224.

[108] M.L. Slevin, E.M. Piall, G.W. Aherne, V.J. Harvey, A. Johnston and T.A. Lister, *Effect of dose and schedule on pharmacokinetics of high-dose cytosine arabinoside in plasma and cerebrospinal fluid*, Journal of Clinical Oncology 1, (1983), pp. 546–551.

[109] R. Smaaland, O.D. Laerum, K. Lote, O. Sletvold, R.B. Sothern and R. Bjerknes, *DNA synthesis in human bone marrow is circadian stage dependent*, Blood 77, (1991), pp. 2603–2611.

[110] R. Smaaland, R.B. Sothern, O.D. Laerum and J.F. Abrahamsen, *Rhythms in human bone marrow and blood cells*, Chronobiol Int. 19, (2002), pp. 101–27.

[111] S.L Spencer, R.A. Gerety, K.J. Pienta, S. Forrest, *Modeling somatic evolution in tumorigenesis*, PLoS Comput. Biol. 2 (8), (2006), e108.

[112] J.L. Spivak, T. Pham, M. Isaacs, W.D. Hankins, *Erythropoietin is both a mitogen and a survival factor*, Blood 77, (1991), pp. 1228–1233.

[113] A. Stéphanou, S.R. McDougall, A.R.A. Anderson and M.A.J. Chaplain, *Mathematical modelling of flow in 2D and 3D vascular networks : Applications to anti-angiogenic and chemotherapeutic drug strategies*, Mathematical and Computer Modelling 41 (10), (2005), pp. 1137-1156.

[114] X. Sui, S.B. Krantz, Z.J. Zhao, *Stem cell factor and erythropoietin inhibit apoptosis of human erythroid progenitor cells through different signalling pathways*, Br. J. Haematol. 110, (2000), pp. 63–70.

[115] A.S. Tsiftsoglou, I.S. Vizirianakis, J. Strouboulis, *Erythropoiesis : model systems, molecular regulators, and developmental programs*, IUBMB Life., 61(8), (2009), pp. 800–830.

[116] Y. Tang and H. G. Othmer, *A G protein-based model of adaptation in Dictyostelium discoideum*, 120 (1), (1994), pp. 25–76.

[117] P. Veng-Pedersen, S. Chapel, P.R.L. Schmidt, N.H. Al-Huniti, R.T. Cook et al. *An integrated pharmacodynamic analysis of erythropoietin, reticulocyte, and hemoglobin responses in acute anemia*, Pharm Res 19, (2002), pp. 1630–1635.

[118] M.Y. Yang, J.G. Chang, P.M. Lin, K.P. Tang, Y.H. Chen, H.Y. Lin, T.C. Liu, H.H. Hsiao, Y.C. Liu and S.F. Lin, *Downregulation of circadian clock genes in chronic myeloid leukemia : alternative methylation pattern of hPER3*, Cancer Sci. 97, (2006), pp. 1298–1307.

[119] H.E. Wichmann, M.D. Gerhardts, H. SPechtmeyer, R. Gross, *A mathematical model of thrombopoiesis in rats*, Cell Tissue Kinet. 12, (1979), pp. 551–567.

[120] H.E. Wichmann, M. Loeffler, K. Pantel, H. Wulff, *A mathematical model of erythropoiesis in mice and rats. Part 2. Stimulated erythropoiesis.*, Cell Tissue Kinet. 22, (1989), pp. 31–49.

[121] H.E. Wichmann, M. Loeffler, *Mathematical Modeling of Cell Proliferation*, Boca Raton, FL, CRC, (1985).

[122] H.E. Wichmann, M. Loeffler, S. Schmitz, *A concept of hemopoietic regulation and its biomathematical realisation.* Blood Cells 14, (1985), pp. 411–429.

[123] S. Woo, W. Krzyzanski and W. J. Jusko, *Pharmacokinetic and Pharmacodynamic Modeling of Recombinant Human Erythropoietin after Intravenous and Subcutaneous Administration in Rats*, JPET 319 (3), (2006), pp. 1297–1306.

[124] S. Woo, W. Krzyzanski and W. J. Jusko, *Pharmacodynamic model for chemotherapy-induced anemia in rats*, Cancer Chemother. Pharmacol. 62 (1), (2008), pp. 123–133.

[125] H. Wulff, H.E. Wichmann, M. Loeffler, K. Pantel, *A mathematical model of erythropoiesis in mice and rats. Part 3. Suppressed erythropoiesis*, Cell Tissue Kinet. 22, (1989), pp. 51–61.